

V

**THE EFFECTS OF ATMOSPHERIC TURBULENCE
IN OPTICAL ASTRONOMY**

BY

F. RODDIER

*Département d'Astrophysique de l'I.M.S.P., Equipe de recherche associée au C.N.R.S. no 669,
Université de Nice, Parc Valrose, 06034 Nice Cedex, France*

CONTENTS

	PAGE
§ 1. INTRODUCTION	283
§ 2. STATISTICAL PROPERTIES OF ATMOSPHERIC TUR- BULENCE	284
§ 3. STATISTICAL PROPERTIES OF THE PERTURBED COMPLEX FIELD	291
§ 4. LONG-EXPOSURE IMAGES	297
§ 5. SHORT-EXPOSURE IMAGES	309
§ 6. EXPOSURE-TIME AND NON-ISOPLANICITY EF- FECTS	319
§ 7. OPTICAL PATH FLUCTUATIONS.	328
§ 8. STELLAR SCINTILLATION	341
§ 9. APPLICATIONS TO HIGH RESOLUTION IMAGING .	350
§ 10. SEEING MONITORS AND SITE TESTING.	360
§ 11. CONCLUSION	367
REFERENCES	368

§ 1. Introduction

Atmospheric turbulence is a major problem in optical astronomy as it drastically reduces the angular resolution of telescopes. The diameter of the image of a star, also called the seeing disk, varies approximately from 0.3 arcsecond to 10 arcseconds or more, according to weather conditions. A typical diameter is 2 arcseconds, which is the resolution limit of a 6 cm aperture in the visible.

When a stellar image is observed through a telescope with high magnification, the observed image structure, even with perfect optics, is usually far from the theoretical diffraction pattern and changes rapidly with time. The appearance of the image depends strongly on the aperture of the telescope. With small apertures a random motion of the image is often the main effect. With large apertures spreading and blurring of the image occur. A speckle structure is often observed, somewhat similar in appearance to a bunch of grapes, as noted by RÖSCH [1958b].

In the early sixties, the physics of image degradation by atmospheric turbulence was still little understood. Several techniques were worked out on an empirical basis in order to make quantitative estimates of the amount of degradation. They are reviewed by STOCK and KELLER [1960], MEINEL [1960], and in the Proceedings of the I.A.U. Symposium no 19 (RÖSCH, COURTES and DOMMANGET [1963]). The influence of the telescope location on image quality was recognised and these techniques were extensively used during the site testing campaigns leading up to the construction of most of our modern observatories. An I.A.U. working group on site testing was created and a Symposium on this subject held in Rome in October 1962. Several questions arose: is it possible to describe image degradation with a single atmospheric parameter? Is it possible to predict image behaviour through a large telescope from measurements through a small one? No answer could be given due to the absence of any theory of image formation through turbulence.

Since that time, the situation has evolved considerably. Observation sites once having been chosen, astronomers became less and less

interested in measuring image degradation. At the same time, due to the discovery of the laser, optical physicists became more and more interested in optical propagation through turbulence, leading to considerable advances in this field. Unfortunately, the work of optical physicists has often remained unknown to astronomers (for example LINFOOT and WITCOMB [1972] and GRIFFIN [1973]). At the same time, the application by A. LABEYRIE [1970] of speckle interferometry techniques to stellar images gave a new impetus to high resolution imaging techniques as well as to the theory of image formation through turbulence. This theory is now well established on a solid experimental basis but its importance is not yet fully appreciated by the majority of astronomers.

The purpose of this paper is to summarise the present state of the theory, review the experimental checks that have been made and discuss the implications in the domain of astronomical observations. We hope that this review will help to acquaint the astronomical community with recent advances in this field.

§ 2 briefly summarises the theory of energy cascades due to KOLMOGOROV [1941] and the related spectral properties of temperature and refractive index fluctuations in the atmosphere derived by OBUKHOV [1949], YAGLOM [1949] and CORRSIN [1951]. § 3 summarises the spectral properties of the complex amplitude fluctuations of a perturbed plane wave, derived by CHERNOV [1955] and TATARSKI [1956]. In order to minimise mathematical calculations we have adopted a phase screen approach similar to that of LEE and HARP [1969]. § 4, § 5 and § 6 deal with the statistical properties of a point source image derived mainly by HUFNAGEL and STANLEY [1964], FRIED [1966] and KORFF [1973]. Application to Michelson stellar interferometry and aperture synthesis is also discussed. In § 7 and § 8, the phase screen approach is used again to derive the statistical properties of amplitude and phase fluctuations, i.e. of stellar scintillation and of optical path or angle-of-arrival fluctuations. Applications to high resolution imaging are discussed in § 9. Applications to site testing and the measurement of image quality are discussed in § 10.

§ 2. Statistical Properties of Atmospheric Turbulence

2.1. STRUCTURE OF TURBULENCE

Mathematical descriptions of turbulence are presented in the books by BATCHELOR [1970] and by HINZE [1959]. A didactic presentation, with

particular emphasis on atmospheric turbulence, can be found in the book by TENNEKES and LUMLEY [1972]. Properties of atmospheric turbulence are described in detail in the book by LUMLEY and PANOFSKY [1964]. Here we shall briefly summarise the results pertinent to optical propagation, as reviewed by TATARSKI [1961].

A flow becomes turbulent when the Reynolds number $Re = V_0 L_0 / \nu_0$ exceeds a critical value which depends only upon the geometrical structure of the flow. Here, V_0 is a characteristic velocity and L_0 a characteristic size of the flow; ν_0 is the kinematic viscosity of the fluid. Atmospheric air flow is nearly always turbulent. Since the kinematic viscosity of air is of the order of $\nu_0 = 15 \times 10^{-6} \text{ m}^2 \text{ s}^{-1}$, taking $V_0 = 1 \text{ m/s}$ and $L_0 = 15 \text{ m}$ leads to $Re = 10^6$ which, in general, corresponds to fully developed turbulence.

KOLMOGOROV [1941] suggested that, in fully developed turbulence, the kinetic energy of large scale motions is transferred to smaller and smaller scale motions. Motions on a small scale are statistically isotropic. Motions at scale L have a characteristic velocity V . When the Reynolds number VL/ν_0 becomes small enough, the break up process stops and the kinetic energy is dissipated into heat by viscous friction. In a stationary state, the rate ε_0 of viscous dissipation must be equal to the rate of production of turbulent energy. It is therefore reasonable to assume that the velocity V of motions at scale L depends only upon L and upon the rate ε_0 of energy production and dissipation. A dimensional reasoning then easily shows that

$$V \propto \varepsilon_0^{\frac{1}{3}} L^{\frac{1}{3}}. \quad (2.1)$$

In a spectral analysis of the kinetic energy as a function of the modulus κ of the wave vector κ , the energy $E(\kappa) d\kappa$ between κ and $\kappa + d\kappa$ is proportional to $V^2(\kappa)$. Taking (2.1) into account, with $L \propto 1/\kappa$, leads to:

$$E(\kappa) d\kappa \propto \kappa^{-\frac{5}{3}} \quad \text{or} \quad E(\kappa) \propto \kappa^{-\frac{5}{3}} \quad (2.2)$$

which expresses the Kolmogorov law, valid only in the inertial range $L_0^{-1} \ll \kappa \ll l_0^{-1}$, where L_0 is the outer scale (generally the scale of the motions which give rise to turbulence) and l_0 is the inner scale at which viscous dissipation arises.

In the troposphere, l_0 ranges from a few millimetres near the ground to about 1 cm near the tropopause. L_0 is of the order of the thickness of turbulent layers, that is about 100 m. Near the ground, it is of the order of the height above the ground. We shall see that the size of the wavefront perturbations, degrading astronomical images, ranges between a few

centimetres and the size of the telescope aperture. Kolmogorov's law therefore entirely applies and is indeed found consistent with observations. However in the case of long baseline interferometry it may become questionable.

2.2. TEMPERATURE AND HUMIDITY FLUCTUATIONS

Temperature and humidity are both functions of height in the atmosphere. Turbulent mixing therefore creates inhomogeneities of temperature and humidity at scales comparable to eddy sizes. OBUKHOV [1949] and YAGLOM [1949] have shown that, in a turbulent flow, the concentration of an additive which is passive (i.e. does not affect the dynamics of turbulence) and which is conservative (i.e. does not disappear by chemical reaction of the other), also follows Kolmogorov's law. The inner and outer scales differ, in principle, from l_0 and L_0 , the inner scale being related to molecular diffusion. However, as far as we are concerned, they happen to be of the same order of magnitude. This result applies, to a good approximation, to the mixing of air with water vapour or the mixing of cool air with warm air. The power spectrum $\Phi_T(\kappa)$ of temperature fluctuations and the power spectrum $\Phi_C(\kappa)$ of humidity fluctuations are therefore also described by

$$\Phi_T(\kappa) \propto \kappa^{-\frac{5}{3}}, \quad \Phi_C(\kappa) \propto \kappa^{-\frac{5}{3}}. \quad (2.3)$$

In the following, we shall deal with three-dimensional spectra $\Phi(\kappa) = \Phi(\kappa_x, \kappa_y, \kappa_z)$. One-dimensional spectra are related to three-dimensional spectra by integration over all directions so that, in the isotropic case

$$\Phi(\kappa) = 4\pi\kappa^2\Phi(\kappa),$$

therefore

$$\Phi_T(\kappa) \propto \kappa^{-\frac{11}{3}} \quad \text{and} \quad \Phi_C(\kappa) \propto \kappa^{-\frac{11}{3}}. \quad (2.4)$$

The covariance of the temperature fluctuations $\Theta = T - \langle T \rangle$ is

$$B_T(\rho) = \langle \Theta(r)\Theta(r+\rho) \rangle. \quad (2.5)$$

According to the Wiener-Khinchine theorem, it is the three-dimensional Fourier transform of $\Phi_T(\kappa)$ defined as

$$B_T(\rho) = \int \Phi_T(\kappa) \exp(i\kappa \cdot \rho) d\kappa. \quad (2.6)$$

However it cannot be derived from (2.4) since integral (2.6) would diverge at the origin (where (2.4) is not valid). Following TATARSKI [1961] and others, it is convenient to consider the structure function

$$D_T(\rho) = \langle |\Theta(r+\rho) - \Theta(r)|^2 \rangle \quad (2.7)$$

related to the covariance by

$$D_T(\rho) = 2[B_T(0) - B_T(\rho)] \quad (2.8)$$

which remains finite as long as $|\rho|$ is finite. Again, an expression for $D_T(\rho)$, valid in the inertial range, can easily be derived by dimensional reasoning, assuming that it depends only upon $|\rho| = \rho$, upon the rate ε_0 of production of turbulent energy and upon the rate η_0 of production of temperature fluctuation (which is also the rate of molecular dissipation). Then necessarily $D_T(\rho)$ is proportional to

$$D_T(\rho) \propto \eta_0 \varepsilon_0^{-\frac{1}{3}} \rho^{\frac{5}{3}} \quad (2.9)$$

as derived by OBUKHOV [1949]. Eq. (2.9) is usually written

$$D_T(\rho) = C_T^2 \rho^{\frac{5}{3}} \quad (2.10)$$

defining C_T^2 as the structure constant of temperature fluctuations. With such a definition, TATARSKI [1961] has shown that (2.4) becomes

$$\Phi_T(\kappa) = \frac{\Gamma(\frac{8}{3}) \sin(\pi/3)}{4\pi^2} C_T^2 \kappa^{-\frac{11}{3}} = 0.033 C_T^2 \kappa^{-\frac{11}{3}}. \quad (2.11)$$

Similar expressions can be derived for humidity fluctuations $c = C - \langle C \rangle$.

2.3. REFRACTIVE INDEX FLUCTUATIONS

The refractive index N of air is a function $N(T, C)$ of the temperature T and of the concentration C of water vapour. Its fluctuations $n = N - \langle N \rangle$ are therefore given by

$$n = \frac{\partial N}{\partial T} \Theta + \frac{\partial N}{\partial C} c = \mathbb{A} \Theta + \mathbb{B} c \quad (2.12)$$

with variance

$$\langle n^2 \rangle = \mathbb{A}^2 \langle \Theta^2 \rangle + 2\mathbb{A}\mathbb{B} \langle \Theta c \rangle + \mathbb{B}^2 \langle c^2 \rangle. \quad (2.13)$$

In optical propagation the last term is always negligible. FRIEHE and LARUE [1974], ANTONIA, CHAMBERS and FRIEHE [1978] have shown that

the second term can be a significant correction factor, either positive or negative, in a marine boundary layer. However, it seems to be negligible in the case of most astronomical observations.

An expression for the coefficient \mathbb{A} can easily be derived from Gladstone's relation. Assuming pressure equilibrium leads to:

$$\mathbb{A} = 80 \times 10^{-6} P/T^2, \quad (2.14)$$

where the air pressure P is expressed in millibars and the air temperature T in Kelvin degrees. Since $n = \mathbb{A} \theta$, the structure function of n also follows Obukhov's law

$$D_N(\rho) = C_N^2 \rho^{\frac{2}{3}} \quad (2.15)$$

where C_N is the index structure constant. It is related to the temperature structure constant C_T by

$$C_N = \mathbb{A} C_T. \quad (2.16)$$

Similarly, the power spectrum of the index fluctuations is given by

$$\Phi_N(k) = 0.033 C_N^2 k^{-\frac{11}{3}}. \quad (2.17)$$

The parameter C_N^2 expresses the contribution of turbulence to optical propagation. Measuring its dependence upon height has been the aim of many investigations, the results of which will be now reviewed.

2.4. DEPENDENCE OF C_N^2 WITH HEIGHT AND TIME

An old, but good description of the origin of astronomical seeing can be found in the book by TEXEREAU [1961]. The sources of image degradation can be roughly divided into four origins: turbulence associated with the telescope and the dome, turbulence in the surface boundary layer or due to ground convection, turbulence in the planetary boundary layer or associated with orographic disturbances, and turbulence in the tropopause or above.

Turbulence inside the telescope and the dome are due to temperature gradients and can therefore be avoided. Turbulence due to velocity gradients at the interface between still air inside the dome and wind driven air outside the dome cannot be avoided and is a major source of image degradation. However the associated temperature or refractivity fluctuations are entirely due to temperature gradients. They can therefore

be considerably reduced by carefully equalising inside and outside air temperatures. Difficulties arise during daytime observations because of the solar heating of the instrument.

Turbulence in the surface boundary layer and its diurnal cycle has long been known by astronomical observers. During the last decade, it has been extensively studied by people interested in laser beam propagation in the atmosphere. A review of the results can be found in the monograph by CLIFFORD [1978]. This turbulence layer extends roughly up to several tens of meters above the ground. C_T^2 values have been derived from high-speed temperature sensors either ground based (LAWRENCE, OCHS and CLIFFORD [1970]) or tower mounted (KALLISTRATOVA and TIMANOVSKIY [1971], OCHS and LAWRENCE [1972], NEFF [1975]). They can also be derived from heat flux estimates (WESELY and ALCARAZ [1973]). Acoustic soundings allow direct visualisation of refractivity fluctuations up to about 1 km. This new technique, reviewed by SINGAL [1974] and AUBRY [1975] also leads to C_T^2 estimates (NEFF [1975]). Radar soundings (METCALF [1975]) and aircraft soundings (TSVANG [1969], OCHS and LAWRENCE [1972]) have also been used to study refractivity fluctuations within the first kilometre above the ground.

The diurnal cycle, well known to solar observers, is due to the solar heating of the ground (HESS [1959]). Typically, turbulence reaches a minimum just after sunrise and steeply increases until early afternoon. Growing thermal plumes are seen on acoustic sounding records. Then, turbulence decreases to a secondary minimum after sunset. It slightly increases again during nighttime. 12 m above the ground, KALLISTRATOVA and TIMANOVSKIY [1971] find typical C_N^2 values of the order of 10^{-13} m^{-2} during daytime and 10^{-14} m^{-2} during nighttime. A $h^{-\frac{4}{3}}$ height dependence has been predicted by WYNGAARD, IZUMI and COLLINS [1971], under unstable daytime conditions on flat land, and has been found to agree with observations (TSVANG [1969], NEFF [1975]). They also predict a $h^{-\frac{2}{3}}$ dependence under neutral conditions and a slower decrease under the stable conditions that occur during nighttime.

The behaviour of turbulence above 1 km has been little known until recently. An exponential decrease of C_N^2 with height was often assumed (REIGER [1962, 1963], YOUNG [1969]). A more realistic model was derived by HUFNAGEL [1966] taking into account both atmospheric data and stellar scintillation data. The use of balloon-borne thermal probes initiated by COULMAN [1973] and BUFTON [1973a, b] greatly improved our knowledge. The same technique has since been extensively used by

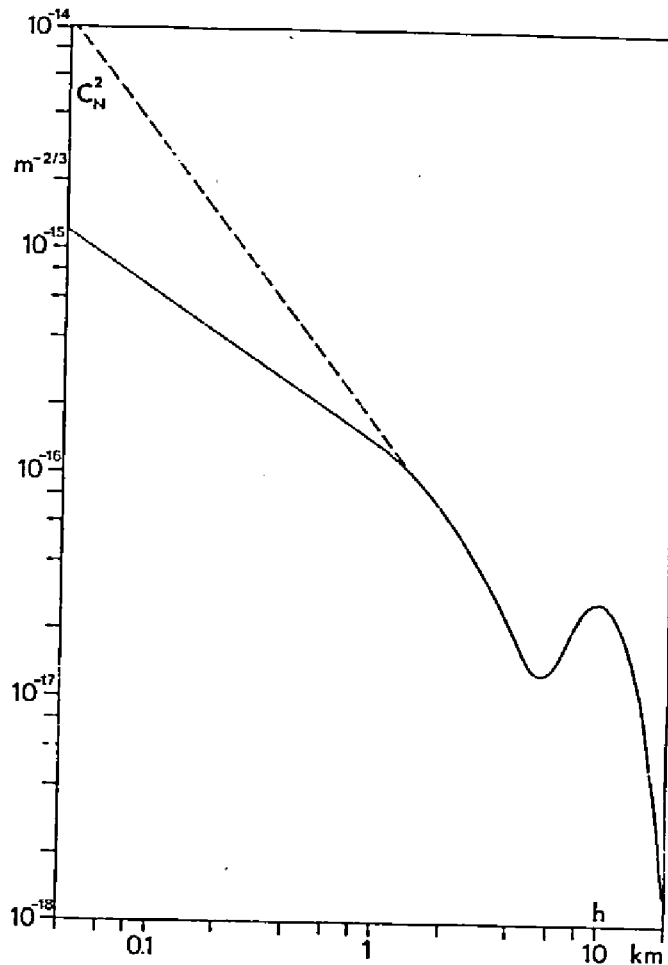


Fig. 1. Average C_N^2 profile (HUFNAGEL [1974]) extended towards low altitudes according a $h^{-\frac{2}{3}}$ law (neutral nighttime conditions). Dotted line: extension according a $h^{-\frac{2}{3}}$ law (unstable daytime conditions).

BARLETTI, CEPPATELLI, MORODER, PATERNO and RIGHINI [1974] and BARLETTI, CEPPATELLI, PATERNO, RIGHINI and SPERONI [1977] during the J.O.S.O. site testing campaign. Turbulence appears to be concentrated into thin layers with a typical thickness of 100–200 m where C_N^2 increases by more than one order of magnitude above its background level. Below 4 km, orographic disturbances certainly play an important role, but above 4 km, BARLETTI, CEPPATELLI, PATERNO, RIGHINI and SPERONI [1976] conclude that the behaviour of turbulence is almost independent of the location. Indeed, when the layered structure is smoothed out, and the average of many profiles is taken, a typical behaviour is observed. It reaches a minimum of the order of $10^{-17} \text{ m}^{-\frac{2}{3}}$ around 6–9 km, slightly increases to a secondary maximum near the tropopause and decreases again in the stratosphere. Low resolution C_N^2 profiles showing this general behaviour have also been obtained from stellar scintillation analysis by

OCHS, TIN-I-WANG, LAWRENCE and CLIFFORD [1976] and by VERNIN, BARLETTI, CEPPATELLI, PATERNO, RIGHINI and SPERONI [1979] who found a good agreement with simultaneous thermal soundings. Radar measurements of C_N^2 profiles have also been reported by VANZANDT, GREEN, GAGE and CLARK [1977, 1978]. Turbulence near the tropopause is due to strong wind shears frequently occurring in this region. Its time evolution can be followed by radar soundings (BROWNING [1971]) or by stellar scintillation analysis as recently shown by AZOUI and VERNIN [1980].

An improved model for the average C_N^2 profile and its fluctuations has been proposed by HUFNAGEL [1974] and found to agree well with the observations of BARLETTI, CEPPATELLI, PATERNO, RIGHINI and SPERONI [1976] who also derived a lucky observer model by plotting the smallest C_N^2 value ever observed at each altitude. Hufnagel's average C_N^2 profile is presented in Fig. 1 with an extension towards lower altitudes according to the predicted power laws. Although individual atmospheric measurements show considerable departures from the model, the order of magnitude of the predicted effects on seeing are well reproduced, as discussed in the following sections.

§ 3. Statistical Properties of the Perturbed Complex Field

Because the atmosphere determines the ultimate limitations of optical telescopes, astronomers were among the first to be interested in optical propagation through turbulence (see LITTLE [1951], CHANDRASEKHAR [1952], KELLER [1953, 1955]). VAN ISACKER [1954] attempted to derive the spectral distribution of thermal fluctuations in the atmosphere from scintillation measurements. However CHERNOV [1955] and TATARSKI [1956] were the first to introduce Kolmogorov's law into their theory. The English translation of their monographs (CHERNOV [1960], TATARSKI [1961, 1971]) made available the first complete treatment of the problem of wave propagation in turbulent media. Applications to optical propagation in the atmosphere and discussions on the limitations of the theory can be found in several articles by STROHBEHN [1968, 1970a, 1971, 1973] and CLIFFORD [1978]. A simple physical approach has been derived by LEE and HARP [1969]. Modern theories include the effect of strong fluctuations and multiple scattering. They are discussed by USCINSKI [1977], ISHIMARU [1978] and STROHBEHN [1978]. In this section, we shall

deal only with the complex amplitude. We shall briefly derive its properties relevant to image formation (coherence functions) using a phase-screen approach similar to that of LEE and HARP [1969] and the formalism of Fourier optics as presented by GOODMAN [1968]. Fluctuations of amplitude (scintillation) and of angle-of-arrival, will be similarly examined in § 7 and § 8, using the small perturbation approximation.

For the sake of simplicity, we shall consider only horizontal monochromatic plane waves, at wavelength λ , propagating downward from a star at the zenith, towards a ground-based observer. Each point of the atmosphere will be designated by a horizontal coordinate vector x and an altitude h above the ground. The scalar vibration located at coordinates (x, h) will be described by its complex amplitude

$$\Psi_h(x) = |\Psi_h(x)| \exp[i\varphi_h(x)]. \quad (3.1)$$

At each altitude h , the phase $\varphi_h(x)$ will be referred to its average value so that, for any h , $\langle \varphi_h(x) \rangle = 0$. Furthermore, we shall normalise to unity the unperturbed complex amplitude outside the atmosphere, so that $\Psi_\infty(x) = 1$. Finally we shall consider the atmosphere as non-absorbing and horizontally stratified (its statistical properties depend only upon h).

3.1. OUTPUT OF A THIN TURBULENCE LAYER

Let us now assume that the earth atmosphere is still and homogeneous everywhere except inside a thin horizontal layer, between altitude h and $h + \delta h$. The layer thickness is chosen to be large compared to the correlation scale of the inhomogeneities but small enough for diffraction effects to be negligible over the distance δh (thin screen approximation). Since, at the layer input, $\Psi_{h+\delta h}(x) = 1$, at the output

$$\Psi_h(x) = \exp[i\varphi(x)] \quad (3.2)$$

where $\varphi(x)$ is the phase shift introduced by index fluctuations $n(x, h)$ inside the layer

$$\varphi(x) = k \int_h^{h+\delta h} dz \cdot n(x, z) \quad (3.3)$$

where $k = 2\pi/\lambda$ is the wavenumber of the vibration.

The second order moment of the complex random field $\Psi_h(x)$ at the

layer output is the coherence function

$$B_h(\xi) = \langle \Psi_h(x) \Psi_h^*(x + \xi) \rangle. \quad (3.4)$$

Putting eq. (3.2) into eq. (3.4) leads to

$$B_h(\xi) = \langle \exp i[\varphi(x) - \varphi(x + \xi)] \rangle. \quad (3.5)$$

Since $\varphi(x)$ is the sum of a great number of independent variables (eq. (3.3)), it has Gaussian statistics. The expression between square brackets in (3.5) is therefore also Gaussian and has a zero mean. Since $B_h(\xi)$ is its characteristic function (Fourier transform of the probability density function) at unit frequency, it is equal to

$$B_h(\xi) = \exp -\frac{1}{2} \langle |\varphi(x) - \varphi(x + \xi)|^2 \rangle \quad (3.6)$$

or, introducing the two-dimensional (horizontal) structure function $D_\varphi(\xi)$ of the phase $\varphi(x)$,

$$B_h(\xi) = \exp -\frac{1}{2} D_\varphi(\xi). \quad (3.7)$$

We must now relate $D_\varphi(\xi)$ to the statistics of the index fluctuations. Let $B_\varphi(\xi)$ be the covariance of $\varphi(x)$

$$B_\varphi(\xi) = \langle \varphi(x) \varphi(x + \xi) \rangle. \quad (3.8)$$

Putting (3.3) into (3.8) leads to

$$B_\varphi(\xi) = k^2 \int_h^{h+\delta h} dz \int_h^{h+\delta h} dz' \langle n(x, z) n(x + \xi, z') \rangle.$$

Introducing $\zeta = z' - z$ and the three-dimensional covariance $B_N(\xi, \zeta)$ of the index fluctuations, gives

$$B_\varphi(\xi) = k^2 \int_h^{h+\delta h} dz \int_{h-z}^{h+\delta h-z} d\zeta \cdot B_N(\xi, \zeta). \quad (3.9)$$

Since δh has been assumed to be much larger than the correlation scale of the index fluctuations, the integration over ζ can be taken from $-\infty$ to $+\infty$ so that

$$B_\varphi(\xi) = k^2 \delta h \int d\zeta \cdot B_N(\xi, \zeta). \quad (3.10)$$

The phase structure function is related to its covariance by

$$D_\varphi(\xi) = 2[B_\varphi(0) - B_\varphi(\xi)].$$

Taking (3.10) into account gives

$$D_\varphi(\xi) = 2k^2 \delta h \int d\zeta [B_N(0, \zeta) - B_N(\xi, \zeta)]$$

or

$$D_\varphi(\xi) = k^2 \delta h \int d\zeta [D_N(\xi, \zeta) - D_N(0, \zeta)] \quad (3.11)$$

where

$$D_N(\xi, \zeta) = 2[B_N(0, 0) - B_N(\xi, \zeta)]$$

is the index structure function. Assuming Obukhov's law (2.15)

$$D_N(\xi, \zeta) = C_N^2 (\xi^2 + \zeta^2)^{\frac{1}{3}}$$

where $\xi = |\xi|$, so that (3.11) leads to

$$D_\varphi(\xi) = k^2 C_N^2 \delta h \int d\zeta [(\xi^2 + \zeta^2)^{\frac{1}{3}} - \zeta^{\frac{2}{3}}]$$

or after integration

$$D_\varphi(\xi) = 2.91 k^2 C_N^2 \delta h \xi^{\frac{5}{3}}. \quad (3.12)$$

Putting (3.12) into (3.7) gives the second order moment of the complex field $\Psi_h(x)$ at the layer output

$$B_h(\xi) = \exp -\frac{1}{2}(2.91 k^2 C_N^2 \delta h \xi^{\frac{5}{3}}). \quad (3.13)$$

The complex field $\Psi_0(x)$ at ground level is the field diffracted by the layer. Since optical wavelengths are much smaller than the scale of the observed wavefront perturbations, the Fresnel approximation can be used safely. Therefore (GOODMAN [1968])

$$\Psi_0(x) = \Psi_h(x) * \frac{1}{i\lambda h} \exp \left(i\pi \frac{x^2}{\lambda h} \right) \quad (3.14)$$

where the symbol $*$ denotes a two-dimensional convolution with respect to the variable x . A remarkable property is that coherence functions $B_h(\xi)$ are invariant by Fresnel diffraction. Indeed, the coherence function $B_0(\xi)$ at ground level is

$$\begin{aligned} B_0(\xi) &= \langle \Psi_0(x) \Psi_0^*(x + \xi) \rangle \\ &= \langle \Psi_h(x) \Psi_h^*(x + \xi) \rangle * \frac{1}{i\lambda h} \exp \left(i\pi \frac{x^2}{\lambda h} \right) * -\frac{1}{i\lambda h} \exp \left(-i\pi \frac{(x + \xi)^2}{\lambda h} \right). \end{aligned}$$

Now, as easily shown by taking the Fourier transform,

$$\frac{1}{i\lambda h} \exp\left(i\pi \frac{x^2}{\lambda h}\right) * -\frac{1}{i\lambda h} \exp\left(-i\pi \frac{x^2}{\lambda h}\right) = \delta(x)$$

where $\delta(x)$ is Dirac's impulse symbol. Therefore

$$B_0(\xi) = B_h(\xi) \quad (3.15)$$

or, taking (3.7) into account,

$$B_0(\xi) = \exp -\frac{1}{2} D_\varphi(\xi). \quad (3.16)$$

For high altitude layers, the complex field $\Psi_0(x)$ at ground level will fluctuate both in amplitude (scintillation) and in phase. Therefore, in (3.16), D_φ must not be taken as the structure function of the phase at ground level. However, as discussed in § 7.3, the correction remains small in the conditions of astronomical observations. Taking D_φ as the phase structure function at ground level is called the near-field approximation.

3.2. MULTIPLE LAYERS AND THICK LAYERS

Let us now assume (as is often true) that turbulence is located in a number of thin layers between altitudes h_j and $h_j + \delta h_j$. The complex amplitude Ψ_{h_j} at the output of layer j is related to the complex amplitude $\Psi_{h_j + \delta h_j}$ at the input by

$$\Psi_{h_j}(x) = \Psi_{h_j + \delta h_j}(x) \cdot \exp [i\varphi_j(x)] \quad (3.17)$$

where $\varphi_j(x)$ is the phase fluctuation introduced by layer j . Since φ_j is statistically independent of $\Psi_{h_j + \delta h_j}$, the coherence at the output is related to the coherence at the input by

$$\begin{aligned} \langle \Psi_{h_j}(x) \cdot \Psi_{h_j}^*(x + \xi) \rangle &= \langle \Psi_{h_j + \delta h_j}(x) \cdot \Psi_{h_j + \delta h_j}^*(x + \xi) \rangle \\ &\times \langle \exp i[\varphi_j(x) - \varphi_j(x + \xi)] \rangle. \end{aligned} \quad (3.18)$$

Following (3.5), and (3.13), we obtain

$$\langle \exp i[\varphi_j(x) - \varphi_j(x + \xi)] \rangle = \exp -\frac{1}{2}[2.91k^2 C_N^2(h_j) \delta h_j \xi^2]. \quad (3.19)$$

Through each layer, the coherence function is multiplied by expression (3.19). Between layers, it remains unaffected. Its value on the ground is

therefore

$$\begin{aligned} B_0(\xi) &= \prod_i \exp -\frac{1}{2}[2.91k^2 C_N^2(h_i) \delta h_i \xi^{\frac{2}{3}}] \\ &= \exp -\frac{1}{2}\left[2.91k^2 \xi^{\frac{2}{3}} \sum_j C_N^2(h_j) \delta h_j\right] \end{aligned} \quad (3.20)$$

which easily generalises, for a continuous distribution of turbulence, into

$$B_0(\xi) = \exp -\frac{1}{2}\left[2.91k^2 \xi^{\frac{2}{3}} \int dh \cdot C_N^2(h)\right] \quad (3.21)$$

the integral being extended all over the earth's atmosphere.

When observing at an angular distance γ from the zenith, the thickness δh of each layer is multiplied by $(\cos \gamma)^{-1}$ and, to a good approximation, the coherence function $B_0(\xi)$ on the telescope aperture plane is

$$B_0(\xi) = \exp -\frac{1}{2}\left[2.91k^2 (\cos \gamma)^{-1} \xi^{\frac{2}{3}} \int dh \cdot C_N^2(h)\right]. \quad (3.22)$$

It will be shown, in § 4, that the properties of long exposure images are entirely determined by the coherence of the complex field Ψ_0 . Expression (3.22) is therefore of fundamental importance. It has been criticised by LUTOMIRSKI and YURA [1971] who demonstrated the influence of a finite outer scale. The influence of both finite inner and outer scales has recently been investigated by VALLEY [1979]. Departures from Kolmogorov's spectrum at small scales have also been reported and their influence on optical propagation have been examined by HILL and CLIFFORD [1978]. Experimental evidence for departures from the 5/3 power law in (3.22) has been reported by BOURICIUS and CLIFFORD [1970], by CLIFFORD, BOURICIUS, OCHS and ACKLEY [1971] and by BUSER [1971] in the case of horizontal propagation near the ground. However, no departure has been observed in the experiments, described in § 4 and § 7, made under the conditions of astronomical observations. Expression (3.22) can therefore be considered as a good approximation for describing astronomical seeing.

3.3. FOURTH ORDER MOMENTS

In order to describe the statistical behaviour of short exposure images, an expression will be needed for the fourth order moment

$$M_0(\xi, \xi') = \langle \Psi_0(x) \Psi_0^*(x + \xi) \Psi_0^*(x + \xi') \Psi_0(x + \xi + \xi') \rangle. \quad (3.23)$$

Such an expression cannot be derived without any additional assumption about the statistics of complex field Ψ_0 . When turbulence is located near the ground, expression (3.2) holds with a Gaussian phase φ . Ψ_0 is said to be log-normal. As shown in § 7.3, (3.2) still holds to a good approximation in the case of astronomical observations, although scintillation occurs.

Putting (3.2) into (3.23) leads to

$$M_0(\xi, \xi') = \langle \exp i[\varphi(x) - \varphi(x + \xi) - \varphi(x + \xi') + \varphi(x + \xi + \xi')]\rangle. \quad (3.24)$$

Since the quantity between square brackets has Gaussian statistics, the same arguments used to derive (3.6) lead to

$$M_0(\xi, \xi') = \exp -\frac{1}{2}([\varphi(x) - \varphi(x + \xi) - \varphi(x + \xi') + \varphi(x + \xi + \xi')]^2). \quad (3.25)$$

Introducing the phase structure function D_φ , we find after some manipulations

$$M_0(\xi, \xi') = \exp -[D_\varphi(\xi) + D_\varphi(\xi') - \frac{1}{2}D_\varphi(\xi + \xi') - \frac{1}{2}D_\varphi(\xi - \xi')]. \quad (3.26)$$

Since we assume turbulence to be located near the ground, (3.12) holds and leads to

$$M_0(\xi, \xi') = \exp -2.91k^2 \int dh \cdot C_N^2(h)[|\xi|^{\frac{5}{3}} + |\xi'|^{\frac{5}{3}} - \frac{1}{2}|\xi + \xi'|^{\frac{5}{3}} - \frac{1}{2}|\xi - \xi'|^{\frac{5}{3}}]. \quad (3.27)$$

Statistics of stellar speckle patterns described in § 5 are found to agree with this expression.

§ 4. Long-Exposure Images

The appearance of a turbulence degraded image, as seen through a telescope, has been briefly discussed in the introduction. The structure of the image undergoes random changes related to the motion of atmospheric inhomogeneities in front of the telescope. Exposure times as short as a few milliseconds are necessary in order to freeze the image. The eye is therefore unable to follow the most rapid changes. In a conventional astronomical photograph, the exposure time easily exceeds a few seconds,

in which case the recorded image is no longer random. It is an average and we shall refer to it as a "long exposure image". Properties of long exposure images were first derived by HUFNAGEL and STANLEY [1964] and FRIED [1965, 1966]. Applications to astronomy have been discussed by YOUNG [1974].

4.1. RELATION BETWEEN THE OBJECT AND THE IMAGE

Let us denote $O(\alpha)$ the irradiance distribution from the object as a function of the direction α on the sky. $I(\alpha)$ will be the observed irradiance distribution, in the instantaneous image, as a function of the same variable α . A long exposure image will be considered as the ensemble average $\langle I(\alpha) \rangle$. Since astronomical objects are entirely incoherent, the relation between $\langle I(\alpha) \rangle$ and $O(\alpha)$ is linear. We shall moreover assume that it is shift invariant, i.e. the telescope is isoplanatic and the average effect of turbulence is the same all over the telescope field of view. In such a case, $\langle I(\alpha) \rangle$ is related to $O(\alpha)$ by a convolution relation

$$\langle I(\alpha) \rangle = O(\alpha) * \langle S(\alpha) \rangle \quad (4.1)$$

the point spread function $\langle S(\alpha) \rangle$ being the average image of a point source.

We shall define the two-dimensional complex Fourier transform $\tilde{I}(\gamma)$ of $I(\alpha)$ as

$$\tilde{I}(\gamma) = \int d\alpha \cdot I(\alpha) \cdot \exp(-2i\pi\alpha \cdot \gamma) \quad (4.2)$$

with similar relations for the Fourier transform \tilde{O} and \tilde{S} of O and S . In these expressions the spatial frequency vector γ has the dimension of the inverse of the angle α and must therefore be expressed in radian⁻¹. With such a definition, (4.1) becomes, in the Fourier space

$$\langle \tilde{I}(\gamma) \rangle = \tilde{O}(\gamma) \cdot \langle \tilde{S}(\gamma) \rangle \quad (4.3)$$

where $\langle \tilde{S}(\gamma) \rangle$ is the optical transfer function of the whole system, telescope and atmosphere.

4.2. EXPRESSION FOR THE OPTICAL TRANSFER FUNCTION

In order to relate this transfer function to atmospheric properties, we shall assume that we are observing, through the atmosphere, a mono-

chromatic point source, of wavelength λ . Again, we shall denote $\Psi_0(x)$ as the complex amplitude at the telescope aperture. The complex amplitude $\mathcal{A}(\alpha)$ diffracted at an angle α in the telescope focal plane is proportional to

$$\mathcal{A}(\alpha) \propto \int dx \cdot \Psi_0(x) P_0(x) \exp(-2i\pi\alpha \cdot x/\lambda) \quad (4.4)$$

where $P_0(x)$ is the transmission function of the telescope aperture. For an ideal diffraction-limited telescope,

$$P_0(x) = \begin{cases} 1 & \text{inside the aperture} \\ 0 & \text{outside the aperture.} \end{cases} \quad (4.5)$$

In the case of aberrated optics, wavefront errors are introduced as an argument of the complex transmission $P_0(x)$.

In the following, we shall make extensive use of the non-dimensional reduced variable

$$u = x/\lambda. \quad (4.6)$$

Let us call

$$\Psi(u) = \Psi_0(\lambda u) \quad \text{and} \quad P(u) = P_0(\lambda u). \quad (4.7)$$

With such notation (4.4) becomes

$$\mathcal{A}(\alpha) \propto \mathcal{F}[\Psi(u) \cdot P(u)] \quad (4.8)$$

where \mathcal{F} is the complex Fourier transform defined by (4.2). The point spread function is the irradiance diffracted in the direction α

$$S(\alpha) = |\mathcal{A}(\alpha)|^2 \propto |\mathcal{F}[\Psi(u)P(u)]|^2. \quad (4.9)$$

Its Fourier transform is given by the autocorrelation function of $\Psi(u)P(u)$

$$\tilde{S}(\gamma) \propto \int du \cdot \Psi(u)\Psi^*(u+\gamma)P(u)P^*(u+\gamma). \quad (4.10)$$

In the absence of any turbulence, we assume that $\Psi(u) = 1$ (§ 3) so that, normalising $\tilde{S}(\gamma)$ to unity at the origin,

$$\tilde{S}(\gamma) = \mathcal{S}^{-1} \int du \cdot P(u)P^*(u+\gamma) = T(\gamma) \quad (4.11)$$

where \mathcal{S} is the pupil area (in wavelength squared units). Eq. (4.11) is the classical expression for the optical transfer function $T(\gamma)$ of a telescope.

In the presence of turbulence (4.11) becomes

$$\tilde{S}(\gamma) = \mathcal{S}^{-1} \int du \cdot \Psi(u) \Psi^*(u + \gamma) P(u) P^*(u + \gamma) \quad (4.12)$$

and the optical transfer function for long exposures is

$$\langle \tilde{S}(\gamma) \rangle = \mathcal{S}^{-1} \int du \langle \Psi(u) \cdot \Psi^*(u + \gamma) \rangle P(u) P^*(u + \gamma). \quad (4.13)$$

In (4.13) appears the second order moment

$$B(\gamma) = \langle \Psi(u) \cdot \Psi^*(u + \gamma) \rangle = B_0(\lambda \gamma) \quad (4.14)$$

the properties of which have been studied in § 3. Since $B(\gamma)$ depends only upon γ , (4.13) can be written, taking (4.11) into account,

$$\langle \tilde{S}(\gamma) \rangle = B(\gamma) \cdot T(\gamma) \quad (4.15)$$

showing the fundamental result that, for long exposures, the optical transfer function of the whole system, telescope and atmosphere, is the product of the transfer function of the telescope with an atmospheric transfer function equal to the coherence function $B(\gamma)$.

4.3. RESOLVING POWER

Following FRIED [1966] we shall use Strehl's criterion (see for instance O'NEILL [1963]), defining the resolving power \mathcal{R} as the integral of the optical transfer function, which is analogous to the bandwidth in electronics. According to (4.15) the resolution of a telescope through turbulence is

$$\mathcal{R} = \int d\gamma \cdot B(\gamma) T(\gamma). \quad (4.16)$$

It is limited either by the telescope or the atmosphere according to the relative width of the two functions $B(\gamma)$ and $T(\gamma)$. For a small, diffraction-limited telescope of diameter D , turbulence effects are negligible and, assuming a free circular aperture,

$$\mathcal{R} \approx \mathcal{R}_d = \int d\gamma \cdot T(\gamma) = \frac{1}{4}\pi(D/\lambda)^2. \quad (4.17)$$

For a large good telescope, the resolving power depends only upon

turbulence and

$$\mathcal{R} \approx \mathcal{R}_\infty = \int d\gamma \cdot B(\gamma). \quad (4.18)$$

According to eq. (3.22), $B(\gamma)$ can be written

$$B(\gamma) = B_0(\lambda\gamma) = \exp - K\gamma^5 \quad (4.19)$$

where K describes the seeing conditions and $\gamma = |\gamma|$. With such a notation (4.18) becomes, after integration,

$$\mathcal{R}_\infty = (6\pi/5)K^{-\frac{1}{3}}\Gamma(6/5) \quad (4.20)$$

where Γ is the usual gamma function.

A very convenient measure of seeing introduced by FRIED [1966] is the critical diameter r_0 of the telescope for which

$$\int d\gamma \cdot B(\gamma) = \int d\gamma \cdot T(\gamma). \quad (4.21)$$

Putting $D = r_0$ in (4.17) and equating it with (4.20) leads to

$$K = [(24/5)\Gamma(6/5)]^{\frac{1}{5}}(r_0/\lambda)^{-\frac{5}{3}} = 3.44(r_0/\lambda)^{-\frac{5}{3}}$$

so that expression (4.19) can be written

$$B(\gamma) = \exp - 3.44(\lambda\gamma/r_0)^{\frac{5}{3}} \quad (4.22)$$

or

$$B_0(\xi) = \exp - 3.44(\xi/r_0)^{\frac{5}{3}}. \quad (4.23)$$

Expressions (4.22) and (4.23) will be used in all that follows. The resolving power is limited by the telescope when its diameter D is smaller than r_0 . It is limited by the atmosphere when D is greater than r_0 . Large r_0 values mean good seeing, small values mean bad seeing.

The relation between Fried's parameter r_0 and the profile C_N^2 with height is obtained by equating (4.23) and (3.22). We get

$$r_0 = \left[0.423k^2(\cos \gamma)^{-1} \int dh \cdot C_N^2(h) \right]^{-\frac{3}{5}} \quad (4.24)$$

which shows that r_0 also depends upon the zenith angle γ and the wavelength $\lambda = 2\pi/k$. The wavelength dependence is given by

$$r_0 \propto (\lambda^{-2})^{-\frac{3}{5}} = \lambda^{\frac{3}{5}} \quad (4.25)$$

as confirmed experimentally by BOYD [1978] and by SELBY, WADE and

SANCHEZ MAGRO [1979]. In the following, whenever γ or λ are not specified, we assume $\gamma = 0$ (observations at the zenith) and $\lambda = 0.5 \mu\text{m}$. Table 1 gives r_0 values at three different wavelengths as a function of $\int dh \cdot C_N^2(h)$.

Measurements of r_0 are described in detail in the last section. Typical values for astronomical observations in the visible lie between 2 cm and 20 cm, which shows that the telescope resolving power is always limited by the atmosphere. However, under favourable circumstances, it can be diffraction limited in the infrared. When limited by the atmosphere, the seeing angle ω_∞ , also given in Table 1, is of the order of λ/r_0 (§ 7.6). According to (4.25), it varies as $\lambda^{-\frac{1}{2}}$, which shows that seeing slowly improves at increasing wavelengths as already noticed by astronomers observing in the infrared.

4.4. APPLICATION TO MICHELSON'S STELLAR INTERFEROMETRY

Expression (4.15) applies whatever the shape of the telescope entrance pupil. It therefore applies to Michelson's stellar interferometry, if we assume that the entrance pupil is made of two small apertures at some distance λ/γ_0 apart. In such a case, the pupil transmission function can be written

$$P(\mathbf{u}) = p(\mathbf{u}) + p(\mathbf{u} - \gamma_0) \quad (4.26)$$

where $p(\mathbf{u})$ is the transmission function of each aperture. Assuming no turbulence occurs, the optical transfer function is obtained by putting (4.26) into (4.11) leading to

$$T(\gamma) = t(\gamma) + \frac{1}{2}t(\gamma + \gamma_0) + \frac{1}{2}t(\gamma - \gamma_0) \quad (4.27)$$

where

$$t(\gamma) = s^{-1} \int d\mathbf{u} \cdot p(\mathbf{u})p(\mathbf{u} + \gamma) \quad (4.28)$$

is the optical transfer function of each aperture of area s . In the limit of very small apertures (4.27) can be written as a sum of Dirac's δ distributions, or after renormalisation,

$$T(\gamma) = \delta(\gamma) + \frac{1}{2}\delta(\gamma + \gamma_0) + \frac{1}{2}\delta(\gamma - \gamma_0) \quad (4.29)$$

and the image Fourier transform is

$$\tilde{I}_0(\gamma) = \tilde{O}(\gamma) \cdot T(\gamma) = \tilde{O}(0) \delta(\gamma) + \frac{1}{2}\tilde{O}(-\gamma_0) \delta(\gamma + \gamma_0) + \frac{1}{2}\tilde{O}(\gamma_0) \delta(\gamma - \gamma_0). \quad (4.30)$$

TABLE 1
Fried's parameter r_0 , coherence area $\lambda^2\sigma$ and seeing angle ω_x at three different wavelengths, for typical values of $\int dh \cdot C_N^2(h)$, according to eqs. (4.24), (5.13) and (7.70').

$\int dh \cdot C_N^2(h)$ (m ³)	$\lambda = 0.5 \mu\text{m}$			$\lambda = 2.2 \mu\text{m}$			$\lambda = 10 \mu\text{m}$		
	r_0 (cm)	$\lambda^2\sigma$ (cm ²)	ω_x (arc second)	r_0 (cm)	$\lambda^2\sigma$ (cm ²)	ω_x (arc second)	r_0 (cm)	$\lambda^2\sigma$ (cm ²)	ω_x (arc second)
2×10^{-13}	21.1	152	0.62	125	5.34×10^3	0.46	769	202×10^3	0.34
3×10^{-13}	16.5	93.7	0.79	97.9	3.28×10^3	0.59	603	124×10^3	0.43
4×10^{-13}	13.9	66.3	0.94	82.4	2.32×10^3	0.70	507	87.9×10^3	0.52
6×10^{-13}	10.9	40.8	1.20	64.6	1.43×10^3	0.89	398	54.1×10^3	0.66
8×10^{-13}	9.19	28.9	1.43	54.5	1.01×10^3	1.06	335	38.3×10^3	0.78
10×10^{-13}	8.04	22.1	1.63	47.6	774	1.21	293	29.3×10^3	0.89
15×10^{-13}	6.30	13.6	2.08	37.3	476	1.55	229	18.0×10^3	1.14
20×10^{-13}	5.30	9.62	2.47	31.4	337	1.84	193	12.8×10^3	1.36
30×10^{-13}	4.16	5.91	3.15	24.6	207	2.34	151	7.84×10^3	1.73
40×10^{-13}	3.50	4.19	3.74	20.7	147	2.78	127	5.55×10^3	2.06
60×10^{-13}	2.74	2.57	4.77	16.2	90.1	3.55	100	3.41×10^3	2.62
100×10^{-13}	2.02	1.39	6.49	11.9	48.8	4.82	73.5	1.85×10^3	3.56

Since $\tilde{O}(\gamma)$ is hermitian, the irradiance distribution in the image plane is

$$I_0(\alpha) = \tilde{O}(0) + \operatorname{Re} [\tilde{O}(\gamma_0) \exp(2i\pi\alpha \cdot \gamma_0)] \quad (4.31)$$

or, introducing the argument θ_0 of the complex quantity $\tilde{O}(\gamma_0)$

$$I_0(\alpha) = \tilde{O}(0) + |\tilde{O}(\gamma_0)| \cos(2\pi\alpha \cdot \gamma_0 + \theta_0). \quad (4.32)$$

Expression (4.32) describes the interference fringe pattern observed in the telescope focal plane. The fringe visibility

$$V = |\tilde{O}(\gamma_0)|/\tilde{O}(0) \quad (4.33)$$

is related to the modulus $|\tilde{O}(\gamma_0)|$, whereas the fringe position is related to the argument θ_0 of $\tilde{O}(\gamma_0)$.

When turbulence occurs, according to (4.15), the Fourier transform of the long exposure image is obtained by multiplying $T(\gamma)$ and $B(\gamma)$ so that (4.30) becomes

$$\begin{aligned} \langle \tilde{I}(\gamma) \rangle &= \tilde{O}(\gamma) \cdot T(\gamma) \cdot B(\gamma) \\ &= \tilde{O}(0) \delta(\gamma) + \frac{1}{2} \tilde{O}(-\gamma_0) B(-\gamma_0) \delta(\gamma + \gamma_0) + \frac{1}{2} \tilde{O}(\gamma_0) B(\gamma_0) \delta(\gamma - \gamma_0) \end{aligned} \quad (4.34)$$

and the long exposure fringe pattern is described by

$$\begin{aligned} \langle I(\alpha) \rangle &= \tilde{O}(0) + \operatorname{Re} [\tilde{O}(\gamma_0) B(\gamma_0) \exp(-2i\pi\alpha \cdot \gamma_0)] \\ &= \tilde{O}(0) + |\tilde{O}(\gamma_0)| B(\gamma_0) \cos(2\pi\alpha \cdot \gamma_0 + \theta_0). \end{aligned} \quad (4.35)$$

The related fringe visibility is

$$V = B(\gamma_0) \cdot |\tilde{O}(\gamma_0)|/\tilde{O}(0). \quad (4.36)$$

When observing a stellar point source, $\tilde{O}(\gamma) = 1$ and the fringe visibility becomes

$$V = B(\gamma_0). \quad (4.37)$$

This is the essence of the interferometric measurements of the atmospheric transfer function $B(\gamma)$, described in § 4.5. Expression (4.34) shows that, when long exposures are taken through a Michelson stellar interferometer, the attenuation of spectral components of the object is exactly the same as in normal imaging. As we shall see, this attenuation is mainly due to the motion of the fringes during the exposure. In the actual Michelson experiment (MICHELSON [1920]) fringes were observed visually. The success of the experiment comes from the ability of the eye to follow fringe motions.

Let us call Ψ_1 and Ψ_2 the instantaneous complex field at each aperture. The instantaneous transfer function is obtained by multiplying $p(\mathbf{u})$ with Ψ_1 and $p(\mathbf{u} - \mathbf{y}_0)$ with Ψ_2 so that (4.29) becomes

$$\tilde{S}(\mathbf{y}) = \frac{1}{2}(|\Psi_1|^2 + |\Psi_2|^2) \delta(\mathbf{y}) + \frac{1}{2}\Psi_1\Psi_2^* \delta(\mathbf{y} + \mathbf{y}_0) + \frac{1}{2}\Psi_1^*\Psi_2 \delta(\mathbf{y} - \mathbf{y}_0) \quad (4.38)$$

and (4.30) becomes

$$\begin{aligned} \tilde{I}(\mathbf{y}) &= \tilde{O}(\mathbf{y}) \cdot \tilde{S}(\mathbf{y}) = \frac{1}{2}(|\Psi_1|^2 + |\Psi_2|^2)\tilde{O}(\mathbf{0})\delta(\mathbf{y}) \\ &\quad + \frac{1}{2}\tilde{O}(-\mathbf{y}_0)\Psi_1\Psi_2^* \delta(\mathbf{y} + \mathbf{y}_0) + \frac{1}{2}\tilde{O}(\mathbf{y}_0)\Psi_1^*\Psi_2 \delta(\mathbf{y} - \mathbf{y}_0). \end{aligned} \quad (4.39)$$

The instantaneous irradiance distribution in the image plane is therefore

$$I(\boldsymbol{\alpha}) = \frac{1}{2}(|\Psi_1|^2 + |\Psi_2|^2)\tilde{O}(\mathbf{0}) + \operatorname{Re}[\tilde{O}(\mathbf{y}_0)\Psi_1^*\Psi_2 \exp(-2i\pi\boldsymbol{\alpha} \cdot \mathbf{y}_0)]. \quad (4.40)$$

Since turbulence introduces mainly phase disturbances

$$\Psi_1 \approx \exp i\varphi_1 \quad \text{and} \quad \Psi_2 \approx \exp i\varphi_2$$

so that

$$I(\boldsymbol{\alpha}) \approx \tilde{O}(\mathbf{0}) + \operatorname{Re}[\tilde{O}(\mathbf{y}_0) \exp -i(2\pi\boldsymbol{\alpha} \cdot \mathbf{y}_0 + \varphi_1 - \varphi_2)] \quad (4.41)$$

showing that fringes are mainly shifted by a random amount $(\varphi_1 - \varphi_2)/2\pi|\mathbf{y}_0|$. When the r.m.s. shift is greater or equal to about one fringe spacing, fringes will disappear in a long exposure. However they are still visible to the eye as long as their motion can be followed (see § 7.4).

An expression for the long exposure fringe pattern is obtained by taking the average of (4.40). Since the average irradiance is not affected by turbulence,

$$\langle |\Psi_1|^2 \rangle = \langle |\Psi_2|^2 \rangle = 1 \quad (4.42)$$

and (4.40) leads to

$$\langle I(\boldsymbol{\alpha}) \rangle = \tilde{O}(\mathbf{0}) + \operatorname{Re}[\tilde{O}(\mathbf{y}_0)\langle \Psi_1^*\Psi_2 \rangle \exp(-2i\pi\boldsymbol{\alpha} \cdot \mathbf{y}_0)] \quad (4.43)$$

which is equivalent to (4.35) since $\langle \Psi_1^*\Psi_2 \rangle = B(\mathbf{y}_0)$. Instead of making a long exposure, we can envisage recording a sequence of short exposures or rapid photoelectric scans in order to freeze the instantaneous fringe pattern. In each recorded pattern, the variance of the modulation is, according to (4.40),

$$\sigma_F^2 = \frac{1}{2}|\tilde{O}(\mathbf{y}_0)|^2 \cdot |\langle \Psi_1^*\Psi_2 \rangle|^2. \quad (4.44)$$

Averaging over a large number of independent scans, the variance

becomes

$$\langle \sigma_F^2 \rangle = \frac{1}{2} |\tilde{O}(\gamma_0)|^2 \langle |\Psi_1^* \Psi_2|^2 \rangle. \quad (4.45)$$

The quantity

$$\langle |\Psi_1^* \Psi_2|^2 \rangle = \langle |\Psi_1|^2 \cdot |\Psi_2|^2 \rangle \quad (4.46)$$

is the second order moment of the intensity fluctuations on each aperture. As shown in § 8 (Fig. 14) these fluctuations become uncorrelated when the baseline exceeds about 10 cm, in which case

$$\langle |\Psi_1^* \Psi_2|^2 \rangle \approx \langle |\Psi_1|^2 \rangle \langle |\Psi_2|^2 \rangle = 1$$

and (4.45) becomes

$$\langle \sigma_F^2 \rangle = \frac{1}{2} |\tilde{O}(\gamma_0)|^2 \quad (4.47)$$

which is exactly the variance that we would obtain by scanning an undisturbed fringe pattern as described by (4.32). This is the principle of photoelectric interferometry as developed by CURRIE, KNAPP and LIEWER [1974]. The object energy spectrum $|\tilde{O}(\gamma)|^2$ is entirely recovered through turbulence but the phase of $\tilde{O}(\gamma)$ is lost. It will be shown in § 5 that the object energy spectrum can similarly be recovered by a second-order statistical analysis of a sequence of short-exposure images taken with the full telescope aperture (the so-called speckle interferometry technique).

4.5. EXPERIMENTAL MEASUREMENTS OF THE LONG-EXPOSURE TRANSFER FUNCTION

Astronomers have long tried to measure the photometric profile of star images on long-exposure photographs. Because of the non-linearity and small dynamic range of photographic emulsions, images of several stars of different magnitudes must be analysed on a single carefully calibrated plate (see for instance KING [1971]). The observed profile is always nearly Gaussian so astronomers are used to fitting their stellar profiles with Gaussian curves. According to the theory presented here, stellar profiles are given by the two-dimensional Fourier transform of the atmospheric transfer function $B(\gamma)$ described by (4.22). Since $5/3$ is not far from $6/3=2$, $B(\gamma)$ and therefore its Fourier transform, are nearly, but not exactly, Gaussian functions. Numerical computations of the predicted stellar profile are presented in Table 2. The core is indeed nearly Gaussian but the fall off in the wings is not as steep as that of a Gaussian

TABLE 2
Theoretical profile of a long exposure stellar image, through a large telescope, obtained by taking the Hankel transform of Fried's transfer function (eq. (4.22)), after KADIRI [1979]. For $r_0 = 10$ cm, $\Delta\alpha = 0.16$ arcsecond.

$\alpha/\Delta\alpha$	0	1	2	3	4	5	6	7	8
$I(\alpha)/I(0)$	1.00000	0.92893	0.74724	0.52615	0.33039	0.19005	0.10364	0.05567	0.03052
$\alpha/\Delta\alpha$	9	10	11	12	13	14	15	16	17
$I(\alpha)/I(0)$	0.01751	0.01062	0.00681	0.00459	0.00322	0.00234	0.00175	0.00134	0.00104
$\alpha/\Delta\alpha$	18	19	20	21	22	23	24	25	26
$I(\alpha)/I(0)$	0.00083	0.00067	0.00055	0.00045	0.00038	0.00032	0.00027	0.00023	0.00020
$\alpha/\Delta\alpha$	27	28	29	30	31	32	33	34	35
$I(\alpha)/I(0)$	0.00018	0.00016	0.00014	0.00012	0.00011	0.00010	0.00009	0.00008	0.00007

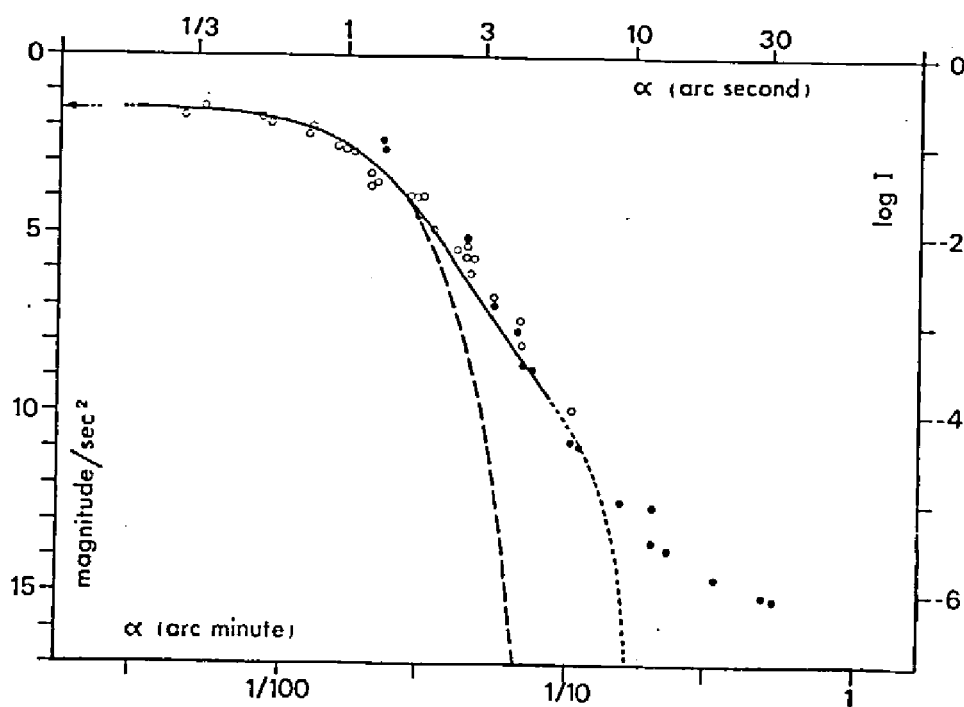


Fig. 2. Open and full circles: profile of a stellar image after KING [1971]. Solid line: theoretical profile from Table 2 assuming $r_0 = 5.5$ cm. Dashed line: Gaussian profile. Dotted line: expected inner scale cut-off.

curve. Fig. 2 shows a stellar profile published by KING [1971] together with a fit of the central core with a Gaussian curve and a fit with the theoretical profile of Table 2. Experimental points clearly agree well with the extended wing predicted by Table 2, at least up to 6 arcseconds. At larger angular distances an inverse-square slope aureole is observed. Since a turbulence inner scale of the order of a few millimeters implies a steep fall-off of the profile in this region, the aureole has necessarily a different origin. It is probably due to scattering by small particles or scratches in the telescope, since Fraunhöfer diffraction by a sharp edge leads to an inverse square law.

The atmospheric transfer function $B(\gamma)$ is best measured interferometrically. The principle of such measurements has been given in § 4.4. Compared to stellar profile measurements, it eliminates both the emulsion dynamic range problem and the effects of telescope aberrations or focusing errors. Interferometric measurements of $B(\gamma)$ had initially been made by optical physicists in the case of horizontal laser beam propagation (WESSELY and BOLSTAD [1970], BERTOLOTTI, MUZII and SETTE [1970], BOZEC, CAGNET and ROGER [1971]). They provided the first experimental check of expression (4.22). Similar measurements were later performed on stellar sources by C. RODDIER and F. RODDIER [1973], KELSALL [1973], DAINTY and SCADDAN [1974, 1975], C. RODDIER [1976]

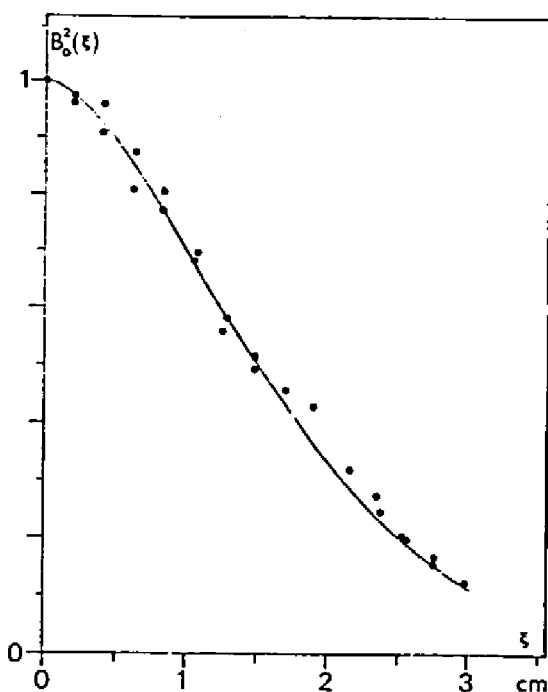


Fig. 3. Square of the coherence function $B_0(\xi)$. Full circles: experimental measurements made with a rotation interferometer (C. RODDIER [1976]). Solid line: theoretical curve assuming $r_0 = 6$ cm (eq. (4.23)).

and BROWN and SCADDAN [1979]. Fig. 3 shows experimental data obtained with a rotation interferometer by C. RODDIER [1976], together with a best fit with expression (4.23). A check of the 5/3 law is obtained by plotting experimental values of $\log [-\log B(\gamma)]$ as a function of $\log \gamma$ as shown on Fig. 4. Experimental results are found entirely consistent with the expected 5/3 slope. More accurate checks of the 5/3 law will be discussed in § 7.

§ 5. Short-Exposure Images

Because of turbulence, the instantaneous illumination in the focal plane of a telescope must be considered as a random function. In the last section we studied its first moment or average value. Here, we shall be interested in its second order statistics or energy spectrum.

5.1. THE IMAGE ENERGY SPECTRUM

We will again assume that the image $I(\alpha)$ is related to the object $O(\alpha)$ by a convolution relation

$$I(\alpha) = O(\alpha) * S(\alpha). \quad (5.1)$$

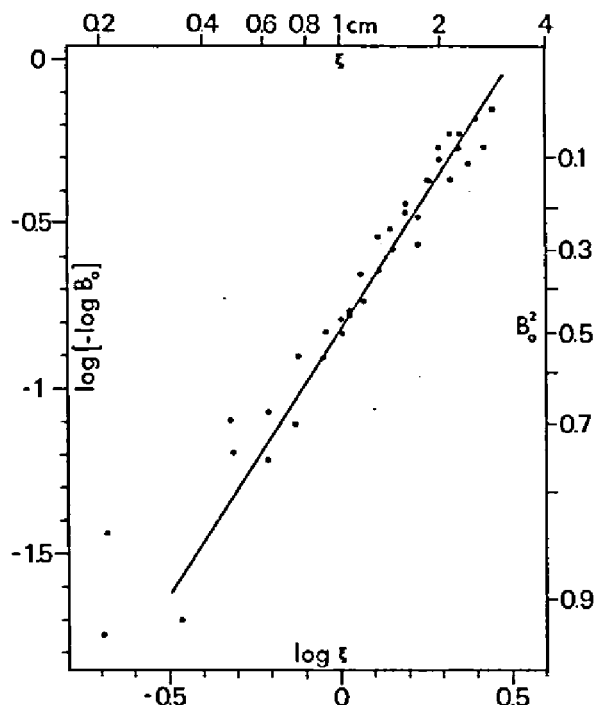


Fig. 4. Full circles: experimental data from C. RODDIER [1976]. Solid line: least square fit with a $5/3$ slope allowing an accurate estimation of r_0 . Here $r_0 = 3.9$ cm.

The relation is indeed linear but shift invariance is now a crude assumption. Here $I(\alpha)$ and $S(\alpha)$ are both random functions and (5.1) means that, at any given instant, the distorted point spread function is the same for all points of the image, which implies that the instant wavefront perturbations are identical for all wavefront directions. As easily seen in Fig. 5 this can only be true if turbulence is entirely located near the telescope aperture. Since it is not the case, our assumption is an approximation valid only in a limited field of view called the isoplanatic patch.

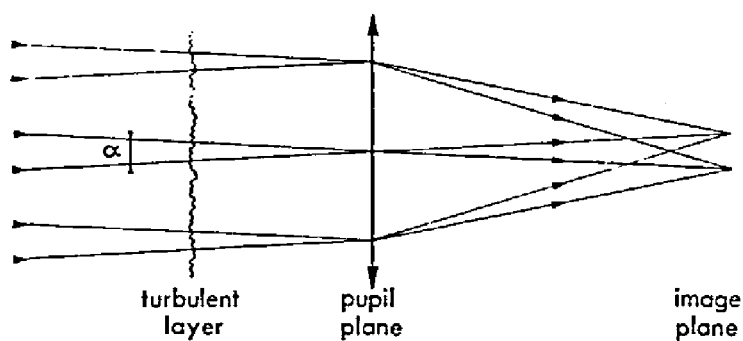


Fig. 5. If the observed object has sufficiently small angular dimensions α , or if the turbulence is localised near the telescope pupil, beams originating from any point on the object and arriving on the pupil can be considered to have encountered almost identical regions of the perturbing atmosphere. The related image aberrations are isoplanatic.

Observations and theoretical estimations show that, in the case of astronomical images, the size of the isoplanatic patch is of the order of a few arcseconds. The isoplanicity approximation will be discussed in details in the next section.

From (5.1), the image energy spectrum is given by

$$\langle |\tilde{I}(\gamma)|^2 \rangle = |\tilde{O}(\gamma)|^2 \langle |\tilde{S}(\gamma)|^2 \rangle \quad (5.2)$$

where $|\tilde{O}(\gamma)|^2$ is the object energy spectrum and $\langle |\tilde{S}(\gamma)|^2 \rangle$ is the energy spectrum of a point source image. $\langle |\tilde{S}(\gamma)|^2 \rangle$ describes the transmission of the spectral components in the image energy spectrum. Its square root is sometimes called the speckle modulation transfer function. It will be shown that, in contrast with the long exposure transfer function, it has a high frequency component, extending up to the telescope cut-off frequency, corresponding to a speckle structure observed in monochromatic short exposures. This high frequency component allows retrieval of high resolution information by the so-called speckle interferometry technique (see § 9.4).

Assuming monochromaticity, the random instantaneous transfer function $\tilde{S}(\gamma)$ is given by expression (4.10) derived in § 4.2. Its average squared modulus is therefore

$$\begin{aligned} \langle |\tilde{S}(\gamma)|^2 \rangle &= S^{-2} \int du du' \langle \Psi(u) \Psi^*(u + \gamma) \Psi^*(u') \Psi(u' + \gamma) \rangle \\ &\times P(u) P^*(u + \gamma) P^*(u') P(u' + \gamma) \end{aligned} \quad (5.3)$$

which depends upon the fourth order moment

$$M(\gamma, \gamma') = \langle \Psi(u) \Psi^*(u + \gamma) \Psi^*(u + \gamma') \Psi(u + \gamma + \gamma') \rangle \quad (5.4)$$

where $\gamma' = u' - u$. Putting (5.4) into (5.3) leads to

$$\langle |\tilde{S}(\gamma)|^2 \rangle = S^{-2} \int d\gamma' \cdot M(\gamma, \gamma') A(\gamma, \gamma') \quad (5.5)$$

where

$$A(\gamma, \gamma') = \int du \cdot P(u) P^*(u + \gamma) P^*(u + \gamma') P(u + \gamma + \gamma') \quad (5.6)$$

describes the telescope contribution. In contrast with the long exposure transfer function, $\langle |\tilde{S}(\gamma)|^2 \rangle$ is no longer the product of a telescope function with an atmospheric function, because of the integral in (5.5).

Let us first derive the general asymptotic behaviour of $\langle |\tilde{S}(\gamma)|^2 \rangle$ for a large telescope ($D \gg r_0$), at high spatial frequencies ($\gamma \gg r_0/\lambda$). In this case,

$\Psi(\mathbf{u})\Psi^*(\mathbf{u}+\boldsymbol{\gamma}')$ is uncorrelated with $\Psi^*(\mathbf{u}+\boldsymbol{\gamma})\Psi(\mathbf{u}+\boldsymbol{\gamma}+\boldsymbol{\gamma}')$ except when $\boldsymbol{\gamma}' = -\boldsymbol{\gamma}$, so that

$$M(\boldsymbol{\gamma}, \boldsymbol{\gamma}') \simeq \langle \Psi(\mathbf{u})\Psi^*(\mathbf{u}+\boldsymbol{\gamma}') \rangle \langle \Psi^*(\mathbf{u}+\boldsymbol{\gamma})\Psi(\mathbf{u}+\boldsymbol{\gamma}+\boldsymbol{\gamma}') \rangle \quad (5.7)$$

everywhere in the $\boldsymbol{\gamma}'$ plane, except near $\boldsymbol{\gamma}' = -\boldsymbol{\gamma}$, the contribution of which is negligible in the integral (5.5). Therefore, when $\boldsymbol{\gamma} \gg r_0/\lambda$,

$$\langle |\tilde{S}(\boldsymbol{\gamma})|^2 \rangle \simeq \mathcal{S}^{-2} \int d\boldsymbol{\gamma}' \cdot B^2(\boldsymbol{\gamma}') A(\boldsymbol{\gamma}, \boldsymbol{\gamma}') \quad (5.8)$$

or, taking (5.6) into account,

$$\langle |\tilde{S}(\boldsymbol{\gamma})|^2 \rangle \simeq \mathcal{S}^{-2} \int d\mathbf{u} P(\mathbf{u}) P^*(\mathbf{u}+\boldsymbol{\gamma}) \int d\boldsymbol{\gamma}' \cdot B^2(\boldsymbol{\gamma}') P^*(\mathbf{u}+\boldsymbol{\gamma}') P(\mathbf{u}+\boldsymbol{\gamma}+\boldsymbol{\gamma}'). \quad (5.9)$$

Since $B^2(\boldsymbol{\gamma}')$ falls off very rapidly on a distance of the order r_0/λ , whereas the pupil transmission P has slow variations,

$$\begin{aligned} \langle |\tilde{S}(\boldsymbol{\gamma})|^2 \rangle &\simeq \mathcal{S}^{-2} \sigma \int d\mathbf{u} \cdot |P(\mathbf{u})|^2 |P(\mathbf{u}+\boldsymbol{\gamma})|^2 \\ &\simeq (\sigma/\mathcal{S}) T_0(\boldsymbol{\gamma}) \end{aligned} \quad (5.10)$$

where

$$\sigma = \int d\boldsymbol{\gamma}' \cdot B^2(\boldsymbol{\gamma}') \quad (5.11)$$

is a measure of the coherence area of the wavefront perturbations and

$$T_0(\boldsymbol{\gamma}) = \mathcal{S}^{-1} \int d\mathbf{u} \cdot |P(\mathbf{u})|^2 |P(\mathbf{u}+\boldsymbol{\gamma})|^2 \quad (5.12)$$

is the transfer function of an ideal diffraction limited telescope of the same aperture. Eq. (5.10) shows that $\langle |\tilde{S}(\boldsymbol{\gamma})|^2 \rangle$ extends up to the telescope diffraction cut off f_c and that, to a first approximation, telescope aberrations and focusing errors have a negligible influence. Eq. (5.10) also shows that, in the image, the typical speckle size is of the order of $f_c^{-1} = \lambda/\mathbb{D}$. Since the size of the seeing disk is of the order of λ/r_0 , the number of speckles in the image is of the order of $(\mathbb{D}/r_0)^2$. Putting (4.22) into (5.11) leads, after integration, to

$$\sigma = 0.342(r_0/\lambda)^2. \quad (5.13)$$

Values of $\lambda^2\sigma$ are given in Table 1 (p. 303) in cm^2 units. Since $\mathcal{S} \simeq$

$(D/\lambda)^2$, the number of speckles is also of the order of S/σ , so that the attenuation factor in (5.10) is approximately the inverse of the number of speckles in the image.

A complete analytical expression for $\langle |\tilde{S}(\gamma)|^2 \rangle$ can be derived if $\Psi(u)$ is assumed to follow circular Gaussian statistics (DAINTY [1975]). This assumption is widely used in optics when dealing with ground-glass diffusers. In this case

$$M(\gamma, \gamma') = B^2(\gamma) + B^2(\gamma'). \quad (5.14)$$

Putting (5.14) into (5.5) and still assuming $D \gg r_0$, leads to

$$\langle |\tilde{S}(\gamma)|^2 \rangle = B^2(\gamma) |T(\gamma)|^2 + (\sigma/S) T_0(\gamma)$$

or, taking (4.15) into account,

$$\langle |\tilde{S}(\gamma)|^2 \rangle = \langle \tilde{S}(\gamma) \rangle^2 + (\sigma/S) T_0(\gamma) \quad (5.15)$$

which describes the speckle energy spectrum $\langle |\tilde{S}(\gamma)|^2 \rangle$ as the sum of the low frequency long-exposure energy spectrum and the high frequency component previously derived.

In the case of atmospheric fluctuations, $\Psi(u)$ is better described by log-normal statistics and the fourth-order moment is given by (3.26). Comparison between (3.16) and (4.23) shows that, at the near-field approximation,

$$D_\varphi(\xi) = 6.88(\xi/r_0)^{\frac{1}{3}}. \quad (5.16)$$

Putting (5.16) into (3.26) leads to

$$\begin{aligned} M(\gamma, \gamma') &= M_0(\lambda\gamma, \lambda\gamma') \\ &= \exp \left\{ -6.88(\lambda/r_0)^{\frac{1}{3}} \cdot [|\gamma|^{\frac{5}{3}} + |\gamma'|^{\frac{5}{3}} - \frac{1}{2}|\gamma + \gamma'|^{\frac{5}{3}} - \frac{1}{2}|\gamma - \gamma'|^{\frac{5}{3}}] \right\}. \end{aligned} \quad (5.17)$$

In such a case, $\langle |\tilde{S}(\gamma)|^2 \rangle$ has no simple analytical expression. Integration of (5.5) was performed numerically for the first time by KORFF [1973] using (5.17). The general shape of $\langle |\tilde{S}(\gamma)|^2 \rangle$ remains the same. The asymptotic behaviour at high frequencies is still described by (5.10). However, the low frequency part is slightly wider than the long exposure energy spectrum. As shown by KORFF [1973], it fits the energy spectrum of a long exposure made with a fast automatic guider removing image motion, i.e. wavefront tilts, on the telescope aperture. Such a spectrum has been studied by FRIED [1966] who derived the approximate expression, in the

near-field case (see § 7.6)

$$\langle |\tilde{S}(\gamma)|^2 \rangle = |T(\gamma)|^2 \exp \{-6.88(\lambda\gamma/r_0)^{\frac{1}{3}}[1 - (\lambda\gamma/D)^{\frac{1}{3}}]\}. \quad (5.18)$$

Its square root, called the "short exposure" transfer function by Fried, must be distinguished from the speckle transfer function.

Accurate experimental checks of Korff's calculations are difficult since short exposure stellar images are always noisy. However, since the two-dimensional speckle energy spectrum is expected to have a circular symmetry, its values along any axis can be found by taking the average squared Fourier transform of the speckle image integrated along a direction perpendicular to that axis. In the experiment by KARO and SCHNEIDERMAN [1976b], the integration was performed electronically along each line scanned by a T.V. camera. In a more recent experiment by AIME, KADIRI, RICORT, RODDIER and VERNIN [1979] a photomultiplier is used in association with a scanning slit. One of their typical results is presented in Fig. 6 showing a good agreement with Korff's theory. Excellent agreement has also been obtained in the infrared by CHELLI, LENA, C. RODDIER, F. RODDIER and SIBILLE [1979] again using a single detector and a scanning slit.

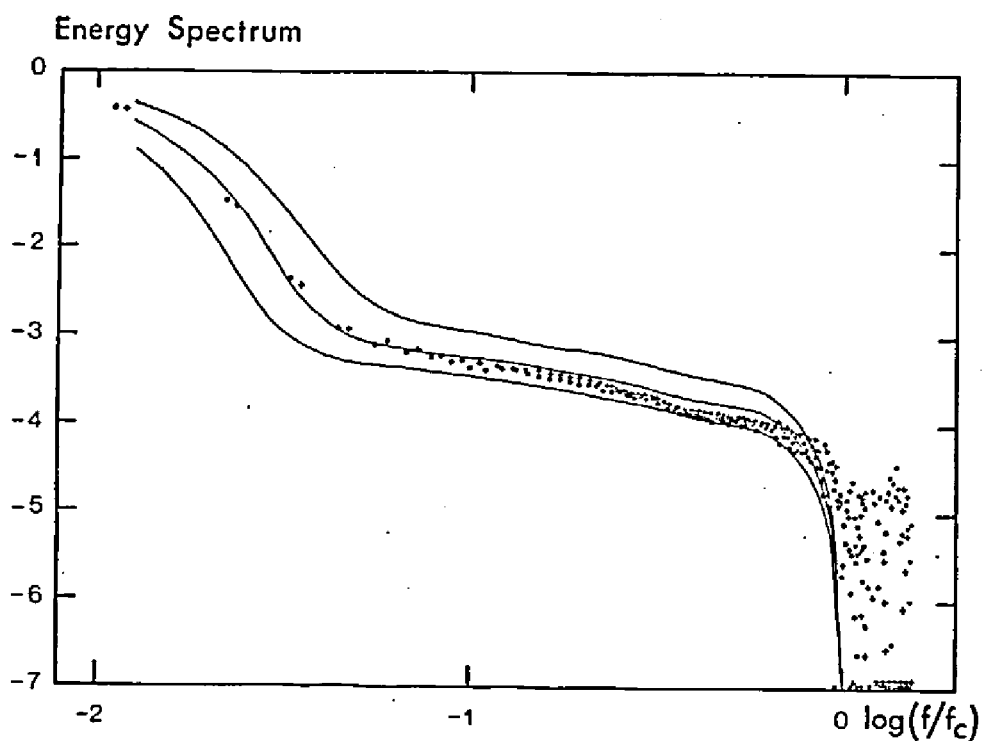


Fig. 6. Spatial energy spectrum of the image of an unresolved star. Dots: experimental data obtained by AIME, KADIRI, RICORT, RODDIER and VERNIN [1979], on star Vega, with the 193 cm telescope of the Haute Provence Observatory (France). Solid lines: theoretical curves, according to Korff's theory, for $r_0 = 4.3$ cm, 5.6 cm and 6.9 cm. The telescope central obscuration has been taken into account in the calculations.

5.2. THE APERTURE-SYNTHESIS APPROACH

In § 4.4, we investigated the influence of atmospheric turbulence on a Michelson stellar interferometer. Let us generalise the results to an array of N_0 small identical apertures. The pupil transmission function will be

$$P(\mathbf{u}) = \sum_{i=1}^{N_0} p(\mathbf{u} - \mathbf{f}_i). \quad (5.19)$$

Assuming no turbulence, the related optical transfer function is

$$T(\mathbf{f}) = \frac{1}{N_0} \sum_{i=1}^{N_0} \sum_{j=1}^{N_0} t(\mathbf{f} + \mathbf{f}_i - \mathbf{f}_j) \quad (5.20)$$

where $t(\mathbf{f})$ is the optical transfer function of each aperture. In the limit of very small apertures, (5.20) can be written after renormalisation

$$T(\mathbf{f}) = \frac{1}{N_0} \sum_{i=1}^{N_0} \sum_{j=1}^{N_0} \delta(\mathbf{f} + \mathbf{f}_i - \mathbf{f}_j). \quad (5.21)$$

Several pairs of apertures may have the same separation

$$\mathbf{f}_i - \mathbf{f}_i = \mathbf{f}_m. \quad (5.22)$$

Let N_m be the number of aperture pairs separated by \mathbf{f}_m . N_m is called the redundancy coefficient of the array at frequency \mathbf{f}_m . Grouping these pairs together in (5.21) and assuming $\mathbf{f}_0 = 0$, leads to

$$T(\mathbf{f}) = \sum_m c_m \delta(\mathbf{f} - \mathbf{f}_m) \quad (5.23)$$

with

$$c_m = N_m / N_0. \quad (5.24)$$

The image Fourier transform is

$$\begin{aligned} \tilde{I}(\mathbf{f}) &= \tilde{O}(\mathbf{f}) T(\mathbf{f}) \\ &= \sum_m \frac{N_m}{N_0} \tilde{O}(\mathbf{f}_m) \delta(\mathbf{f} - \mathbf{f}_m). \end{aligned} \quad (5.25)$$

Let us now consider the entrance pupil of a large diffraction limited telescope as an array of small adjacent apertures. As seen in Fig. 7, within such a pupil, the number N_m of small-aperture pairs separated by \mathbf{f}_m is proportional to the overlap area of two pupil images shifted by \mathbf{f}_m . The ratio N_m/N_0 is therefore given by the integral (5.12) so that

$$N_m/N_0 = T_0(\mathbf{f}_m). \quad (5.26)$$

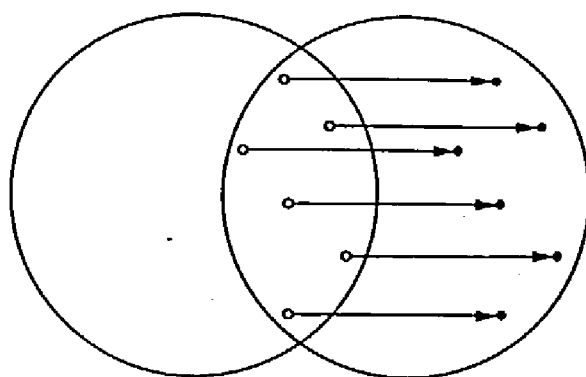


Fig. 7. The number of pairs of points (open and full circles) separated by a vector γ (arrow) within a given pupil is proportional to the overlap area of two such pupils separated by the vector γ . This number, as a function of γ , determines the telescope optical transfer function.

The optical transfer function of a diffraction limited telescope is a measure of the redundancy of its pupil. Putting (5.26) into (5.25) leads to

$$\tilde{I}(\gamma) = \sum_m T_0(\gamma_m) \tilde{O}(\gamma_m) \delta(\gamma - \gamma_m) \quad (5.27)$$

or, in the limit of infinitely small apertures,

$$\tilde{I}(\gamma) = \int d\gamma' \cdot T_0(\gamma') \tilde{O}(\gamma') \delta(\gamma - \gamma') = T_0(\gamma) \tilde{O}(\gamma) \quad (5.28)$$

thus recovering the usual expression for a diffraction limited telescope.

The effect of atmospheric turbulence on a two-aperture stellar interferometer has been described in § 4.4. Following a similar approach, we shall now investigate the effect of turbulence on an array of N_0 small apertures. Let Ψ_i be the instantaneous complex field at aperture i . The instantaneous transfer function is obtained by multiplying $p(u - \gamma_i)$ with Ψ_i in (5.19) so that (5.20) becomes

$$\tilde{S}(\gamma) = \frac{1}{N_0} \sum_{i=1}^{N_0} \sum_{j=1}^{N_0} \Psi_i \Psi_j^* t(\gamma + \gamma_i - \gamma_j). \quad (5.29)$$

Let us group again aperture pairs having the same separation

$$\gamma_i - \gamma_j = \gamma_m \quad (5.22)$$

and let N_m be the number of such pairs. Renumbering the apertures, we shall call $\Psi_{m,q}$ and $\Psi'_{m,q}$ the two values of the complex field associated with the q th pair separated by γ_m . Hence (5.29) becomes, in the limit of

very small apertures,

$$\tilde{S}(\gamma) = \frac{1}{N_0} \sum_m \sum_{q=1}^{N_m} \Psi_{m,q} \Psi'_{m,q}^* \delta(\gamma - \gamma_m). \quad (5.30)$$

The instantaneous transfer function still has the form

$$\tilde{S}(\gamma) = \sum_m c_m \delta(\gamma - \gamma_m) \quad (5.31)$$

with

$$c_m = \frac{1}{N_0} \sum_{q=1}^{N_m} \Psi_{m,q} \Psi'_{m,q}^*. \quad (5.32)$$

The long exposure transfer function $\langle \tilde{S}(\gamma) \rangle$ is obtained by taking the average of (5.31). The related coefficients are

$$\langle c_m \rangle = \frac{1}{N_0} \sum_{q=1}^{N_m} \langle \Psi_{m,q} \Psi'_{m,q}^* \rangle = \frac{N_m}{N_0} B(\gamma_m) \quad (5.33)$$

in agreement with (4.15). In the following, we shall assume that, for $m \neq 0$, the separation $|\gamma_m|$ between the apertures is always larger than Fried's parameter r_0 so that

$$\langle \Psi_{m,q} \Psi'_{m,q}^* \rangle = B(\gamma_m) \approx 0. \quad (5.34)$$

According to (5.31), the energy spectrum of a point source image is a discrete spectrum with components

$$\langle c_m^2 \rangle = \frac{1}{N_0^2} \left\langle \left| \sum_{q=1}^{N_m} \Psi_{m,q} \Psi'_{m,q}^* \right|^2 \right\rangle. \quad (5.35)$$

Since the quantities $\Psi_{m,q} \Psi'_{m,q}^*$ have been assumed statistically independent with zero mean (5.34), the variance of their sum in (5.35) is the sum of their variances and

$$\begin{aligned} \left\langle \left| \sum_{q=1}^{N_m} \Psi_{m,q} \Psi'_{m,q}^* \right|^2 \right\rangle &= \sum_{q=1}^{N_m} \langle |\Psi_{m,q} \Psi'_{m,q}^*|^2 \rangle \\ &= \sum_{q=1}^{N_m} \langle |\Psi_{m,q}|^2 \rangle \langle |\Psi'_{m,q}|^2 \rangle = N_m \end{aligned} \quad (5.36)$$

the average irradiances $\langle |\Psi_{m,q}|^2 \rangle$ and $\langle |\Psi'_{m,q}|^2 \rangle$ being normalised to unity. Hence, for $m \neq 0$, (5.35) becomes

$$\langle c_m^2 \rangle = N_m / N_0^2. \quad (5.37)$$

This is to be compared with the energy spectrum of a point-source image without turbulence. According to (5.23) and (5.24), it has components

$$c_m^2 = N_m^2/N_0^2. \quad (5.38)$$

Turbulence therefore introduces the attenuation factor $1/N_m$. For a non-redundant pupil such as the two-aperture pupil of a Michelson interferometer, there is no attenuation as seen in § 4.4. The significance of pupil redundancy in the degradation of images by aberrations was first underlined by RUSSELL and GOODMAN [1971] and by RHODES and GOODMAN [1973].

Let us again consider the entrance pupil of a large telescope as an array of adjacent apertures with size of the order of r_0 , so that the wavefront perturbations on each aperture are uncorrelated. According to (5.37), the energy spectrum of a point-source image, for $f \geq r_0/\lambda$, can be approximated as

$$\langle |\tilde{S}(f)|^2 \rangle \approx \sum_m (N_m/N_0^2) \delta(f - f_m) \quad (5.39)$$

or, taking (5.26) into account,

$$\langle |\tilde{S}(f)|^2 \rangle \approx N_0^{-1} \sum_m T(f_m) \delta(f - f_m) \quad (5.40)$$

and, approximating the sum as an integral,

$$\begin{aligned} \langle |\tilde{S}(f)|^2 \rangle &\approx N_0^{-1} \int d\gamma' \cdot T(\gamma') \delta(f - \gamma') \\ &= N_0^{-1} T(f). \end{aligned} \quad (5.41)$$

Thus recovering expression (5.10) where $N_0 = S/\sigma$ is the number of coherence areas on the pupil, or the number of speckles in the image. This heuristic derivation of (5.10) is due to KORFF, DRYDEN and MILLER [1972]. Application to aperture synthesis was considered by F. RODDIER [1974].

5.3. THE PROBABILITY DENSITY FUNCTIONS OF STELLAR SPECKLES

A laser speckle pattern is generally considered as an interference pattern formed by the combination of light beams issued from a large number of independent scatterers. The resulting complex amplitude, being the sum of a large number of independent random fields, tends to a

complex Gaussian process, as a result of the central limit theorem (GOODMAN [1975], DAINTY [1976]). According to § 5.2, the same result applies to stellar speckles provided that the telescope diameter D is much larger than the correlation scale of the wavefront perturbations, that is $D \gg r_0$. In such a case the complex amplitude $\mathcal{A}(\alpha)$ in the image plane is a circular Gaussian process and the related illumination $S(\alpha) = |\mathcal{A}(\alpha)|^2$ has an exponential distribution

$$\mathcal{P}(S) = \langle S \rangle^{-1} \exp(-S/\langle S \rangle) \quad (5.42)$$

as suggested by LABEYRIE [1975]. Accurate experimental verification of (5.42) is difficult because the speckle pattern is always blurred by the finite width of the scanning aperture, the finite optical bandwidth or the finite "exposure time". GOODMAN [1975] and DAINTY [1976] have given an approximate expression for the probability density function of such blurred speckles which has been found to agree well with observations through a 91 cm telescope (SCADDAN and WALKER [1978]).

The probability density function of the illumination in the image plane of a small telescope cannot be derived from the central limit theorem and will depend upon the statistics of the wavefront perturbations. However no simple analytical expression can be derived unless we assume that the wavefront perturbations have Gaussian statistics in which case $\mathcal{A}(\alpha)$ is also Gaussian.

§ 6. Exposure-Time and Non-Isoplanicity Effects

In the last section, we assumed that images were recorded with an exposure time short enough to freeze the instantaneous wavefront perturbations. Here, we shall investigate the effect of a longer exposure time, i.e. the effect of the evolution of wavefront perturbations during the exposure time. We shall also investigate the effect of non-isoplanicity, i.e. the effect of the evolution of wavefront perturbations with the direction of observation. The two theories are very similar. Both involve the calculation of speckle cross-spectra.

6.1. SPECKLE CROSS-SPECTRA

Let $\Psi_1(u)$ and $\Psi_2(u)$ describe two different wavefronts and let $S_1(\alpha)$ and $S_2(\alpha)$ be the associated speckle patterns. Their Fourier transforms

$\tilde{S}_1(\gamma)$ and $\tilde{S}_2(\gamma)$ are given by (4.12) and the cross-spectrum is

$$\langle \tilde{S}_1(\gamma) \tilde{S}_2^*(\gamma') \rangle = S^{-2} \int d\gamma' \cdot M_{12}(\gamma, \gamma') A(\gamma, \gamma') \quad (6.1)$$

where $A(\gamma, \gamma')$ is defined by (5.6) and

$$M_{12}(\gamma, \gamma') = \langle \Psi_1(u) \Psi_1^*(u + \gamma) \Psi_2^*(u + \gamma') \Psi_2(u + \gamma + \gamma') \rangle. \quad (6.2)$$

In the following, we shall assume that Ψ_1 and Ψ_2 obey the same Gaussian statistics. Although log-normal statistics would be more realistic, we know from § 5 that Gaussian statistics give a fairly good qualitative account of the observations. Moreover, the high frequency tail of the image energy-spectrum (which is of interest in speckle interferometry experiments) does not depend upon the statistics of Ψ . Assuming Gaussian statistics,

$$M_{12}(\gamma, \gamma') = B^2(\gamma) + B_{12}^2(\gamma') \quad (6.3)$$

with

$$B_{12}(\gamma') = \langle \Psi_1(u) \Psi_2^*(u + \gamma') \rangle. \quad (6.4)$$

Putting (6.3) into (6.1) leads to

$$\langle \tilde{S}_1(\gamma) \cdot \tilde{S}_2^*(\gamma') \rangle = B^2(\gamma) |T(\gamma)|^2 + S^{-2} \int d\gamma' \cdot B_{12}(\gamma') A(\gamma, \gamma'). \quad (6.5)$$

6.2. EFFECT OF NON-ISOPLANICITY

Let us drop the assumption of isoplanicity. The relation between the image I and the object O takes the more general form

$$I(\alpha) = \int d\beta \cdot O(\beta) S(\alpha - \beta, \beta) \quad (6.6)$$

where the point-spread function S now depends upon the direction of observation. Taking the Fourier transform of (6.6) leads to

$$\tilde{I}(\gamma) = \int d\beta \cdot O(\beta) \tilde{S}(\gamma, \beta) \exp(-2i\pi\beta \cdot \gamma). \quad (6.7)$$

The image energy spectrum therefore becomes

$$\begin{aligned} \langle |\tilde{I}(\gamma)|^2 \rangle &= \iint d\beta \cdot d\beta' \cdot O(\beta) O(\beta') \langle \tilde{S}(\gamma, \beta) \tilde{S}^*(\gamma, \beta') \rangle \\ &\times \exp[-2i\pi(\beta - \beta') \cdot \gamma] \end{aligned} \quad (6.8)$$

or, with $\boldsymbol{\theta} = \boldsymbol{\beta} - \boldsymbol{\beta}'$,

$$\begin{aligned}\langle |\tilde{I}(\boldsymbol{\gamma})|^2 \rangle &= \int \int d\boldsymbol{\beta} \cdot d\boldsymbol{\theta} \cdot O(\boldsymbol{\beta})O(\boldsymbol{\beta} - \boldsymbol{\theta})\langle \tilde{S}(\boldsymbol{\gamma}, \boldsymbol{\beta})\tilde{S}^*(\boldsymbol{\gamma}, \boldsymbol{\beta} - \boldsymbol{\theta}) \rangle \\ &\quad \times \exp(-2i\pi\boldsymbol{\theta} \cdot \boldsymbol{\gamma}) \\ &= \int d\boldsymbol{\theta} \cdot C_0(\boldsymbol{\theta})\langle \tilde{S}(\boldsymbol{\gamma}, \boldsymbol{\beta})\tilde{S}^*(\boldsymbol{\gamma}, \boldsymbol{\beta} - \boldsymbol{\theta}) \rangle \exp(-2i\pi\boldsymbol{\theta} \cdot \boldsymbol{\gamma})\end{aligned}\quad (6.9)$$

where $C_0(\boldsymbol{\theta})$ is the object autocorrelation function. Putting (6.5) into (6.9) leads to

$$\begin{aligned}\langle |\tilde{I}(\boldsymbol{\gamma})|^2 \rangle &= B^2(\boldsymbol{\gamma}) |T(\boldsymbol{\gamma})|^2 |\tilde{O}(\boldsymbol{\gamma})|^2 \\ &\quad + S^{-2} \int \int d\boldsymbol{\theta} \cdot d\boldsymbol{\gamma}' \cdot C_0(\boldsymbol{\theta})B_\theta^2(\boldsymbol{\gamma}')A(\boldsymbol{\gamma}, \boldsymbol{\gamma}') \exp(-2i\pi\boldsymbol{\theta} \cdot \boldsymbol{\gamma}')\end{aligned}\quad (6.10)$$

where

$$B_\theta(\boldsymbol{\gamma}') = \langle \Psi(\boldsymbol{u}, \boldsymbol{\beta})\Psi^*(\boldsymbol{u} + \boldsymbol{\gamma}', \boldsymbol{\beta}') \rangle \quad (6.11)$$

describes the covariance between wavefront perturbations associated with directions $\boldsymbol{\beta}$ and $\boldsymbol{\beta}'$.

Let us first assume a single thin turbulent layer at altitude h . The related perturbations $\Psi(\boldsymbol{u}, \boldsymbol{\beta})$ and $\Psi(\boldsymbol{u}, \boldsymbol{\beta}')$ will be identical but shifted one from the other by an amount $\boldsymbol{\theta}h$ so that

$$\begin{aligned}B_\theta(\boldsymbol{\gamma}') &= \langle \Psi(\boldsymbol{u} + \boldsymbol{\beta}h/\lambda, 0)\Psi^*(\boldsymbol{u} + \boldsymbol{\gamma}' + \boldsymbol{\beta}'h/\lambda, 0) \rangle \\ &= B(\boldsymbol{\gamma}' - \boldsymbol{\theta}h/\lambda).\end{aligned}\quad (6.12)$$

For a moderate to large size telescope $A(\boldsymbol{\gamma}, \boldsymbol{\gamma}')$ does not vary appreciably over the width of the function $B^2(\boldsymbol{\gamma}' - \boldsymbol{\theta}h/\lambda)$. In (6.10) we shall therefore approximate this function with a Dirac distribution

$$B_\theta^2(\boldsymbol{\gamma}') = B^2(\boldsymbol{\gamma}' - \boldsymbol{\theta}h/\lambda) \approx \sigma \delta(\boldsymbol{\gamma}' - \boldsymbol{\theta}h/\lambda) \quad (6.13)$$

where σ is defined by (5.11). Putting (6.13) into (6.10) leads to

$$\begin{aligned}\langle |\tilde{I}(\boldsymbol{\gamma})|^2 \rangle &= B^2(\boldsymbol{\gamma}) |T(\boldsymbol{\gamma})|^2 |\tilde{O}(\boldsymbol{\gamma})|^2 \\ &\quad + \sigma S^{-2} \int d\boldsymbol{\theta} \cdot C_0(\boldsymbol{\theta})A(\boldsymbol{\gamma}, \boldsymbol{\theta}h/\lambda) \exp(-2i\pi\boldsymbol{\theta} \cdot \boldsymbol{\gamma}).\end{aligned}\quad (6.14)$$

When both $|\boldsymbol{\gamma}|$ and $|\boldsymbol{\theta}h/\lambda|$ are much smaller than the telescope frequency

cut off $f_c = D/\lambda$, $A(\mathbf{f}, \theta h/\lambda)$ can be approximated with

$$A(\mathbf{f}, \theta h/\lambda) \approx S T(\mathbf{f}) T(\theta h/\lambda). \quad (6.15)$$

Putting (6.15) into (6.14) shows that, within a large frequency range $r_0/\lambda < |\mathbf{f}| \ll D/\lambda$, the image energy spectrum is approximately described by

$$\langle |\tilde{I}(\mathbf{f})|^2 \rangle = S^{-1} \sigma T(\mathbf{f}) \int d\theta \cdot C_0(\theta) T(\theta h/\lambda) \exp(-2i\pi\theta \cdot \mathbf{f}). \quad (6.16)$$

In this frequency range, the object spectrum is smoothed by convolution with the Fourier transform of $T(\theta h/\lambda)$. The related features in the object autocorrelation are attenuated by the factor $T(\theta h/\lambda)$. Half attenuation occurs when $|\theta| \approx D/2h$. With $D = 1$ m and $h = 10^4$ m, the isoplanatic patch size is of the order of 10 arcseconds.

Observed values are smaller than that, of the order of 4 arcseconds (NISENSEN and STACHNIK [1978], SCHNEIDERMAN and KARO [1978a], POLLAIN, BUFFINGTON and CRAWFORD [1979]). This is not surprising since turbulence can hardly be assumed to be concentrated into a single layer. According to (4.22) and (6.12), the single layer model leads to

$$B_\theta^2(\mathbf{f}') = \exp\{-6.88(\lambda/r_0)^{\frac{5}{3}} |\mathbf{f}' - \theta h/\lambda|^{\frac{5}{3}}\}. \quad (6.17)$$

A reasoning similar to that of § 3.2 shows that, in the case of several layers at altitudes h_j , (6.17) becomes

$$B_\theta^2(\mathbf{f}') = \prod_i \exp\{-6.88(\lambda/r_{0,j})^{\frac{5}{3}} |\mathbf{f}' - \theta h_j/\lambda|^{\frac{5}{3}}\} \quad (6.18)$$

where $r_{0,j}$ is Fried's parameter that would produce layer j alone. Eq. (6.18) can also be written

$$B_\theta^2(\mathbf{f}') = \exp\left\{-6.88(\lambda/r_0)^{\frac{5}{3}} \frac{\sum_j (r_{0,j})^{-\frac{5}{3}} |\mathbf{f}' - \theta h_j/\lambda|^{\frac{5}{3}}}{r_0^{-\frac{5}{3}}}\right\} \quad (6.19)$$

or, assuming layers of thickness δh_j with a uniform turbulence of structure constant $C_N^2(h_j)$,

$$B_\theta^2(\mathbf{f}') = \exp\left\{-6.88(\lambda/r_0)^{\frac{5}{3}} \frac{\sum_j C_N^2(h_j) \delta h_j |\mathbf{f}' - \theta h_j/\lambda|^{\frac{5}{3}}}{\sum_i C_N^2(h_i) \delta h_i}\right\} \quad (6.20)$$

since $r_{0,j}$ and $C_N^2(h_j) \delta h_j$ are related by (4.24). For a continuous distribution of turbulence, (6.20) easily generalises into

$$B_\theta^2(\gamma') = \exp \left\{ -6.88(\lambda/r_0)^{\frac{5}{3}} \frac{\int_0^\infty dh \cdot C_N^2(h) |\gamma' - \theta h/\lambda|^{\frac{5}{3}}}{\int_0^\infty dh \cdot C_N^2(h)} \right\}. \quad (6.21)$$

In such a case, approximation (6.13) becomes

$$B_\theta^2(\gamma') \approx \sigma(\theta) \delta(\gamma' - \theta \bar{h}/\lambda) \quad (6.22)$$

where \bar{h} is an average turbulence altitude and

$$\sigma(\theta) = \int d\gamma' \cdot B_\theta^2(\gamma'). \quad (6.23)$$

The quantity $\sigma(\theta)$ can be computed numerically from (6.21). It is clear from (6.18) that $\sigma(\theta)$ will fall to zero as soon as $|\theta| \approx r_0/\Delta h$ where Δh is some measure of the height dispersion of turbulence layers. FRIED [1976, 1979] suggests that

$$\Delta h \approx \left[\frac{\int_0^\infty dh \cdot h^{\frac{5}{3}} C_N^2(h)}{\int_0^\infty dh \cdot C_N^2(h)} \right]^{\frac{3}{5}}. \quad (6.24)$$

Under different assumptions, SHAPIRO [1976] gives

$$\Delta h \approx \left[\frac{\int_0^\infty dh \cdot h^2 C_N^2(h)}{\int_0^\infty dh \cdot C_N^2(h)} \right]^{\frac{1}{2}}. \quad (6.25)$$

Recently LOOS and HOGGE [1979] have quoted the similarity between these integrals and eqs. (8.11) and (8.12) giving the scintillation index (see § 8). They suggested that scintillation measurements through an aperture of appropriate size (about 10 cm) would give the parameter Δh , as defined by (6.24), thus permitting $r_0/\Delta h$ to be evaluated, giving the order of magnitude of the isoplanatic patch size.

Putting (6.22) into (6.10) and using approximation (6.15) again shows that, in the frequency range $r_0/\lambda < |\gamma| \ll D/\lambda$ the image energy spectrum is

approximately given by

$$\langle |\tilde{I}(\gamma)|^2 \rangle \approx S^{-1} \sigma T(\gamma) \int d\theta \cdot C_0(\theta) [\sigma(\theta)/\sigma(0)] T(\theta \bar{h}/\lambda) \exp(-2i\pi\theta \cdot \gamma). \quad (6.26)$$

Since for a large telescope $\sigma(\theta)$ decreases steeper than $T(\theta \bar{h}/\lambda)$, in this frequency range, the image spectrum is mainly smoothed by convolution with the Fourier transform of $\sigma(\theta)/\sigma(0)$. The related features in the object autocorrelation are attenuated by the factor $\sigma(\theta)/\sigma(0)$. Using Hufnagel's model (§ 2.4) in (6.21) and (6.23) shows that half attenuation should occur when $|\theta| \approx 2$ arcsecond which is smaller than observed values (see FRIED [1979]). This is not surprising since turbulence is never continuously distributed as in the model, which must be considered as a measure of the probability of observing a turbulence layer at a given altitude. As shown in § 2, any true distribution of turbulence with height consists of discrete layers so that the observed isoplanatic patch size will lie between the average model value and the single layer value.

Detailed calculations of the cross correlation $\langle \tilde{S}(\gamma, \beta) \cdot \tilde{S}^*(\gamma, \beta') \rangle$ have been made by KORFF, DRYDEN and LEAVITT [1975] using log-normal statistics. A discussion of isoplanicity can also be found in WANG [1975] under the assumption of Gaussian statistics.

6.3. THE TIME EVOLUTION OF SPECKLES

Let $\Psi_1(\mathbf{u}) = \Psi(\mathbf{u}, t)$ and $\Psi_2(\mathbf{u}) = \Psi(\mathbf{u}, t - \tau)$ describe the wavefront perturbations at time t and $t - \tau$. According to (6.5) the cross-spectrum of the associated speckle patterns is

$$\langle \tilde{S}(\gamma, t) \tilde{S}^*(\gamma, t - \tau) \rangle = B^2(\gamma) |T(\gamma)|^2 + S^{-2} \int d\gamma' \cdot B_\tau^2(\gamma') A(\gamma, \gamma') \quad (6.27)$$

where

$$B_\tau(\gamma') = \langle \Psi(\mathbf{u}, t) \Psi^*(\mathbf{u} + \gamma', t - \tau) \rangle \quad (6.28)$$

describes the spatio-temporal covariance of Ψ . The temporal correlation function of speckles $C(\tau)$ is obtained by integrating (6.27) over all

frequencies, leading to

$$C(\tau) = \int d\gamma' \cdot B^2(\gamma') |T(\gamma')|^2 + \int d\gamma' \cdot B_\tau^2(\gamma') |T(\gamma')|^2. \quad (6.29)$$

As yet, little is known about the function $B_\tau^2(\gamma')$. It is often assumed that a wind, uniform throughout the turbulence, merely drives the wave-front perturbations without deformation over the telescope pupil plane (Taylor's approximation). In such a case, v being the wind velocity,

$$\begin{aligned} B_\tau(\gamma') &= \langle \Psi(u, 0) \Psi^*(u + \gamma' - v\tau/\lambda, 0) \rangle \\ &= B(\gamma' - v\tau/\lambda), \end{aligned} \quad (6.30)$$

an expression similar to (6.12). According to (4.22)

$$B_\tau^2(\gamma') = \exp \{-6.88(\lambda/r_0)^{\frac{2}{3}} |\gamma' - v\tau/\lambda|^{\frac{2}{3}}\}. \quad (6.31)$$

Measurements of the spatio-temporal covariance of irradiance fluctuations $|\Psi|^2$ indeed show evidence for propagation. They also show a steep decay of the correlation with time delay τ (Fig. 16, p. 348). A similar behaviour is therefore expected for $B_\tau^2(\gamma')$. Assuming several turbulent layers with wind velocities v_j leads to an expression similar to (6.18)

$$B_\tau^2(\gamma') = \prod_j \exp \{-6.88(\lambda/r_{0,j})^{\frac{2}{3}} |\gamma' - v_j\tau/\lambda|^{\frac{2}{3}}\} \quad (6.32)$$

where $r_{0,j}$ is Fried's parameter produced by layer j alone. For a continuous distribution of turbulence, eq. (6.32) generalises into

$$B_\tau^2(\gamma') = \exp \left\{ -6.88(\lambda/r_0)^{\frac{2}{3}} \frac{\int_0^\infty dh \cdot C_N^2(h) |\gamma' - v(h)\tau/\lambda|^{\frac{2}{3}}}{\int_0^\infty dh \cdot C_N^2(h)} \right\}. \quad (6.33)$$

Expressions (6.32) and (6.33) are both able to describe the decay of $B_\tau^2(\gamma')$ with τ . For a moderate to large size telescope, $|T(\gamma')|^2$ does not vary appreciably over the width of the functions $B^2(\gamma)$ and $B_\tau^2(\gamma')$. In eq. (6.29), we shall therefore approximate these functions with Dirac distributions

$$B^2(\gamma) = \sigma \delta(\gamma) \quad (6.34)$$

$$B_\tau^2(\gamma') = \sigma(\tau) \delta(\gamma' - \bar{v}\tau/\lambda) \quad (6.35)$$

where \bar{v} is an average wind velocity,

$$\sigma(\tau) = \int d\gamma' \cdot B_\tau^2(\gamma'), \quad (6.36)$$

and $\sigma = \sigma(0)$ is given by (5.13). The quantity $\sigma(\tau)$ can be computed numerically from (6.33), knowing both the atmospheric wind and turbulence profiles. It is clear from (6.32) that $\sigma(\tau)$ will fall to zero as soon as $\tau = r_0/\Delta v$ where Δv is some measure of the velocity dispersion of turbulence layers.

Putting (6.34) and (6.35) into (6.29) leads to

$$C(\tau) = \sigma \{1 + [\sigma(\tau)/\sigma(0)] |T(\bar{v}\tau/\lambda)|^2\}. \quad (6.37)$$

Measurements of $C(\tau)$ by SCADDAN and WALKER [1978] and PARRY, WALKER and SCADDAN [1979] reveal a steep decay due to speckle boiling and a slow decay due to image motion (neglected in our approximations). According to (6.37), the normalised covariance of the speckle boiling is given by

$$\frac{C(\tau) - C(\infty)}{C(\infty)} = [\sigma(\tau)/\sigma(0)] |T(\bar{v}\tau/\lambda)|^2. \quad (6.38)$$

Assuming a single wind velocity implies that $\sigma(\tau) = \sigma(0)$ so that the speckle lifetime becomes equal to the transit time of perturbations over the telescope pupil. The measurements quoted above clearly show a smaller lifetime, typically 10 ms which must be attributed to the decay of $\sigma(\tau)$. It is therefore of the order of $r_0/\Delta v$. This leads to a velocity dispersion $\Delta v = 5 \text{ m/s}$ for $r_0 = 5 \text{ cm}$. The lifetime is also found to increase with wavelength as expected, since r_0 increases as $\lambda^{\frac{1}{3}}$ (eq (4.25)).

6.4. EFFECT OF THE EXPOSURE TIME ON THE IMAGE SPECTRUM

For an exposure time T , the optical transfer function is given by

$$\tilde{S}_T(\mathcal{J}) = T^{-1} \int_{-T/2}^{+T/2} dt \cdot \tilde{S}(\mathcal{J}, t) = T^{-1} \int dt \cdot \Pi(t/T) \tilde{S}(\mathcal{J}, t) \quad (6.39)$$

where $\Pi(t/T)$ is a rectangle function of width T . The energy spectrum of a point-source image is therefore

$$\begin{aligned} \langle |\tilde{S}_T(\mathcal{J})|^2 \rangle &= T^{-2} \iint dt \cdot d\tau \cdot \Pi\left(\frac{t}{T}\right) \Pi\left(\frac{t-\tau}{T}\right) \langle \tilde{S}(\mathcal{J}, t) \tilde{S}^*(\mathcal{J}, t-\tau) \rangle \\ &= T^{-1} \int d\tau \cdot \Lambda(\tau/T) \langle \tilde{S}(\mathcal{J}, t) \tilde{S}^*(\mathcal{J}, t-\tau) \rangle \end{aligned} \quad (6.40)$$

where $T\Lambda(\tau/T)$ is the autocorrelation function of $H(t/T)$. Putting (6.27) into (6.40) leads to

$$\langle |\tilde{S}_T(\gamma)|^2 \rangle = B^2(\gamma) |T(\gamma)|^2 + S^{-2} T^{-1} \int d\tau \cdot \Lambda(\tau/T) \int d\gamma' \cdot B_\tau^2(\gamma') A(\gamma, \gamma') \quad (6.41)$$

or, using approximation (6.35),

$$\langle |\tilde{S}_T(\gamma)|^2 \rangle = B^2(\gamma) |T(\gamma)|^2 + S^{-2} T^{-1} \int d\tau \cdot \Lambda(\tau/T) \sigma(\tau) A(\gamma, \bar{v}\tau/\lambda). \quad (6.42)$$

When both $|\gamma|$ and $|\bar{v}\tau/\lambda|$ are much smaller than the telescope frequency cut-off $f_c = D/\lambda$, $A(\gamma, \bar{v}\tau/\lambda)$ can again be approximated as

$$A(\gamma, \bar{v}\tau/\lambda) \approx ST(\gamma) T(\bar{v}\tau/\lambda) \quad (6.43)$$

so that (6.42) becomes

$$\begin{aligned} \langle |\tilde{S}_T(\gamma)|^2 \rangle &= B^2(\gamma) |T(\gamma)|^2 \\ &+ \sigma S^{-1} T^{-1} T(\gamma) \int d\tau \cdot \Lambda(\tau/T) [\sigma(\tau)/\sigma(0)] T(\bar{v}\tau/\lambda). \end{aligned} \quad (6.44)$$

Since the equivalent width of $\sigma(\tau)/\sigma(0)$ is of the order of $r_0/\Delta v$, expression (6.44) shows that the high frequency wing of the image spectrum is uniformly depressed by a factor

$$T^{-1} \int d\tau \cdot \Lambda(\tau/T) [\sigma(\tau)/\sigma(0)] T(\bar{v}\tau/\lambda) \approx T^{-1} \min [T, r_0/\Delta v, D/|\bar{v}|] \quad (6.45)$$

where "min" stands for "the smallest value among". As seen in § 6.3, for a large telescope, $r_0/\Delta v$ is smaller than $D/|\bar{v}|$ so that, within a large frequency range $r_0/\lambda < |\gamma| \ll D/\lambda$ the attenuation factor is uniform and equal to $r_0/T \Delta v$, as soon as $T \geq r_0/\Delta v$. Such a uniform depression of the energy spectrum has been observed by KARO and SCHNEIDERMAN [1978]. The observed amount of depression is consistent with $r_0/\Delta v$ values of the order of 20 ms. This is also consistent with the exposure time of speckle interferometers based on standard T.V. systems. It has been shown (see § 9) that the signal-to-noise ratio in speckle interferometry is, for a single exposure, proportional to the number N_s of photons per speckle, as long as $N_s \ll 1$. Since N_s is proportional to T , whereas the signal decreases as

T^{-1} , the signal-to-noise ratio for a single exposure remains constant independent of T , whenever $T \geq r_0 \Delta v$ and $N_s \ll 1$.

Detailed numerical computations of the theoretical shape of the image energy spectrum as a function of the exposure time have been done by C. RODDIER and F. RODDIER [1975], assuming log-normal statistics. Unfortunately, a single wind velocity is also assumed which now appears to be unrealistic.

§ 7. Optical Path Fluctuations

Up to now, we have considered the statistical properties of the complex field $\Psi_0(x)$ only. We shall now examine the statistical properties of its modulus $|\Psi_0(x)|$ and of its argument or phase $\varphi_0(x)$. Fluctuations of the squared modulus $|\Psi_0(x)|^2$ describe the random illumination at the telescope aperture or the stellar shadow pattern easily seen when directly viewing the telescope objective mirror. The motion of the shadows produces stellar scintillation as seen with the naked eye. Fluctuations of the phase $\varphi_0(x)$ or of the optical path $\lambda\varphi_0(x)/2\pi$ describe the shape of the wavefront surface. They are related to the fluctuations of the angle of arrival of light, that is to the image motion as seen through a very small aperture.

When dealing with imaging, scintillation or angle-of-arrival fluctuations need not to be considered separately, as we have seen. They are, however, to be considered in some other cases. For instance, scintillation interferes directly with photometric observations, especially in occultation measurements. Angle-of-arrival fluctuations interfere with astrometric measurements. In § 10, we shall see that scintillation and angle-of-arrival measurements are useful tools for probing atmospheric turbulence and testing astronomical sites.

As we did in § 3, we shall again use the phase screen approach and the formalism of Fourier optics in order to derive briefly the fundamental relations due to CHERNOV [1955] and TATARSKI [1956] and presented in detail in the books quoted in § 3.

7.1. EFFECT OF A THIN TURBULENT LAYER

Let us consider again horizontal monochromatic plane waves propagating downward, towards a ground based observer. As in § 3.1, we shall

first assume that the atmosphere is homogeneous everywhere except inside a thin horizontal layer between altitudes h and $h + \delta h$, introducing a phase shift $\varphi(x)$ described by (3.3).

We shall now make a new and very restrictive assumption that we did not make in § 3. We shall assume that

$$\varphi(x) \ll 1. \quad (7.1)$$

This assumption, called the small perturbation approximation, is not valid for most of the experiments made on propagation along horizontal paths. Many efforts have been made during the last decade to account for the saturation of scintillation which occurs when this approximation is not valid (see for instance STROHBEHN [1978]). In the case of astronomical observations, saturation effects have been considered by YOUNG [1970]. Saturation regimes usually occur when the distance from the zenith exceeds 60° . Near the zenith, they are exceptional and (7.1) can be taken as a good approximation, so that the field at the layer output given by (3.2) can be written

$$\Psi_h(x) = 1 + i\varphi(x). \quad (7.2)$$

The complex field $\Psi_0(x)$ at ground level is given by the Fresnel convolution described by eq. (3.14) of § 3.1, so that

$$\Psi_0(x) = [1 + i\varphi(x)] * \frac{1}{i\lambda h} \exp\left(i\pi \frac{x^2}{\lambda h}\right). \quad (7.3)$$

Since, as is easily seen from its Fourier transform,

$$1 * \frac{1}{i\lambda h} \exp\left(i\pi \frac{x^2}{\lambda h}\right) = 1 \quad (7.4)$$

eq. (7.3) becomes

$$\Psi_0(x) = 1 + \varepsilon(x) \quad (7.5)$$

where the complex quantity

$$\varepsilon(x) = \varphi(x) * \frac{1}{\lambda h} \exp\left(i\pi \frac{x^2}{\lambda h}\right) \quad (7.6)$$

describes the relative fluctuations of the complex amplitude at ground level.

Its real part

$$\chi(x) = \varphi(x) * \frac{1}{\lambda h} \cos\left(\pi \frac{x^2}{\lambda h}\right) \quad (7.7)$$

describes the relative fluctuations of the modulus $|\Psi_0(x)|$.

Its imaginary part

$$\varphi_0(x) = \varphi(x) * \frac{1}{\lambda h} \sin \left(\pi \frac{x^2}{\lambda h} \right) \quad (7.8)$$

describes the fluctuations of the phase.

Since $\varphi(x)$ has Gaussian statistics (see § 3), the linearly related quantities $\varepsilon(x)$, $\chi(x)$ and $\varphi_0(x)$ also have Gaussian statistics. Let us define the two-dimensional power spectrum $W_\varphi(f)$ of $\varphi(x)$ as†

$$W_\varphi(f) = \int d\xi \cdot B_\varphi(\xi) \exp(-2i\pi f \cdot \xi) \quad (7.9)$$

where $B_\varphi(\xi)$ is the covariance of $\varphi(x)$. With that definition, taking the squared modulus of the Fourier transform of the convolution factor in (7.6), (7.7) and (7.8), leads to the following power spectra for $\varepsilon(x)$, $\chi(x)$ and $\varphi_0(x)$:

$$W_\varepsilon(f) = W_\varphi(f) \quad (7.10)$$

$$W_\chi(f) = W_\varphi(f) (\sin \pi \lambda h f^2)^2 \quad (7.11)$$

$$W_{\varphi_0}(f) = W_\varphi(f) (\cos \pi \lambda h f^2)^2. \quad (7.12)$$

Taking the Fourier transform of (3.10) according to (7.9) gives

$$W_\varphi(f) = k^2 \delta h W_N(f, 0) \quad (7.13)$$

where

$$W_N(f_x, f_y, f_z) = (2\pi)^3 \Phi_N(2\pi f_x, 2\pi f_y, 2\pi f_z) \quad (7.14)$$

is the three-dimensional power spectrum of index fluctuations. Assuming Kolmogorov's law (2.17) to be valid, with $f = |f|$

$$\begin{aligned} W_N(f, 0) &= (2\pi)^3 \times 0.033 C_N^2(h) (2\pi f)^{-\frac{11}{3}} \\ &= 9.7 \times 10^{-3} C_N^2(h) f^{-\frac{11}{3}} \end{aligned} \quad (7.15)$$

so that (7.13) becomes

$$W_\varphi(f) = 9.7 \times 10^{-3} k^2 f^{-\frac{11}{3}} C_N^2(h) \delta h \quad (7.16)$$

† Although this definition is not the most usual, it is consistent with the definition (4.2) of the Fourier transform given in § 4. Care must be taken that the frequency vector f now has the dimension of an inverse length.

and (7.10) to (7.12) can be written, since $k = 2\pi/\lambda$,

$$W_e(f) = 0.38\lambda^{-2}f^{-\frac{11}{3}}C_N^2(h)\delta h \quad (7.17)$$

$$W_x(f) = 0.38\lambda^{-2}f^{-\frac{11}{3}}C_N^2(h)\delta h(\sin \pi\lambda hf^2)^2 \quad (7.18)$$

$$W_{\varphi_0}(f) = 0.38\lambda^{-2}f^{-\frac{11}{3}}C_N^2(h)\delta h(\cos \pi\lambda hf^2)^2. \quad (7.19)$$

7.2. MULTIPLE LAYERS AND THICK LAYERS

Let us first consider two thin layers of turbulence at altitudes h_1 and h_2 (where $h_1 > h_2$) and with thicknesses δh_1 and δh_2 . Let $\varphi_1(x)$ and $\varphi_2(x)$ be the phase shifts introduced by each layers. According to (7.6) the relative fluctuations of the complex amplitude at the input of the lower layer are

$$\varepsilon(x, h_2 + \delta h_2) = i\varphi_1(x) * \frac{1}{i\lambda(h_1 - h_2)} \exp \left[i\pi \frac{x^2}{\lambda(h_1 - h_2)} \right]. \quad (7.20)$$

They are, at the output,

$$\varepsilon(x, h_2) = i\varphi_1(x) * \frac{1}{i\lambda(h_1 - h_2)} \exp \left[i\pi \frac{x^2}{\lambda(h_1 - h_2)} \right] + i\varphi_2(x) \quad (7.21)$$

and, at ground level

$$\begin{aligned} \varepsilon(x) &= \left\{ i\varphi_1(x) * \frac{1}{i\lambda(h_1 - h_2)} \exp \left[i\pi \frac{x^2}{\lambda(h_1 - h_2)} \right] + i\varphi_2(x) \right\} \\ &\quad * \frac{1}{i\lambda h_2} \exp \left(i\pi \frac{x^2}{\lambda h_2} \right). \end{aligned} \quad (7.22)$$

As easily shown by taking its Fourier transform,

$$\begin{aligned} \frac{1}{i\lambda(h_1 - h_2)} \exp \left[i\pi \frac{x^2}{\lambda(h_1 - h_2)} \right] * \frac{1}{i\lambda h_2} \exp \left(i\pi \frac{x^2}{\lambda h_2} \right) \\ = \frac{1}{i\lambda h_1} \exp \left(i\pi \frac{x^2}{\lambda h_1} \right). \end{aligned} \quad (7.23)$$

Therefore

$$\varepsilon(x) = \varphi_1(x) * \frac{1}{\lambda h_1} \exp \left(i\pi \frac{x^2}{\lambda h_1} \right) + \varphi_2(x) * \frac{1}{\lambda h_2} \exp \left(i\pi \frac{x^2}{\lambda h_2} \right) \quad (7.24)$$

showing that, at the small perturbations approximation, fluctuations produced at ground level by several turbulent layers add linearly. Since they are statistically independent, their power spectra also add linearly and

expressions (7.17) to (7.19) easily generalise, for any distribution of turbulence, into

$$W_\epsilon(f) = 0.38\lambda^{-2}f^{-\frac{11}{3}} \int dh \cdot C_N^2(h) \quad (7.25)$$

$$W_x(f) = 0.38\lambda^{-2}f^{-\frac{11}{3}} \int dh \cdot C_N^2(h)(\sin \pi\lambda hf^2)^2 \quad (7.26)$$

$$W_{\varphi_0}(f) = 0.38\lambda^{-2}f^{-\frac{11}{3}} \int dh \cdot C_N^2(h)(\cos \pi\lambda hf^2)^2. \quad (7.27)$$

We note that

$$W_\epsilon(f) = W_x(f) + W_{\varphi_0}(f) \quad (7.28)$$

showing that the cross-spectrum of χ and φ_0 is zero. Since χ and φ_0 are Gaussian variables, this implies that they are statistically independent.

7.3. THE NEAR-FIELD APPROXIMATION

The near field approximation consists of neglecting $W_x(f)$ in (7.28) so that

$$W_\epsilon(f) \approx W_{\varphi_0}(f). \quad (7.29)$$

The validity of this approximation for astronomical observations has been discussed by YOUNG [1974]. From (7.26) and (7.27), it is clear that $W_x(f)$ is negligible at low frequencies. At high frequencies, both spectra take similar but very small values due to their decrease as the $-\frac{11}{3}$ power. Therefore, the near-field approximation holds in many applications. For instance, the variance $\langle \chi^2 \rangle$ of the log-amplitude χ is completely negligible compared to the variance $\langle \varphi_0^2 \rangle$ of the phase

$$\langle \chi^2 \rangle = \int df W_x(f) \ll \langle \varphi_0^2 \rangle = \int df W_{\varphi_0}(f). \quad (7.30)$$

We already know from (3.21) that the coherence function at ground level has the form

$$B_0(\xi) = \exp -\frac{1}{2}D(\xi). \quad (7.31)$$

According to FRIED [1966], the wave structure function can be written

$$D(\xi) = D_x(\xi) + D_{\varphi_0}(\xi) \quad (7.32)$$

where $D_x(\xi)$ and $D_{\varphi_0}(\xi)$ are, respectively, the structure functions of the log-amplitude and of the phase at ground level. Eq. (7.32) is the analog of (7.28) for the structure functions. Comparing (7.31) with (4.23) yields

$$D(\xi) = 6.88(\xi/r_0)^{\frac{5}{3}}. \quad (7.33)$$

Fig. 8 shows a plot of $D(\xi)$ for $r_0 = 11$ cm, together with an estimation of $D_x(\xi)$ from the relation

$$D_x(\xi) = 2[B_x(0) - B_x(\xi)] \quad (7.34)$$

where $B_x(\xi)$ is the covariance of the log-amplitude taken, according to (8.1), as 0.25 times the covariance of the scintillation plotted in Fig. 14 (§ 8), assuming a typical scintillation index of 20% produced by a turbulent layer at 10 km. The phase structure function $D_{\varphi_0}(\xi)$ is obtained by subtracting $D_x(\xi)$ from $D(\xi)$ according to (7.32). Clearly, the near-field approximation

$$D_{\varphi_0}(\xi) \approx D(\xi) \quad (7.35)$$

holds with a maximum error of the order of 8% occurring when $\xi \leq 2.5$ cm.

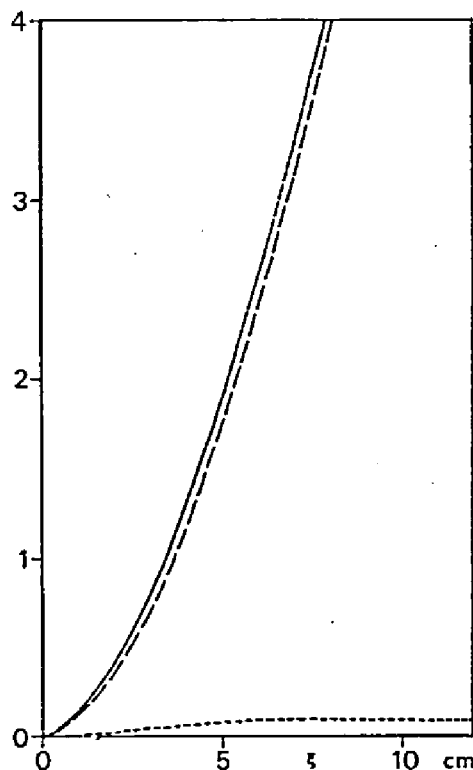


Fig. 8. Wave structure function (solid line), log amplitude structure function (dotted line) and phase structure function (dashed line) assuming $r_0 = 11$ cm and scintillation entirely produced by the tropopause layer with $\sigma_I^2 = 0.2$.

7.4. PHASE FLUCTUATIONS

From (7.33), the near-field approximation (7.35) leads to

$$D_{\varphi_0}(\xi) = \langle |\varphi_0(x) - \varphi_0(x + \xi)|^2 \rangle \approx 6.88(\xi/r_0)^{\frac{5}{3}} \quad (7.36)$$

which shows that the standard deviation of the phase difference between point x and point $x + \xi$

$$\sigma_{\varphi_0}(\xi) = [D_{\varphi_0}(\xi)]^{\frac{1}{2}} = 2.62(\xi/r_0)^{\frac{5}{6}} \quad (7.37)$$

increases as the $\xi^{\frac{5}{6}}$ power of the distance ξ . Interferometric measurements provide an experimental check of (7.36) and (7.37). Such experiments have been done by BUSER [1971] and by CLIFFORD, BOURICIUS, OCHS and ACKLEY [1971] on horizontal laser beam propagation. The first test on stellar sources was done by BRECKINRIDGE [1976] and agreed well with the $5/6$ power law, for displacement values ξ ranging from 0.2 m to 1.5 m. Departures from the $5/6$ power are expected at large distances when ξ becomes comparable with the outer scale of turbulence. However, the distance up to which (7.37) is valid is still unknown.

Since r_0 varies as $\lambda^{\frac{5}{3}}$, σ_{φ_0} varies as λ^{-1} and the standard deviation of the optical path difference

$$\sigma_z = (\lambda/2\pi)\sigma_{\varphi_0} = (2.62/2\pi)\lambda_0(\xi/r_0)^{\frac{5}{6}} \quad (7.38)$$

is wavelength independent. In (7.38), r_0 is the value of Fried's parameter at wavelength λ_0 . Long baseline optical interferometers are now operating in astronomy (LABEYRIE [1975]). Assuming (7.38) is still valid on a 20 m baseline and $r_0 = 11$ cm (at $\lambda_0 = 0.5$ μm) leads to optical path differences of the order of 16 μm , that is typical fringe excursions of the order of 30 fringes in the visible. Assuming frozen turbulence driven by the wind velocity v , the characteristic evolution time is of the order of v/ξ . Taking $v = 2$ m/s and a 20 m baseline leads to a typical fringe motion of the order of 3 fringes per second, which explains that fringes are visible to the eye whenever the seeing is good and the wind speed is low. More rigorous calculations of the fringe visibility as a function of the baseline and the exposure time, assuming frozen wavefronts with log-normal statistics and Kolmogorov's law, can be found in C. RODDIER [1976].

7.5. ANGLE-OF-ARRIVAL FLUCTUATIONS

The deviation $z(x, y)$ of the wave surface from the average plane at ground level is

$$z(x, y) = (\lambda/2\pi)\varphi_0(x, y). \quad (7.39)$$

In terms of geometrical optics, the light rays are normal to the wave surface (see STROHBEHN and CLIFFORD [1967]). Their angle-of-arrival therefore fluctuates. The fluctuations are

$$\alpha(x, y) = -\frac{\partial}{\partial x} z(x, y) = -(\lambda/2\pi) \frac{\partial}{\partial x} \varphi_0(x, y) \quad (7.40)$$

in the x direction and

$$\beta(x, y) = -\frac{\partial}{\partial y} z(x, y) = -(\lambda/2\pi) \frac{\partial}{\partial y} \varphi_0(x, y) \quad (7.41)$$

in the y direction. They obey Gaussian statistics. The power spectra of α and β are related to the power spectrum of φ_0 by

$$W_\alpha(f) = \lambda^2 f_x^2 W_{\varphi_0}(f) \quad (7.43)$$

$$W_\beta(f) = \lambda^2 f_y^2 W_{\varphi_0}(f) \quad (7.44)$$

where f_x and f_y are the x and y components of the frequency vector f . The variance of α and β are

$$\langle \alpha^2 \rangle = \lambda^2 \int df \cdot f_x^2 W_{\varphi_0}(f) \quad (7.45)$$

$$\langle \beta^2 \rangle = \lambda^2 \int df \cdot f_y^2 W_{\varphi_0}(f). \quad (7.46)$$

The standard deviation σ_m of the angle-of-arrival is therefore given by

$$\sigma_m^2 = \langle \alpha^2 \rangle + \langle \beta^2 \rangle = \lambda^2 \int df \cdot f^2 W_{\varphi_0}(f). \quad (7.47)$$

At the near-field approximation (7.29), $W_{\varphi_0}(f)$ is given by (7.25). Putting (7.25) into (7.47) and integrating over all directions in the frequency plane leads to

$$\sigma_m^2 \propto \int_0^\infty dh \cdot C_N^2(h) \int_0^\infty df \cdot f^{-\frac{3}{2}}. \quad (7.48)$$

The integration over f cannot be taken from 0 to ∞ . A more realistic expression is

$$\sigma_m^2 \propto \int_0^\infty dh \cdot C_N^2(h) \int_{L_0}^{D^{-1}} df \cdot f^{-\frac{3}{2}}, \quad (7.49)$$

where L_0 is the turbulence outer scale and D^{-1} is the high frequency cut-off due to averaging over the observing aperture of diameter D .

Integrating (7.49) leads to

$$\sigma_m^2 \propto [\mathbb{D}^{-\frac{1}{3}} - L^{-\frac{1}{3}}] \int_0^\infty dh \cdot C_N^2(h) \quad (7.50)$$

or, neglecting $L^{-\frac{1}{3}}$ compared to $\mathbb{D}^{-\frac{1}{3}}$ (which can be a crude assumption),

$$\sigma_m^2 \propto \mathbb{D}^{-\frac{1}{3}} \int_0^\infty dh \cdot C_N^2(h). \quad (7.51)$$

Expression (7.51) has been established for observations at the zenith. It remains valid at any zenith angle γ by taking h as a distance along the line of sight. Replacing h by $h/\cos \gamma$, (7.51) takes the more general form

$$\sigma_m^2 \propto \mathbb{D}^{-\frac{1}{3}} (\cos \gamma)^{-1} \int_0^\infty dh \cdot C_N^2(h). \quad (7.52)$$

TATARSKI [1971] has indeed shown more rigorously that (7.52) describes the motion of the centre of gravity of a star image as seen through a telescope of diameter \mathbb{D} , when scintillation effects are neglected. The $(\cos \gamma)^{-1}$ law was first established by KRASILNIKOV [1949]. Observations of the quivering of stellar images were reviewed by KOLCHINSKI [1952, 1957] and found consistent with (7.52) (see also IRWIN [1966]). More recent observations by BUFTON and GENATT [1971] agree both with the $\mathbb{D}^{-\frac{1}{3}}$ law and the $(\cos \gamma)^{-1}$ law. It is worthwhile noting that σ_m^2 is independent of wavelength. Introducing Fried's parameter r_0 as expressed by (4.24) leads to

$$\sigma_m^2 \propto \lambda^2 \mathbb{D}^{-\frac{1}{3}} r_0^{-\frac{5}{3}}. \quad (7.53)$$

More rigorous estimations by TATARSKI [1971] and FRIED [1965, 1975] give the following coefficient of proportionality in radians squared

$$\sigma_m^2 \approx (3.44/\pi^2) \lambda^2 \mathbb{D}^{-\frac{1}{3}} r^{-\frac{5}{3}}$$

or

$$\sigma_m^2 \approx 0.36(\lambda/\mathbb{D})^{\frac{1}{3}}(\lambda/r_0)^{\frac{5}{3}}. \quad (7.54)$$

The covariance of angle-of-arrival fluctuations, defined by

$$B_\alpha(\mu, \eta) = \langle \alpha(x, y) \alpha(x + \mu, y + \eta) \rangle \quad (7.55)$$

is obtained by taking the Fourier transform of their power spectrum (7.43). Therefore

$$B_\alpha(\mu, \eta) = -(\lambda^2/4\pi^2) \frac{\partial^2}{\partial \mu^2} B_{\varphi_0}(\mu, \eta) \quad (7.56)$$

or, introducing the phase structure function

$$B_\alpha(\mu, \eta) = (\lambda^2/8\pi^2) \frac{\partial^2}{\partial \mu^2} D_{\varphi_0}(\mu, \eta). \quad (7.57)$$

At the near-field approximation (7.36),

$$D_{\varphi_0}(\mu, \eta) = 6.88r_0^{-\frac{5}{3}}(\mu^2 + \eta^2)^{\frac{5}{6}} \quad (7.58)$$

and

$$\frac{\partial^2}{\partial \mu^2} D_{\varphi_0}(\mu, \eta) = \frac{5}{3} \times 6.88r_0^{-\frac{5}{3}}[(\mu^2 + \eta^2)^{-\frac{1}{6}} - \frac{1}{3}\mu^2(\mu^2 + \eta^2)^{-\frac{7}{6}}]. \quad (7.59)$$

Putting (7.59) into (7.57) gives the longitudinal covariance in radians squared

$$B_\alpha(\mu, 0) = 0.097(\lambda/r_0)^{\frac{5}{3}}(\lambda/\mu)^{\frac{1}{3}} \quad (7.60)$$

and the lateral covariance

$$B_\alpha(0, \eta) = 0.145(\lambda/r_0)^{\frac{5}{3}}(\lambda/\eta)^{\frac{1}{3}}. \quad (7.61)$$

It must be remembered that these expressions are only valid in the inertial range. The divergence at the origin is not physical. In any practical situation, the value at the origin is limited by aperture averaging and given by (7.54). STROHBEHN [1970b] has pointed out the sensitivity of these covariance functions to the shape of the turbulence temperature spectrum. Experimental measurements by BORGNI and MARTIN [1977] and by BORGNI and VERNIN [1978] on the solar limb motion are in excellent agreement with (7.60) and (7.61) for displacement values μ and η ranging from 5 cm to 30 cm. The agreement extends up to 1.1 m in similar measurements made by AZOURI, BORGNI and VERNIN [1978] on lunar limb motion. These measurements provide one of the best proofs of the validity of the inertial model in the case of astronomical observations.

7.6. IMAGE MOTION AND BLURRING

Astronomers are used to describing image degradation in terms of image motion and blurring. Image motion describes the wandering of the image centre of "gravity". As seen in § 7.5, the deviation α' of the image from its average position has a Gaussian probability density

$$\mathcal{P}(\alpha') = \frac{1}{\pi\sigma_m^2} \exp(-|\alpha'|^2/\sigma_m^2) \quad (7.62)$$

with standard deviation σ_m given by eq. (7.54). Image motion does not degrade short exposures. Its effect on long exposures can be removed by using a fast automatic guider or, after detection, by adding short exposures properly centred (see § 9.1). The remaining degradation is called blurring.

Let $S_0(\alpha) = S(\alpha + \alpha')$ be the instantaneous illumination in the centred image of a point source. The classical long exposure $\langle S(\alpha) \rangle$ is related to the improved long exposure $\langle S_0(\alpha) \rangle$ by

$$\begin{aligned}\langle S(\alpha) \rangle &= \left\langle \int d\alpha' \cdot S_0(\alpha - \alpha') \mathcal{P}(\alpha') \right\rangle \\ &= \langle S_0(\alpha) \rangle * \mathcal{P}(\alpha).\end{aligned}\quad (7.63)$$

The associated modulation transfer functions are therefore related to each other by

$$\langle \tilde{S}(f) \rangle = \langle \tilde{S}_0(f) \rangle \cdot \tilde{\mathcal{P}}(f) \quad (7.64)$$

where

$$\tilde{\mathcal{P}}(f) = \exp - \pi^2 \sigma_m^2 f^2 \quad (7.65)$$

is the Fourier transform of $\mathcal{P}(\alpha)$ and $f = |f|$. Putting (7.54) into (7.65) leads to

$$\tilde{\mathcal{P}}(f) = \exp - 3.44 (\lambda f / D)^{\frac{1}{3}} (\lambda f / r_0)^{\frac{5}{3}}. \quad (7.66)$$

Now, putting (4.15), (4.22) and (7.66) into (7.64) gives

$$\begin{aligned}\langle \tilde{S}(f) \rangle &= T(f) \exp - 3.44 (\lambda f / r_0)^{\frac{5}{3}} \\ &= \langle \tilde{S}_0(f) \rangle \exp - 3.44 (\lambda f / D)^{\frac{1}{3}} (\lambda f / r_0)^{\frac{5}{3}}\end{aligned}$$

so that

$$\langle \tilde{S}_0(f) \rangle = T(f) \exp - 3.44 (\lambda f / r_0)^{\frac{5}{3}} [1 - (\lambda f / D)^{\frac{1}{3}}]. \quad (7.67)$$

Expression (7.67) was first derived by FRIED [1966] who defines the associated improved resolution R_0 as (see § 4.3):

$$R_0 = \int df \cdot \langle \tilde{S}_0(f) \rangle. \quad (7.68)$$

R_0 is the resolution obtained after the removal of image motions. It is degraded only by blurring. Astronomers define blurring as a spread angle. Here we shall define it as the diameter ω_0 of a disk, with uniform illumination equal to $\langle S_0(0) \rangle$, having the same integral as $\langle S_0(\alpha) \rangle$. ω_0 is the

equivalent width of $\langle S_0(\alpha) \rangle$. With such a definition

$$(\pi/4)\omega_0^2 = \int d\alpha \cdot [\langle S_0(\alpha) \rangle / \langle S_0(0) \rangle] = 1/\mathcal{R}_0$$

or

$$\omega_0 = (4/\pi\mathcal{R}_0)^{\frac{1}{2}}. \quad (7.69)$$

Similarly, we shall define the spread angle for normal imaging as

$$\omega = (4/\pi\mathcal{R})^{\frac{1}{2}} \quad (7.70)$$

where \mathcal{R} is the resolution for normal imaging given by (4.16). For a small diffraction limited telescope of diameter D

$$\omega \approx \omega_d = (4/\pi)(\lambda/D) = 1.27(\lambda/D). \quad (7.70')$$

For an infinitely large telescope limited by turbulence

$$\omega \approx \omega_\infty = 1.27(\lambda/r_0). \quad (7.70'')$$

Numerical values of \mathcal{R} and \mathcal{R}_0 have been computed by FRIED [1966] as a function of D/r_0 . The associated spread angles ω and ω_0 , expressed in λ/r_0 unit, are plotted in Fig. 9, together with a spread angle ω_m for image motion similarly defined as

$$\omega_m = (4/\pi\mathcal{R}_m)^{\frac{1}{2}} \quad (7.71)$$

where

$$\mathcal{R}_m = \int d\gamma \cdot \tilde{\mathcal{P}}(\gamma). \quad (7.72)$$

With such a definition†

$$\omega_m = 2\sigma_m \quad (7.73)$$

Fig. 9 shows that blurring reaches a minimum for $D/r_0 \approx 3.7$. For smaller D/r_0 values, it is mainly due to diffraction by the telescope aperture. For larger D/r_0 values it is mainly due to turbulence. Fig. 9 also shows that the maximum improvement in resolution, due to image motion removal, is of the order of a factor 2 and occurs when $D/r_0 \approx 3$ (§ 9.1). For large D/r_0 values, image motion is certainly overestimated because the finite outer scale of turbulence has not been taken into account. The effect of the outer scale has been studied by VALLEY [1979]. It must be pointed out

† Care must be taken that the standard deviation of image motion along a given direction is only $\sigma_m/\sqrt{2}$ that is $\omega_m/2\sqrt{2}$.

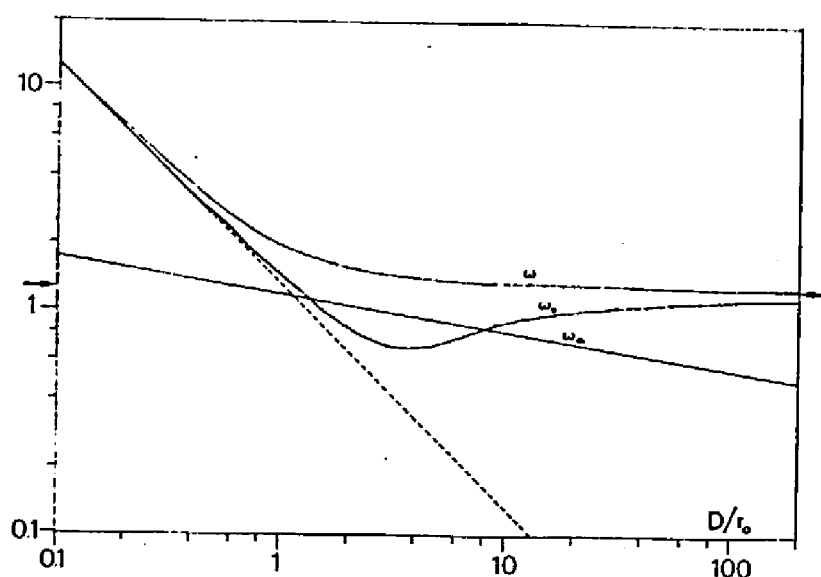


Fig. 9. Image motion ω_m , blurring ω_0 and total spread angle ω , expressed in λ/r_0 unit, as a function of D/r_0 . The asymptotic value $4/\pi$ is indicated with an arrow. Dotted line: blurring due to diffraction by the telescope aperture alone.

that

$$\omega^2 \neq \omega_0^2 + \omega_m^2 \quad (7.74)$$

although such an equality has often been assumed by astronomers in the past. The equality would hold if ω , ω_0 and ω_m were defined as standard deviations. Unfortunately this is not possible since the variance of the spatial irradiance distribution in a long exposure point source image is infinite as it is in an Airy pattern.

The first measurements of blurring as a function of the telescope aperture are due to RÖSCH [1958a]. They were made at the Pic du Midi Observatory on the star α Lyrae. Rösch defines a blurring factor equal to the ratio of the width of the unperturbed Airy pattern to the measured

TABLE 3
Comparison between measurements of blurring by RÖSCH [1958a] and theory. A good fit is obtained when assuming $r_0 = 7.6$ cm.

Telescope diameter D	9 cm	18 cm	27 cm	36 cm	45 cm	54 cm
measured (RÖSCH [1958a])	0.96	0.70	0.51	0.37	0.30	0.23
Rösch's blurring factor	theoretical ($r_0 = 7.6$ cm)	0.90	0.74	0.54	0.40	0.29

width of the instantaneous image. Rösch's blurring factor can be easily read on Fig. 9 by measuring the distance between the curve of blurring and the dotted line. As shown on Table 3, a good fit is obtained with Rösch's measurements by assuming $r_0 = 7.6$ cm. RÖSCH [1958a] also measured image motion. His data agrees very well with a $D^{-\frac{1}{3}}$ law. Measurements of blurring and of image motion are widely used by astronomers to estimate image degradation by atmospheric turbulence (§ 10).

§ 8. Stellar Scintillation

A review of the properties of stellar scintillation has been done recently by JAKEMAN, PARRY, PIKE and PUSEY [1978]. Statistical properties of stellar scintillation have been experimentally investigated by many observers, mainly GAVIOLA [1949], NETTLEBALD [1951], MIKESELL, HOAG and HALL [1951], ELLISON and SEDDON [1952], ELLISON [1954], BUTLER [1952, 1954], MIKESELL [1955], ZHUKOVA [1958], BARNHART, KELLER and MITCHELL [1959], PROTHEROE [1955a, b; 1961a, b; 1964], PROTHEROE and CHEN [1960] and more recently by BUFTON and GENATT [1971], VERNIN and RODDIER [1973], ROCCA, RODDIER and VERNIN [1974], PATERNO [1976], JAKEMAN, PIKE and PUSEY [1976]. Comparisons with simultaneous in situ atmospheric soundings were made by BUFTON [1973b], BARLETTI, CEPPATELLI, PATERNO, RIGHINI and SPERONI [1977] and by VERNIN, BARLETTI, CEPPATELLI, PATERNO, RIGHINI and SPERONI [1979]. Experiments using stellar scintillation analysis as a means for remote sensing of atmospheric turbulence have been developed by ROCCA, RODDIER and VERNIN [1974], OCHS, TING-I-WANG, LAWRENCE and CLIFFORD [1976] and AZOUIT and VERNIN [1980]. The effects of scintillation on astronomical observations have been discussed by YOUNG [1967, 1969], SEDMAK [1973] and BELVEDERE and PATERNO [1976].

8.1. FIRST ORDER STATISTICS

The easiest quantity to measure is the "amount" of scintillation, or scintillation index σ_I^2 , defined as the variance of the relative irradiance fluctuations. It is related to the variance σ_x^2 of the relative amplitude fluctuations χ by

$$\sigma_I^2 = 4\sigma_x^2. \quad (8.1)$$

Since σ_x^2 is the integral of the power spectrum of X

$$\sigma_x^2 = \int d\mathbf{f} \cdot W_x(\mathbf{f}), \quad (8.2)$$

putting (7.26) into (8.2) and (8.1) and integrating over all directions in the frequency plane leads to

$$\sigma_I^2 = 8\pi \times 0.38\lambda^{-\frac{7}{6}} \int_0^\infty dh \cdot C_N^2(h) \int_0^\infty df \cdot f^{-\frac{5}{3}} (\sin \pi\lambda hf^2)^2. \quad (8.3)$$

Introducing the dimensionless variable $w = \pi\lambda hf^2$ gives

$$\sigma_I^2 = 12.5\lambda^{-\frac{7}{6}} \int_0^\infty dh \cdot h^{\frac{5}{6}} C_N^2(h) \int_0^\infty dw \cdot w^{-\frac{11}{6}} (\sin w)^2 \quad (8.4)$$

or, after integration,

$$\sigma_I^2 = 19.12\lambda^{-\frac{7}{6}} \int_0^\infty dh \cdot h^{\frac{5}{6}} C_N^2(h). \quad (8.5)$$

Fig. 10 shows a histogram of σ_I^2 values obtained by VERNIN [1979] in the visible, near the zenith over fifty-two nights. Typical values of σ_I^2 are of the order of 20%. σ_I^2 may be as low as a few percent under good seeing conditions. Eq. (8.5) shows that scintillation decreases with increasing wavelength and becomes very small in the infrared. Eq. (8.5) also shows that the contribution of a turbulence layer to scintillation increases with height as the 5/6 power. Fig. 11a illustrates the average contribution of atmospheric turbulence to scintillation as derived from Hufnagel's model, described in § 2.4 (Fig. 1) for nighttime. There are two maxima, one at 1.2 km and the other at 10.8 km, separated by a minimum at 5 km, showing that scintillation comes mainly from two different parts of the atmosphere: 25% comes from layers lower than 5 km, mainly in the 1–2 km range, while 75% comes from layers above 5 km, mainly in the tropopause and lower stratosphere.

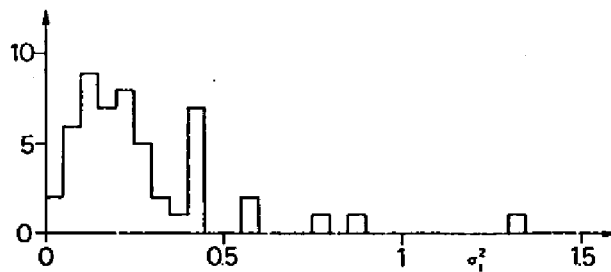


Fig. 10. Histogram of scintillation indexes observed over fifty-two nights by VERNIN [1979].

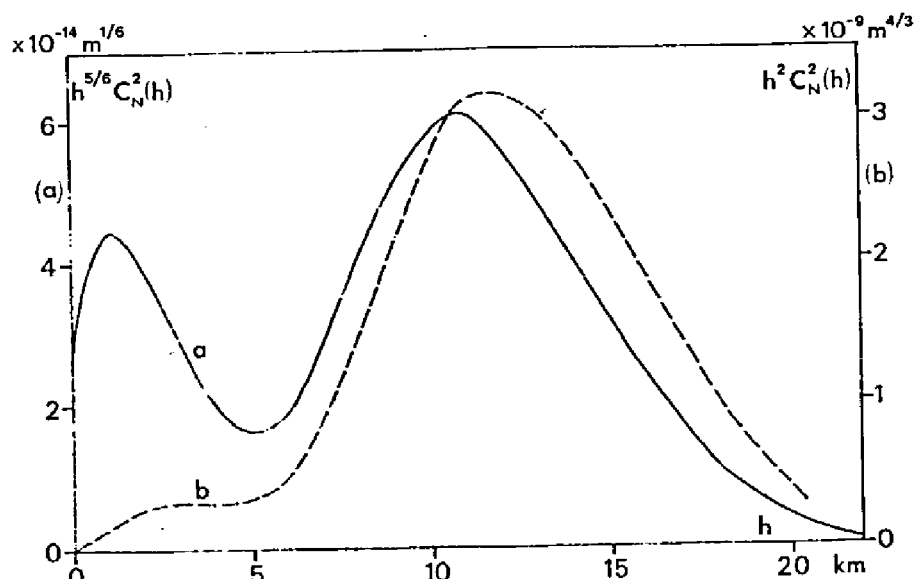


Fig. 11. Average contribution of atmospheric turbulence to stellar scintillation, according to Hufnagel's model; (a) as seen through a small aperture, (b) as seen through a large aperture.

It must be remembered that the results stated above are valid only when irradiance fluctuations are measured through an aperture smaller than their typical scale (in actual practice the aperture diameter must be smaller than or equal to about 3 cm). When a larger telescope is used, high spatial frequency components are smoothed out. Aperture filtering has been described by TATARSKI [1961], YOUNG [1970] and FRIED [1973] and experimentally investigated by YOUNG [1967], MINOTT [1972], BUFTON and GENATT [1971] and IYER and BUFTON [1977]. The telescope filtering function $G(f/f_c) = |\tilde{P}_0(f)|^2$ must be introduced in (8.3). When the aperture frequency cut-off f_c (of the order of the inverse \mathbb{D}^{-1} of the aperture diameter \mathbb{D}) is small enough so that

$$\pi\lambda hf_c^2 \ll 1 \quad (8.6)$$

then the approximation

$$(\sin \pi\lambda hf^2)^2 \approx \pi^2 \lambda^2 h^2 f^4 \quad (8.7)$$

can be used in (8.3) which becomes

$$\sigma_I^2 = 95 \int_0^\infty dh \cdot h^2 C_N^2(h) \int_0^\infty df \cdot f^3 G(f/f_c) \quad (8.8)$$

or, introducing the dimensionless parameter $a = f/f_c$

$$\sigma_I^2 = 95 f_c^7 \int_0^\infty dh \cdot h^2 C_N^2(h) \int da \cdot a^4 G(a) \quad (8.9)$$

or

$$\sigma_I^2 \propto D^{-\frac{2}{3}} \int dh \cdot h^2 C_N^2(h). \quad (8.10)$$

The approximation (8.7) is called the geometrical approximation since it can be derived from geometrical optics (REIGER [1962, 1963]). From (8.6), it is valid whenever $D \gg (\pi \lambda h)^{\frac{1}{2}}$, that is, taking $\lambda = 0.5 \mu\text{m}$ and $h = 10 \text{ km}$, $D \gg 13 \text{ cm}$. Eq. (8.10) shows that, in such a case, the amount of scintillation is independent of wavelength and decreases when the aperture diameter D increases, according to a $-\frac{2}{3}$ power law. Eq. (8.10) also show that, for large apertures, the contribution of turbulent layers to scintillation increases with height h as h^2 instead of $h^{\frac{5}{3}}$. Fig. 11b shows the average contribution of atmospheric turbulence, in this case, as derived from Hufnagel's model. The effect of low altitude layers is clearly filtered out. Experimental checks of the h^2 and $h^{\frac{5}{3}}$ laws have been made by BUFTON [1973b] and by BARLETTI, CEPPATELLI, PATERNO, RIGHINI and SPERONI [1977].

Expressions (8.5) and (8.10) have been established for stellar scintillation at the zenith. It remains valid at any zenith angle γ by taking h as a distance along the line of sight. Replacing h by $h/\cos \gamma$, eqs. (8.5) and (8.10) take the more general form

$$\sigma_I^2 = 19.2 \lambda^{-\frac{2}{3}} (\cos \gamma)^{-\frac{11}{6}} \int_0^\infty dh \cdot h^{\frac{5}{3}} C_N^2(h) \quad (8.11)$$

$$\sigma_I^2 \propto D^{-\frac{2}{3}} (\cos \gamma)^{-3} \int_0^\infty dh \cdot h^2 C_N^2(h). \quad (8.12)$$

Such a dependence on zenith angle was first derived by TATARSKI [1961] and found in reasonable agreement with observations up to $\gamma \approx 60^\circ$. At greater zenith angles σ_I^2 increases less rapidly and even saturates. As already quoted, the phenomenon of saturation of scintillation has been extensively studied on horizontal laser beam propagation (see for instance CLIFFORD, OCHS and LAWRENCE [1974]). In the case of astronomical observations it has been studied by YOUNG [1970] and more recently by PARRY, WALKER and SCADDAN [1979]. To my knowledge, modern theories on saturation (STROHBEHN [1978]) have not yet been applied to the study of stellar scintillation.

The small perturbation theory predicts log-normal statistics for the irradiance fluctuations. The probability density function (p.d.f.) of stellar scintillation has been experimentally investigated by JAKEMAN, PIKE and

PUSEY [1976], JAKEMAN, PARRY, PIKE and PUSEY [1978] and VERNIN [1979]. Results are found to agree well with a log-normal law far from the saturation regime. The Rice distribution is clearly excluded. At large zenith distances, where saturation occurs, data approximately fit a *K* distribution (JAKEMAN and PUSEY [1976]).

8.2. SECOND ORDER STATISTICS

According to (7.26) the spatial power spectrum of the relative irradiance fluctuations is given by

$$W(f) = 4W_x(f) = 3.9 \times 10^{-2} k^2 f^{-\frac{11}{3}} \int_0^\infty dh \cdot C_N^2(h) (\sin \pi \lambda h f^2)^2. \quad (8.13)$$

Fig. 12 shows theoretical spatial spectra that would produce a single turbulent layer at several altitudes. The increase of the fluctuation energy

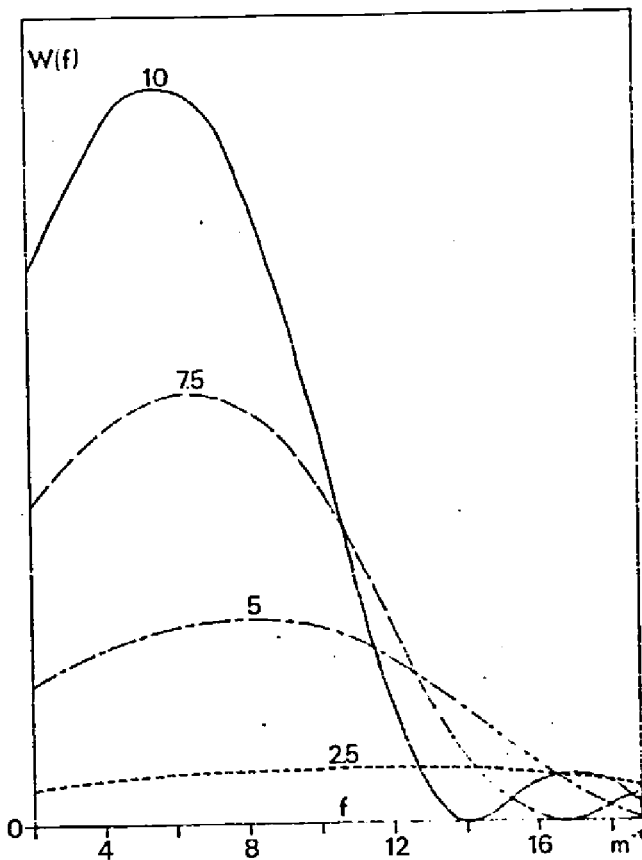


Fig. 12. Theoretical spatial power spectra of stellar shadow patterns, in arbitrary scale, assuming a thin turbulent layer at the latitude indicated in km on each curve (2.5, 5, 7.5 and 10 km). The integral $\int dh \cdot C_N^2(h)$ over the layer thickness is assumed to be the same in each case.

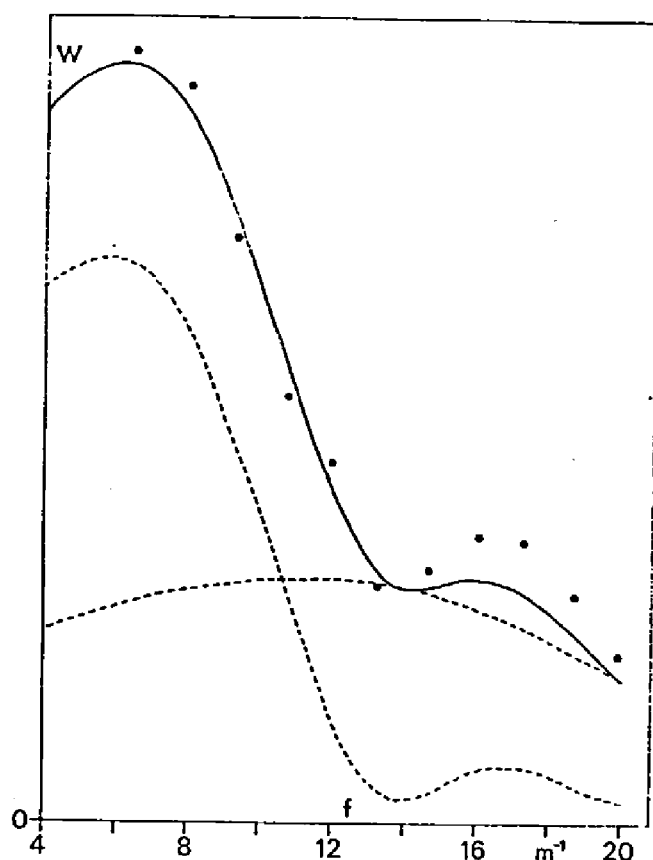


Fig. 13. Typical spatial power spectrum of stellar shadow patterns. Full circles: data from VERNIN and RODDIER [1973]. Solid line: theoretical spectrum assuming two turbulent layers at altitudes 2.5 km and 10 km. Dotted lines: assumed contribution of each layer.

with the altitude is clearly visible. Fig. 12 also shows that the frequency of the energy maximum decreases when the altitude increases. There are few experimental measurements of the spatial spectrum of scintillation. The first measurements were made by PROTHEROE [1961a, b; 1964]. Fig. 13 shows experimental data obtained by Vernin using an improved version of Protheroe's technique described in VERNIN and RODDIER [1973]. A good fit with theory is obtained by assuming that the scintillation is produced by two turbulent layers at approximate altitudes of 2.5 km and 10 km in agreement with the average behaviour described in Fig. 11a (see also TOWNSEND [1965]).

The spatial covariance of irradiance fluctuations is given by the two-dimensional Fourier transform of (8.13). Fig. 14 shows the result of numerical computations for a single turbulent layer at several altitudes. The characteristic size of the shadow pattern clearly increases with the altitude of the layer. Visual observation of shadow patterns often reveals several patterns propagating in different directions. Patterns displaying large shadows can clearly be attributed to turbulence at the tropopause

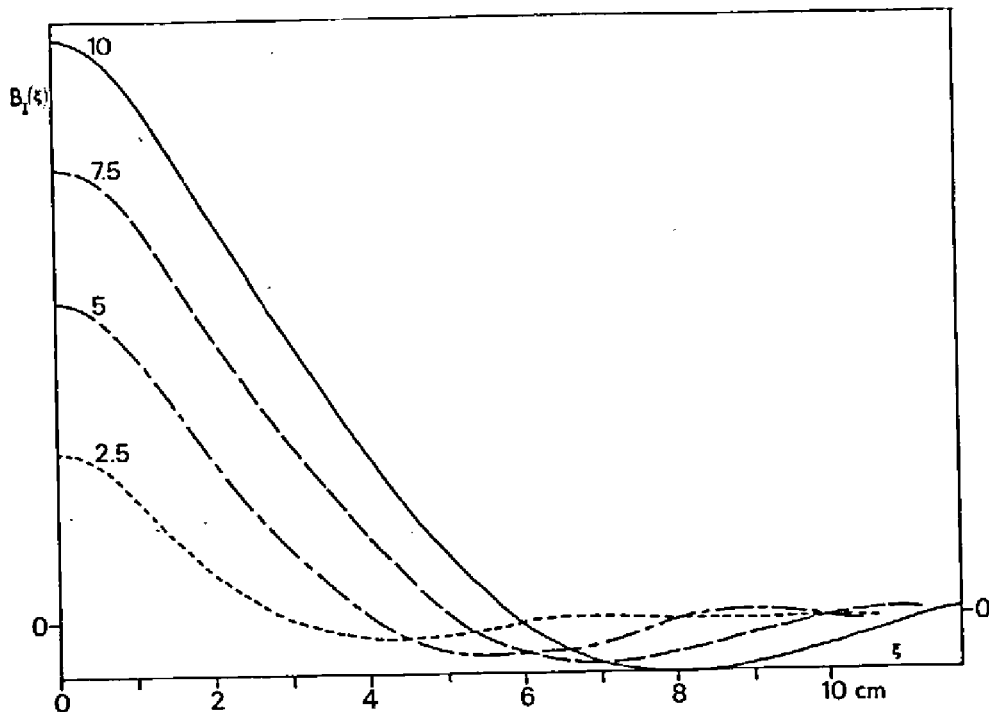


Fig. 14. Theoretical spatial covariance of stellar shadow patterns in arbitrary scale, assuming a thin turbulent layer at the altitude indicated in km on each curve (2.5, 5, 7.5 and 10 km). The integral $\int dh \cdot C_N^2(h)$ over the layer thickness is assumed to be the same in each case.

level, whereas patterns displaying small shadows are produced by low altitude turbulence. Experimental measurements of the spatial covariance were first made by PROTHEROE [1955b] and by BARNHART, KELLER and MITCHELL [1959]. Again experimental results can be interpreted in terms of an appropriate C_N^2 profile.

The problem of inverting the integral in (8.13) in order to derive C_N^2 profiles from experimental spatial spectra or spatial covariance has been discussed by PESKOFF [1968] and FRIED [1969]. The poor accuracy of the method has been underlined by STROHBEHN [1970c]. However, by using combinations of appropriate spatial filters, OCHS, TING-I-WANG, LAWRENCE and CLIFFORD [1976] were able to obtain C_N^2 profiles with about 4 degrees of freedom. Systematic measurements have been done by LOOS and HOGGE [1979]. Spatio-temporal and spatio-angular analysis provide additional useful information for remote sensing of atmospheric turbulence. To a good approximation, the time behaviour of shadow patterns is entirely described by the motion of the wind driven atmospheric inhomogeneities. Fig. 15 shows a two-dimensional spatio-temporal spectrum obtained by VERNIN and RODDIER [1973]. It reveals two different contributions. The associated wind speed and altitudes deduced from the spectrum are in good agreement with meteorological soundings. Fig. 16

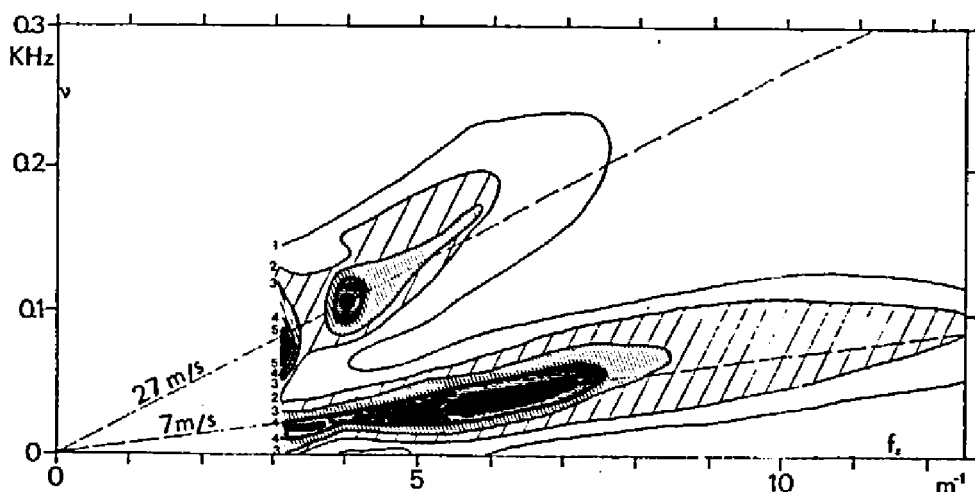


Fig. 15. Two-dimensional spatio-temporal power spectrum of stellar shadow patterns obtained by VERNIN and RODDIER [1973]. Lines of equal power are displayed in a temporal-frequency versus spatial-frequency plot. The spectrum shows evidence for two structures propagating at different speeds. Their velocities projected along γ_x are given by the slope of the dashed line as indicated. They agree with wind velocities at altitudes of 5 and 10 km, as observed in meteorological soundings. Similar altitudes are deduced from the shape of the spatial spectrum associated with each structure.

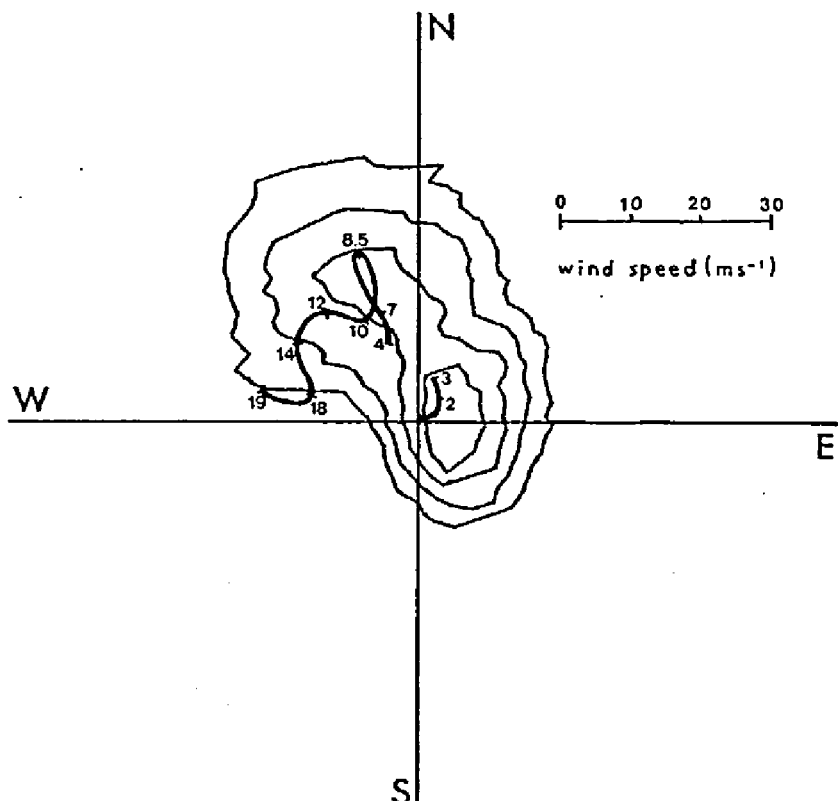


Fig. 16. Two-dimensional spatio-temporal correlation of stellar shadow patterns obtained by AZOURI and VERNIN [1980]. Thin lines: curves of equal correlation for a given time delay $\tau = 4$ ms. Thick line: wind hodograph from meteorological soundings with altitudes indicated in km. In this case, scintillation originates partly from turbulence around 2 km and partly from turbulence near the tropopause.

shows a spatio-temporal covariance, for a given delay $\tau = 4$ ms, obtained by AZOUI and VERNIN [1980]. It also reveals two contributions and their associated wind speed. Altitudes are deduced from meteorological wind hodographs. Spatio-angular analysis on double stars seems highly promising. This technique, first described by ROCCA, RODDIER and VERNIN [1974], allowed AZOUI and VERNIN [1980] to obtain a C_N^2 profile every 10 s with a resolution of 2 km. A typical result, displayed as a time sequence, is presented in Fig. 17.

Since scintillation is a noise source in high speed stellar photometry, purely temporal power spectra are of interest to astronomers. Such measurements have been performed mainly by MIKESELL, HOAG and HALL [1951], MIKESELL [1955], YOUNG [1967] and more recently by PATERNO [1976]. The behaviour of scintillation spectra with the telescope aperture has been theoretically investigated by TATARSKI [1961], REIGER [1962, 1963] and by YOUNG [1967, 1969]. Assuming a single wind velocity v in the x direction, the photoelectric signal is given by

$$Q(t) = F(vt, 0) \quad (8.14)$$

where

$$F(x, y) = \mathcal{J}(x, y) * P(x, y) \quad (8.15)$$

is the convolution of the irradiance $\mathcal{J}(x, y)$ on the aperture plane with the aperture transmission function $P(x, y)$. The power spectrum $W_Q(\nu)$ of

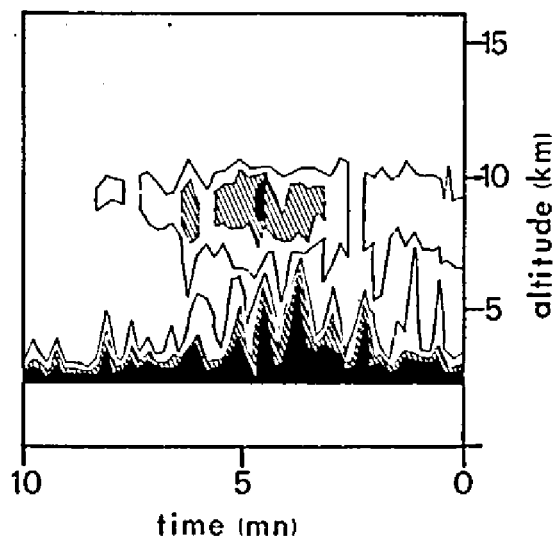


Fig. 17. Time sequence showing the evolution of turbulent layers producing stellar scintillation, from AZOUI and VERNIN [1980]. A C_N^2 profile is obtained every 10 s, with a vertical resolution of about 2 km, from a statistical analysis of the shadow pattern produced by a double star.

$Q(t)$ is therefore

$$W_Q(\nu) = \nu^{-1} \int df_y \cdot W(\nu/v, f_y) |\tilde{P}(\nu/v, f_y)|^2 \quad (8.16)$$

where $W(f_x, f_y)$ is the spatial power spectrum described by (8.13). In the case of a full circular aperture of diameter D , without a central obscuration, the aperture filter function is given by

$$|\tilde{P}(f_x, f_y)|^2 = (D^2/4) |J_1(\pi D f)/f|^2. \quad (8.17)$$

It decreases as the -4 power of the spatial frequency $f = (f_x^2 + f_y^2)^{\frac{1}{2}}$. When the aperture is large, high spatial frequencies are filtered out. According to (8.13), $W(f)$ varies as $f^{\frac{1}{3}}$ in its low frequency part. The product $W(f) |\tilde{P}(f)|^2$ therefore decreases as $f^{-\frac{11}{3}}$ and its integral over f_y decreases as $f^{-\frac{8}{3}}$. Scintillation amplitude spectra [$W(\nu)$] $^{\frac{1}{2}}$ are therefore expected to decrease as $\nu^{-\frac{1}{3}}$. Spectral indexes ranging from -1.5 to -2.5 reported by PATERNO [1976] with 15 cm and 30 cm apertures probably indicate a significant contribution of stratospheric turbulence.

Detailed numerical computations assuming non-uniform wind profiles, and taking into account the telescope central obscuration, have been performed by YOUNG [1969] who also extended the theory to planetary scintillation.

§ 9. Applications to High Resolution Imaging

Many methods have been attempted in order to improve the angular resolution of astronomical observations through atmospheric turbulence. In this section, we shall review these methods in the light of the theory developed in the preceding sections. It will be shown how the parameters describing image degradation limit the possibilities of image restoration.

9.1. CLASSICAL METHODS

A discussion on classical techniques can be found in RÖSCH [1972] and YOUNG [1974]. Expression (4.1) shows that a long exposure image can be restored by deconvolution or Wiener filtering. This has been achieved by HARRIS [1966], MUELLER and REYNOLDS [1967] and McGlamery [1967], with images degraded by laboratory-generated turbulence. It is now also

used for imaging in astronomy (COUPINOT [1973], COUPINOT and HECQUET [1979], HAWKINS [1979]). The point spread function can either be obtained from a reference point source (MUELLER and REYNOLDS [1967]) or be estimated from a priori knowledge of the object (COUPINOT [1973]). It may also be obtained by empirically adjusting a parameter in a theoretical model (HARRIS [1966]). The two-dimensional Fourier transform of the point spread function is the optical transfer function. Its shape is generally assumed to be Gaussian. Fried's theoretical expression (4.22) has – to my knowledge – never been used in a deconvolution procedure.

From the preceding sections, we draw the following conclusions. Fried's theoretical transfer function has been accurately confirmed by experiment. It should therefore be employed in any deconvolution procedure. In certain cases considerable differences might arise if a deconvolved image were obtained using Fried's model instead of that obtained with an assumed Gaussian transfer function. Fried's parameter r_0 can be estimated either from a priori knowledge of the object or from simultaneous measurements of a reference point source. The importance of simultaneity must be underlined because of the great variability of this parameter (KARO and SCHNEIDERMAN [1976a], MILLER and ZIESKE [1977], RICORT and AIME [1979]). Techniques for measuring r_0 are reviewed in § 10. The exponential decrease of the modulation transfer function described by (4.22) implies that the high frequency components of the image become rapidly buried by detector noise. A very low noise level and a good linearity are both essential to an efficient deconvolution. In the case of ultimate photon noise limitation, GOODMAN and BELSHER [1976a, b] have derived an expression for the maximum restorable frequency. In the case of a high signal-to-noise ratio, improved resolution could be obtained by using non-linear techniques, taking into account a priori knowledge of the object (positivity, finite extent) as shown by radio-astronomers (BIRAUD [1969]).

Expression (5.1) shows that – within the limits of isoplanicity – short exposure images can also be restored by deconvolution. In this case, however, the point-spread function has a complicated speckle structure and a reference point source is needed within the isoplanatic patch. Such a deconvolution has been performed by McGlamery [1967] with images degraded by laboratory-generated turbulence. He obtained better results from short exposures than from long exposures, confirming that higher spatial frequencies are recorded in short exposures. Unfortunately astronomical sources are too faint and the isoplanatic patch is too small for

the method to be practicable in astronomy. It becomes practicable when sequences of many short exposures are used, as shown by WEIGELT [1978c].

A method commonly used in astronomy, at least for solar observations (MULLER [1973]), is frame selection. It consists in selecting the best frames in a sequence of many short exposures. The probability of getting a good picture has been theoretically investigated by FRIED [1978]. He defines a good image as one for which the squared wave-front distortion over the aperture is 1 rad^2 or less, and finds that, if the aperture diameter D is greater than $3.5r_0$, the probability of getting such an image is approximately $5.6 \exp[-0.1557(D/r_0)^2]$. For example, with a 40 cm aperture in very good daytime seeing conditions ($r_0 = 8 \text{ cm}$), one image out of ten is good, in reasonable agreement with observations. With $r_0 = 4 \text{ cm}$ (average daytime conditions at a good site), the probability falls to 10^{-6} . The same 10^{-6} probability holds for a larger aperture $D = 80 \text{ cm}$ in very good seeing conditions ($r_0 = 8 \text{ cm}$). This explains why solar astronomers tend to reduce their aperture in order to obtain better images. Selection of the best frames in a sequence of short exposures is effective for bright objects, when $D/r_0 \leq 6$. Owing to the recent advances in I.R. imaging devices, it will probably be an effective method for imaging bright I.R. sources through large telescopes. Indeed, $r_0 = 13 \text{ cm}$ at $\lambda = 0.5 \mu\text{m}$ corresponds to $r_0 = 77 \text{ cm}$ at $2.2 \mu\text{m}$ so that, for a 3.60 m aperture, $D/r_0 \approx 4.7$.

Planetary surfaces are too faint to be properly recorded by a single short exposure. However, composite pictures can be obtained by adding many frames, each being recentred in order to cancel the effect of image wander. The associated transfer function, derived by FRIED [1966], is given by (5.18). Photon noise limitation has also been discussed for this case by GOODMAN and BELSHER [1976a, b]. The maximum increase in resolution is of the order of 2 and occurs when $D/r_0 \approx 3$. Combined with frame selection, the technique should be effective up to $D/r_0 \approx 6$. Image recentring can be obtained automatically, using a high speed servomechanism. This is the simplest form of active or adaptive optics.

9.2. ADAPTIVE OPTICS

Adaptive optical systems are those in which real-time control over optical wavefronts is employed to maximise the angular resolving power of a telescope viewing through atmospheric turbulence. Images are not

only centred but also sharpened. This is achieved by real-time modification of the shape of an optical component, which cancels the wavefront aberrations introduced by turbulence. The beginning of adaptive optics dates from the work of BABCOCK [1953, 1958]. The present state of the art has been reviewed by HARDY [1978a, b]. A special issue of the Journal of the Optical Society of America (Vol. 67, no 3 (1977)) and a meeting of the Society of Photo-optical Instrumentation Engineers (1978) have been dedicated to this topic. Applications to solar observations are discussed by HARVEY [1978].

The necessary performances of an adaptive system are entirely dictated by the statistical properties of wavefront perturbations described in the previous sections. Fried's parameter r_0 again plays a central role. Since r_0 is the diameter of a coherent cell, the number of independently controllable elements required to correct a filled aperture of diameter D is about $(D/r_0)^2$. According to eq. (7.38) in § 7.4, the standard deviation of the optical path difference σ_z over a baseline D is independent of wavelength and equal to $(2.62/2\pi)\lambda_0(D/r_0)^{1/2}$. The peak-to-peak amplitude of the corrections to be made is at least three times larger, that is about ten wavelengths for $D/r_0 = 12$. The perturbations of wavefront amplitudes are negligible and can be ignored as shown in § 7.3.

The response time of the servomechanism is dictated by the "Eulerian" evolution time of wavefront perturbations, or transit time of perturbations over a coherence cell. It is of the order of r_0/v , where v is the typical wind speed of turbulent layers, and may vary from 1 to 10 ms or more, according to weather conditions. It is a little shorter than the speckle lifetime which is related to the "Lagrangian" evolution time of wavefront perturbations and is approximately $r_0/\Delta v$, Δv being the velocity dispersion, as seen in § 6. Corrections made in the pupil plane are valid only within an isoplanatic patch. The effect of non-isoplanicity for adaptive optics has been studied by FRIED [1974, 1975]. The isoplanatic patch size has been found to be essentially the same as that for speckle interferometry (FRIED [1979]). However, the isoplanatic patch can be much wider if several corrections are made along planes conjugate to the locations of turbulence layers. Photon-noise limitations are discussed by GOODMAN and BELSHER [1976a].

Many wavefront correction devices have been developed in order to meet all these requirements. The most successful are active mirrors including segmented mirrors, continuous thin-plate mirrors, monolithic mirrors and membrane or pellicle mirrors. The corrections to be applied

can be determined either by using a wavefront sensing device or by trial and error using an image-sharpening algorithm. For astronomical applications only white-light wavefront sensors, such as Hartmann tests or achromatic interferometers, can be used. Their sensitivity decreases as the inverse of the object size so that, for large objects, image-sharpening algorithms are necessary. Using such techniques, Buffington and his co-workers (MULLER and BUFFINGTON [1974], BUFFINGTON, CRAWFORD, MULLER, SCHWEMIN and SMITS [1977], BUFFINGTON, CRAWFORD, MULLER and ORTH [1977], POLLAIN, BUFFINGTON and CRAWFORD [1979]) have been able to sharpen, in real time, images of single stars (Sirius, Arcturus) and of double stars (α Gem, γ Leo).

9.3. MICHELSON INTERFEROMETRY

Interferometric techniques have already been reviewed by LABEYRIE [1976, 1978]. Applications to solar astronomy are reviewed by F. RODDIER [1978a]. Recent advances are presented in the proceedings of the I.A.U. Colloquium no 50 (DAVIS and TANGO [1979]). Here, we shall mainly discuss the limitations due to atmospheric turbulence. The principle of Michelson interferometry has been described in details in § 4.4. In Michelson's original experiment (MICHELSON [1920], ANDERSON [1920], MICHELSON and PEASE [1921]) the fringe visibility was estimated visually. More recently HARVEY [1972], using the same technique, qualitatively demonstrated the existence of solar features with dimensions of about 100 km or smaller. In § 4.4 we have shown how atmospheric effects can be eliminated in order to make quantitative astronomical measurements. Such measurements had not been attempted until recently, namely by CURRIE, KNAPP and LIEWER [1974] who measured stellar diameters, by KINAHAN [1976] and AIME, RICORT and GREC [1975, 1977] who derived the power spectrum of solar granulation, and by McCARTHY and LOW [1975] and McCARTHY, LOW and HOWELL [1977] who measured stellar envelopes in the infrared. Corrections for atmospheric turbulence can be avoided only if the diameter of the two apertures is much smaller than r_0 , in which case the signal-to-noise ratio is low.

Photon noise limitation has been discussed by GOODMAN and BELSHER [1976a]. At low light level the signal-to-noise ratio is proportional to the number of photons received per "exposure" (see also AIME and RODDIER [1977]). For a given optical bandwidth and a given exposure time, it is

proportional to r_0^2 since the area of the apertures should be comparable in size with r_0 for optimal results. The "exposure time", or maximum integration time allowing fringes to be frozen, is dictated by the transit time of perturbations over the aperture, as for adaptive optics. It is therefore of the order of r_0/v (v being the velocity of the perturbations). When fringes are scanned, it is proportional to r_0^2 as shown by AIME [1978]. For small objects, the optical bandwidth $\Delta\lambda$ is restricted by the condition that the beams from the two apertures must interfere, in spite of the optical path difference σ_z introduced by turbulence. It is therefore proportional to $\lambda^2\sigma_z^{-1}$ or, taking (7.38) into account, for a baseline L ,

$$\Delta\lambda \propto (r_0/L)^{\frac{1}{2}}. \quad (9.1)$$

Since the number of photons per "exposure" is proportional to the aperture area, the exposure time and the bandwidth, the signal-to-noise ratio is proportional to

$$S/N \propto r_0^2(r_0/v)(r_0/L)^{\frac{1}{2}} = r_0^{2.5}v^{-1}L^{-\frac{1}{2}}. \quad (9.2)$$

It increases almost as the fourth power of r_0 . The signal-to-noise ratio is also proportional to the square root of the observation time. In order to obtain a given signal-to-noise ratio, the necessary observation time will therefore increase almost as the 8th power of r_0 . As we shall see, the same result stands for speckle interferometry, thus underlining the fundamental importance of good seeing conditions. The size of the isoplanatic patch for Michelson interferometry does not yet seem to have been considered in the literature. Since Michelson interferometry is a special case of speckle interferometry, it is very likely to be of the same order of magnitude.

An important drawback to Michelson's interferometry is that the Fourier space is explored sequentially. An alternative method envisaged by RUSSELL and GOODMAN [1971] consists of using multiple small apertures. As shown in § 5.2, there is no attenuation of the object Fourier components, as long as the array of apertures is non-redundant. However, the number of Fourier components which can be measured at the same time remains limited. This drawback can be overcome by using shearing interferometers. Such interferometers have already been used for astronomical observation (SAUNDERS [1964, 1967], CURRIE, KNAPP and LIEWER [1974]). They have been suggested as an alternative for speckle interferometry by KENKNIGHT [1972, 1975] and BRECKINRIDGE [1972,

[†] Note the steep improvement of tolerances with increasing wavelength.

1974] as they are equivalent to a large number of Michelson interferometers working together. F. RODDIER and C. RODDIER [1978] have underlined the advantages of a variable rotational shear, and have shown that fringes can be obtained with a wide optical bandwidth by means of a chromatic corrector (see also F. RODDIER [1978b]). The limitations due to atmospheric turbulence are exactly the same as for classical Michelson interferometry.

The main advantage of the two-aperture scheme is that the baseline can be considerably extended as was done by MICHELSON and PEASE [1921] or more recently by LABEYRIE [1975]. Mechanical and atmospheric instabilities are the two main difficulties to overcome. Heterodyne detection solves the problem of mechanical stability at the cost of a drastically reduced bandwidth. The effects of atmospheric turbulence on heterodyne detection are discussed by FRIED [1967] and RABBIA [1978]. The technique has been used in the infrared (SUTTON [1978], ASSUS, CHOPLIN, CORTEGGIANI, CUOT, GAY, JOURNET, MERLIN and RABBIA [1979]). Homodyne detection (or intensity interferometry) solves both the mechanical and the atmospheric problems at the cost of very low sensitivity (HANBURY BROWN [1977, 1978]). The best signal-to-noise ratios are obtained by direct optical interference. The recent success of Labeyrie's two-telescope experiment has opened new hopes and initiated new projects in the visible (University of Maryland, University of Sydney) as well as in the infrared (C.E.R.G.A., Berkeley, Imperial College). Due to the optical bandwidth limitation, the signal-to-noise ratio should decrease as $L^{-\frac{2}{3}}$ (eq. (9.2)) as long as the baseline is much smaller than the outer scale of atmospheric turbulence. The baseline at which the outer scale begins to play a role is still unknown.

LABEYRIE [1974] suggested applying speckle interferometric techniques to long-baseline interferometry with large apertures. The associated theory has been developed by C. RODDIER and F. RODDIER [1976a, b]. They have shown that if the wavefront perturbations on the two apertures are uncorrelated, atmospheric effects are eliminated by defining the fringe contrast as the ratio of high spatial frequency energy of short exposures to the low frequency energy of long exposures. GREENAWAY and DAINTY [1978] have investigated the use of an interferometer working in the pupil space. The signal-to-noise ratios are essentially the same in both cases (DAINTY and GREENAWAY [1978]).

The concept of a telescope array as the basis for a "Next Generation Telescope" has recently attracted attention (PACINI, RICHTER and WILSON [1978]) and the construction of coherent arrays has been envisaged

(LABEYRIE [1977], GUSH [1979]). The effect of atmospheric turbulence on a telescope array has been investigated by F. RODDIER [1974] in the case of small apertures and by AIME and RODDIER [1976] in the case of large apertures. For non-redundant arrays the highest observing efficiency is achieved by arrays containing only a few elements. For highly-redundant arrays, the efficiency is maximised by maximising the number of elements (GREENAWAY [1979]).

9.4. SPECKLE INTERFEROMETRY

The principle of stellar speckle interferometry is due to LABEYRIE [1970] who first recognised the similarity between short exposure stellar images and laser speckles. The method consists of a second order statistical analysis of the image speckle pattern. Short exposures are usually recorded photographically (GEZARI, LABEYRIE and STACHNIK [1972], BRECKINRIDGE, McALISTER and ROBINSON [1979], BEDDOES, DAINTY, MORGAN and SCADDAN [1976], WEIGELT [1978a, b], BALEGA and TIKHONOV [1977]). The image energy spectrum is then obtained by optical processing. The use of a television camera has been initiated by LABEYRIE [1974] and by KARO and SCHNEIDERMAN [1976b]. Electronic image processors have been built in order to compute in real time the energy spectrum of the autocorrelation function of speckled images. On-line digital correlation of photon counting T.V. images, as described by BLAZIT, KOECHLIN and ONETO [1975], seems to be the most promising technique for faint objects. Better photometric accuracy is obtained by photoelectric scans, as pointed out by AIME and RODDIER [1977]. They suggest one-dimensional scans as a good compromise between Michelson interferometry and two-dimensional speckle interferometry. This technique, which has been found valuable for the study of solar granulation (RICORT and AIME [1979]), may provide the best accuracy for the observation of bright objects (see also AIME, KADIRI, RICORT, VERNIN and RODDIER [1979] and KADIRI [1979]). One dimensional scans have also been used for infrared speckle interferometry (SIBILLE, CHELLI and LENA [1979], WADE and SELBY [1978], SELBY, WADE and SANCHEZ MAGRO [1979]). Recent advances in I.R. diode arrays make I.R. speckle interferometry very promising.

Signal-to-noise ratio in speckle interferometry has been studied by many authors. Assuming photon-noise limitation, the uncertainty on the autocorrelation function has been derived more or less heuristically by

LABEYRIE [1974] and DAINTY [1974]. The uncertainty on the energy spectrum has been derived by F. RODDIER [1975] and by GOODMAN and BELSHER [1976a]. Since the autocorrelation function is an integral over all spatial frequencies, the S/N ratio in this quantity exceeds that in the energy spectrum by a factor equal to the square root of the number of speckles. The equivalence of the two expressions have recently been demonstrated by GREENAWAY and DAINTY [1978]. Consequences have been drawn by BARNETT and PARRY [1977] and by WALKER [1978, 1979] for the autocorrelation, by MILLER [1977], and by DAINTY and GREENAWAY [1978, 1979] for the energy spectrum. The signal-to-noise ratio for infrared speckle interferometry has been derived by SIBILLE, CHELLI and LENA [1979] (see also CHELLI [1979]). Whereas, in the visible, photon noise limitations imply that Michelson and speckle interferometry have a similar signal-to-noise ratio, background noise limitations afford the multiplex advantage to I.R. speckle interferometry.

Assuming photon noise only, the signal-to-noise ratio on the energy spectrum, at a very low light level, is proportional to the number of photons per speckle. For a given optical bandwidth and a given exposure time, it is therefore proportional to r_0^2 . The optical bandwidth limitation is similar to that for Michelson interferometry (KARO and SCHNEIDERMAN [1978]) as given by eq. (9.1). It increases as r_0^5 . As shown in § 6.4, the exposure time must be of the order of $r_0/\Delta v$, where Δv is the dispersion of wind velocities in turbulent layers. The signal-to-noise ratio therefore depends upon the atmospheric parameters r_0 and Δv as

$$S/N \propto r_0^{21} \Delta v^{-1}. \quad (9.3)$$

For a given S/N ratio, the observation time increases almost as the 8th power of r_0 , as for Michelson interferometry (§ 9.3).

Eq. (5.2) in § 5 implies that the object energy spectrum $|\tilde{O}(\gamma)|^2$ is obtained by dividing the image energy spectrum $\langle |\tilde{I}(\gamma)|^2 \rangle$ by the energy spectrum of a point source image $\langle |\tilde{S}(\gamma)|^2 \rangle$. The function $\langle |\tilde{S}(\gamma)|^2 \rangle$ describes the atmospheric attenuation of the object spectral components. Its determination remains a major experimental problem. In Labeyrie's initial experiment, calibration of the atmospheric attenuation was obtained by observing unresolved stars between each measurement. Unfortunately, atmospheric effects are often strongly time-dependent. They also depend upon the location of the observed star in the sky, or at least upon its distance from the zenith. Accurate calibration is therefore difficult.

WELTER and WORDEN [1978] have suggested taking the difference between the average autocorrelation of speckle patterns and the average cross-correlation of successive patterns as the autocorrelation for the image effectively uninfluenced by the atmosphere. Indeed, assuming that successive patterns are uncorrelated, their average cross-correlation is equal to the autocorrelation of the long exposure image. In the Fourier space, Welter and Worden's procedure is therefore equivalent to taking the difference between the short exposure spectrum and the long exposure spectrum. According to (5.15) it is effectively proportional to the unperturbed object spectrum multiplied by the diffraction limited transfer function of the telescope. However eq. (5.15) assumes Gaussian statistics which are known to be unrealistic for wavefront perturbations. The low-frequency part of the short exposure spectrum is better represented by (5.18) such that an improvement of Welter and Worden's procedure would consist in subtracting the cross-correlation of successive recentred patterns. Moreover, the short exposure energy spectrum $\langle |\tilde{S}(\gamma)|^2 \rangle$ is often wrongly normalised to unity at the origin, as the long exposure spectrum $\langle \tilde{S}(\gamma) \rangle^2$. In the subtraction, low frequencies are thus incorrectly eliminated. The difference $\langle |\tilde{S}(0)|^2 \rangle - \langle \tilde{S}(0) \rangle^2$ represents the variance of the illumination integrated over the telescope pupil. In the Gaussian approximation (5.15) it is equal to σ/\mathcal{S} and cannot be neglected. Similar criticisms of Welter and Worden's procedure have been made by FANTE [1979] and by BRUCK and SODIN [1980]. Bruck and Sodin suggest a procedure minimising the observed width of the object autocorrelation.

The good agreement recently obtained between observed and theoretical transfer functions, assuming log-normal statistics (AIME, KADIRI, RICORT, RODDIER and VERNIN [1979], CHELLI, LENA, F. RODDIER, C. RODDIER and SIBILLE [1979]) suggests that these theoretical transfer functions could be used to restore information. Only Fried's seeing parameter r_0 needs to be measured. It can be determined simultaneously and independently of the observations or it can be derived from the observations themselves using a known part of the object spectrum, such as the low frequency part, or using a value measured with a Michelson interferometer. A self calibration method has been worked out by RICORT and AIME [1979], based on the consistency of the results obtained from different seeing conditions.

However, theoretical transfer functions apply only to ideal conditions. Corrections for finite optical bandwidths and finite exposure time may be necessary. Focusing errors and telescope aberrations also play a role

when the seeing disk becomes of the order of the transverse aberration (DAINTY [1974], KARO and SCHNEIDERMAN [1977], F. RODDIER, RICORT and C. RODDIER [1978]). The effects of non-isoplanicity as well as finite exposure time have been discussed in detail in § 6.

9.5. IMAGE RECONSTRUCTION

Classical interferometry or speckle interferometry give only the modulus of the Fourier transform of the intensity distribution in the observed object. Although images can be derived from such limited information (FIENUP [1978]), the solution is not in general unique (FIDDY and GREENAWAY [1978]). It may however be unique in many cases (GREENAWAY [1977], BATES, MILNER, LUND and SEAGAR [1978], BRUCK and SODIN [1979]). Techniques of phase recovery have long been developed by radioastronomers (VAN SCHOONEVELD [1979]) and similar techniques are now envisaged in optics. Many proposals have been made to extract the phase information from speckle images. They are reviewed by WORDEN [1977] and by NISENSON and STACHNIK [1979]. Some of them have already been applied to astronomy with some success (LYNDS, WORDEN and HARVEY [1976], WEIGELT [1978c]). The most general method, due to KNOX and THOMPSON [1974], has been applied to the restoration of sunspot images by STACHNIK, NISENSON, EHN, HUDGIN and SCHIRF [1977]. No expression for the signal-to-noise ratio in the Knox and Thompson procedure has yet been given in the literature. However its dependence upon atmospheric parameters is very likely to be the same as for speckle interferometry (eq. (9.3)).

§ 10. Seeing Monitors and Site Testing

Astronomers have long tried to estimate image degradation by atmospheric turbulence for various reasons, such as the choice of an observatory site, comparison between existing sites, selecting observations to be made under given seeing conditions, the decision as to whether an observation is possible, choosing the best instant for a measurement and the calibration of atmospheric effects.

Most of the classical methods of measuring image quality were developed in the early sixties with the intention of selecting optimal sites for the construction of new telescopes. These methods are reviewed by STOCK

and KELLER [1960], MEINEL [1960] and in the proceedings of the I.A.U. Symposium no 19 (RÖSCH, COURTES and DOMMANGET [1963]). The work of Soviet scientists is reviewed in KUCHEROV [1965]. Unfortunately, at that time, the physics of image degradation by atmospheric turbulence was still little understood and experimental efforts were essentially empirical. Questions which arose were: what should be measured? And, more importantly, how many parameters are needed to define the quality of an image? Most of the experimental attempts were based on image motion and blurring measurements. We now know that image motion and blurring are strictly related (§ 7.6) and that image quality can be almost entirely determined by a single parameter such as Fried's parameter r_0 . Other parameters of lesser importance are the size of the isoplanatic patch and the characteristic evolution time of the image structure. Fried's parameter is now universally adopted as a convenient measure of image quality. It can be deduced either directly, from optical measurements (seeing monitors), or indirectly from atmospheric soundings. Both types of measurements will be reviewed in this section.

10.1. SEEING MONITORS

Estimations of image quality are often made visually. Unfortunately, the appearance of the image depends strongly upon the aperture of the telescope. Through a large telescope the size ω of the seeing disk is often estimated by comparison with the known angular separation of a double star. The result slightly depends upon the stellar magnitude. Assuming negligible image motion, r_0 is known to be of the order of λ/ω with $\lambda \approx 0.5 \mu\text{m}$. A calibration by comparison with more quantitative estimates is highly recommended. Slow image motion is difficult to perceive. Inspection of Fig. 9 (p. 340) shows that it may not be negligible. Indeed visual estimations of image quality are known to be often optimistic. Corrections for image motion can be envisaged from the theoretical curves of Fig. 9. However, for large telescopes, care must be taken. In this case the theoretical value of image motion may be overestimated due to the finite outer scale of turbulence being neglected.

Through a small telescope, visual estimations of image quality are difficult and subject to errors. Experience shows that the quality of seeing is always overestimated. A method based on the appearance of stellar diffraction patterns has been proposed by Danjon. Unfortunately, this appearance is not only very sensitive to the telescope diameter but also to

the evolution time of the image structure which is of the order of the response time of the eye. Danjon's scale cannot therefore be calibrated purely in terms of r_0 . Solar observers are used to estimating image quality from the contrast of solar features, such as granulation or sunspot umbrae and penumbrae, and from the appearance of the solar limb. A scale has been proposed by Kiepenheuer. It is subject to the same criticism as Danjon's scale. Visual measurements of image motion with a micrometer probably give the most reliable results. An estimation of r_0 is obtained by means of eq. (7.54). Unfortunately this method is very sensitive to telescope vibrations due to wind shake. A differential method has been developed with a two-aperture telescope (STOCK and KELLER [1960]). It can be considered as a simplified Hartman test and will be discussed below.

Photographic methods are expected to give more quantitative results. In principle the size of the seeing disk can be measured on stellar photographs taken with a large telescope. Exposure times of at least 10 s take image motion into account and can be considered as long exposures. Unfortunately one encounters a considerable magnitude effect. In practice, the image size grows almost indefinitely with the increasing brightness of the stars. As quoted in § 4.5, the size of the seeing disk can be obtained only by a combination of measurements made on a carefully calibrated plate. On the other hand, exposures as short as a few milliseconds taken with an image intensifier reveal the speckle structure of the image. The area of the telescope aperture divided by the estimated number of speckles gives the wavefront coherence area σ , from which r_0 can be deduced by means of expression (5.13).

With small telescopes, the most widely used method consists in photographing star trails. The polar star is generally observed with a fixed telescope mounting. A systematic comparison with visual estimations of the size of the seeing disk through a large telescope has been reported by HARLAN and WALKER [1965]. Star trails provide a continuous record of image motion. Rapid motions are however filtered out. MORODER and RIGHINI [1973] state that the standard deviation measured on photographic plates is about half of that measured visually. After corrections, they derive estimations of r_0 by means of eq. (7.54). A more reliable method seems to derive the line spread function, and hence r_0 , as reported by WALTERS, FAVIER and HINES [1979].

Only photoelectric devices permit continuous monitoring of image quality. Their high sensitivity and small response time allow the instantaneous image structure to be frozen. With large telescopes, rapid scans

through a bright stellar image with a narrow slit give one-dimensional instantaneous intensity profiles. As shown by AIME, KADIRI, RICORT, RODDIER and VERNIN [1979], reliable speckle energy spectra are obtained by processing the signal through a spectrum analyser. Accurate values are obtained by fitting theoretical curves to observations. SCHNEIDERMAN and KARO [1978b] use a similar procedure with a T.V. camera. MILLER and ZIESKE [1977] have developed a seeing monitor in which spectrum analysis is obtained by scanning the stellar image with a variable spatial frequency spinning reticle. The spatial frequency at which the spectrum drops to one half is taken as a measure of blurring. Rapid photoelectric scans are also used to estimate the quality of the solar image through a large telescope. The observed contrast of the solar granulation is taken as a measure of the quality of the image. Theoretical computations have been done by RICORT, AIME, RODDIER and BORGNIKO [1980] in order to calibrate the observed contrast in terms of r_0 . Fig. 18 illustrates the result of their computations. Unfortunately the method is sensitive to scattered light. Spectrum analysis seems preferable to contrast measurements. Rapid image scans apply only to bright objects. When dealing with stars fainter than magnitude 3 or 4, the simplest approach seems to estimate the size of the long exposure seeing disk by measuring the stellar light through a series of diaphragms of different sizes. An iris diaphragm could

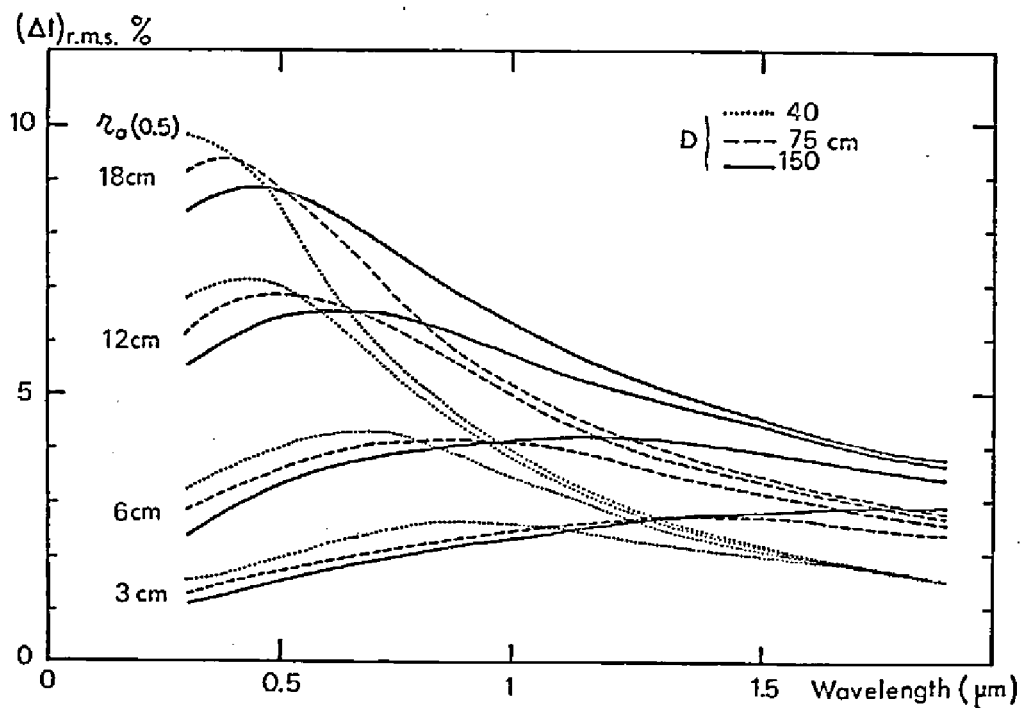


Fig. 18. Observed r.m.s. brightness fluctuations of the solar granulation in % of mean brightness, as a function of wavelength, for 3 telescope diameters and 4 values of r_0 (measured at $\lambda = 0.5 \mu m$), according RICORT, AIME, RODDIER and BORGNIKO [1980].

be automatically driven for continuous monitoring with a response time of the order of 10 s or more. Accurate tracking of the telescope is essential.

With a small telescope, most of the seeing effects appear as image motion. In the astronomical seeing monitor (A.S.M.) of BABCOCK [1963], the motion of a stellar image is measured and recorded with a photoelectric image follower. Babcock's A.S.M. was extensively used in Chile for site testing (IRWIN [1966]). Photoelectric recording of the motion of the solar limb was performed by KALLISTRATOVA [1966]. For the J.O.S.O. site testing campaign, BRANDT [1969, 1970] developed a similar technique allowing motion and blurring of the solar limb to be measured simultaneously. BRANDT [1969] also derived time frequency spectra of the image motion displaying considerable energy at very low frequencies, as could be expected from Kolmogorov's law. A maximum is expected at a frequency of the order of the ratio v/L_0 of the wind speed to the turbulence outer scale. It can easily be as low as 0.1 Hz, showing that integration times of at least 10 s are necessary in order to obtain reliable values for the standard deviation σ_m . BORGNI, VERNIN, AIME and RICORT [1979] have recently brought attention to the spatial and angular filtering associated with the use of a slit on the solar limb. Such filtering must be taken into account in the interpretation of the results.

Up until now, we have reviewed only seeing monitors working in the image plane and measuring atmospheric effects on the image structure. In fact, the best results have been obtained by directly measuring wavefront perturbations in the pupil plane. Hartmann tests have been used by RÖSCH [1954a, b]. However, quantitative statistical analysis of Hartmann photographs is time consuming. A simplified Hartmann test with two apertures can be made with a small, interferometer-like instrument (STOCK and KELLER [1960]). According to (7.54), (7.60) and (7.61), the mean squared amplitude of the relative longitudinal motion of the two stellar images is

$$2[B_\alpha(0, 0) - B_\alpha(\mu, 0)] = 2(\lambda/r_0)^{\frac{1}{3}}[0.18(\lambda/\mathbb{D})^{\frac{1}{3}} - 0.097(\lambda/\mu)^{\frac{1}{3}}] \quad (10.1)$$

and the mean squared amplitude of the relative transverse motion is

$$2[B_\beta(0, 0) - B_\beta(\mu, 0)] = 2(\lambda/r_0)^{\frac{1}{3}}[0.18(\lambda/\mathbb{D})^{\frac{1}{3}} - 0.145(\lambda/\mu)^{\frac{1}{3}}] \quad (10.2)$$

where \mathbb{D} is the diameter of each aperture, assumed to be small and μ the distance between the two apertures (see MILLER and KELLEN [1975]). More reliable estimations of r_0 would be obtained by using three or four

apertures and by following the procedure of BORGNIKO and VERNIN [1978]. The Foucault test, also called occultation, schlieren or stroboscopic technique, consists in focusing a star image onto a knife edge. Irradiance fluctuations proportional to the slope of the wavefront surface are observed in the pupil plane. The use of Foucault tests was also suggested by RÖSCH [1957]. For solar observations, a similar test can be done by observing the telescope pupil through a diaphragm or a slit at the solar limb as shown by KOZHEVNIKOV [1961] and BECKERS [1966]. This method allowed BORGNIKO and VERNIN [1978] to make quantitative estimations of the spatial covariance of angle-of-arrival fluctuations, providing evidence for the inertial structure of atmospheric turbulence. As a by-product, accurate r_0 values are obtained at the near field approximation. They can be used as a standard to calibrate image motion measurements made with a simpler instrument as shown by BORGNIKO, VERNIN, AIME and RICORT [1979]. The results have recently been found to be in excellent agreement with in situ thermal soundings (BORGNIKO, CEPPATELLI, RICORT and RIGHINI [1980]). When dealing with stellar sources, interferometric techniques are by far the most satisfying. The motion of fringes due to atmospheric turbulence was first investigated by DANJON [1955]. The last report is due to BRECKINRIDGE [1976]. Interferometric measurements of the atmospheric transfer function are reviewed in § 4.5. They are direct measurements of the coherence scale of wavefront perturbations according to the definition (4.23) of r_0 . The results must therefore be considered as primary standards from which any seeing monitor should be calibrated.

10.2. ATMOSPHERIC SOUNDINGS

Since the seeing parameter r_0 is related to the integral $\int dh \cdot C_N^2(h)$ of the structure constant of refractive index fluctuations by eq. (4.24), it can be deduced from atmospheric measurements of C_N^2 as a function of altitude. From § 2, we know that C_N^2 is essentially related to the structure constant C_T^2 of temperature fluctuations (eq. (2.16)). Measurements of C_T^2 are made with thin wire thermometers. Such microthermal sensors have been widely used in site testing campaigns. Lynds (in RÖSCH, COURTES and DOMMANGET [1963]) investigated temperature fluctuations in the surface boundary layer at Kitt Peak using seven sensors arrayed along the side of a vertical tower up to 22.5 m. COULMAN [1974] made microthermal measurements in the immediate vicinity of telescopes.

KIEPENHEUER [1972, 1973] made similar measurements from aircraft, for the J.O.S.O. site testing campaigns. For the same campaigns, BARLETTI, LEMMETI and PATERNO [1974] designed a balloon-borne radiosonde. Their results are summarised in a paper by BARLETTI, CEPPATELLI, PATERNO, RIGHINI and SPERONI [1977]. Since radars cannot be easily moved, they are of little use in site testing campaigns. Sodars were used during the J.O.S.O. campaigns. They have been found too sensitive to wind which blows out the return signal. Scintillation measurements have now been proved capable of yielding quantitative results. A comparison between Fig. 11a and 11b (p. 343) shows that scintillation measurements through a 30 cm aperture give the contribution of the tropopause, whereas simultaneous measurements with a 3 cm aperture would give the contribution of the planetary boundary layer by taking the difference. Although more sophisticated, the system developed by OCHS, TIN-I-WANG, LAWRENCE and CLIFFORD [1976] and extensively used by Loos and HOGGE [1979] would certainly be extremely useful in a site testing campaign. The method developed by ROCCA, RODDIER and VERNIN [1974] also gives wind velocities. It has been found to agree with in situ measurements (VERNIN, BARLETTI, CEPPATELLI, PATERNO, RIGHINI and SPERONI [1979]).

10.3. DISCUSSION

We shall now discuss the most appropriate method to be chosen according to the goals briefly outlined at the beginning of this section. For site testing, an approximate knowledge of the origin of atmospheric disturbances is needed and these disturbances must be continuously monitored. Therefore, scintillation measurements seem the most appropriate for turbulence above 1 km. Near the ground, turbulence is best measured with thermal sensors. A gap remains between 1 km and 20 or 30 meters. It is very likely that a carefully calibrated seeing monitor, measuring the integral of C_N^2 over the whole atmosphere, would give that contribution by taking the difference between the results of other measurements. Such a monitor could be a rotation interferometer, as developed by C. RODDIER [1976], mounted on a 20 cm telescope or an interferometrically calibrated image motion monitor. For solar site testing, an image motion monitor calibrated as described by BORGNI, VERNIN, AIME and RICORT [1979] seems appropriate. Considerable efforts have been made in the past to put seeing monitors on top of towers

carefully protected from the wind. There is now no doubt that the measurements of a ground-based monitor could be corrected for the effect of lower layer turbulence, deduced from simultaneous and independent measurements with thermal sensors. The approximate knowledge of the distribution of turbulence with height enables one to estimate the size of the isoplanatic patch for high angular resolution imaging (§ 6). A knowledge of the distribution of wind velocities in turbulence layers is also useful in order to estimate the time scale of speckle boiling (§ 6), which limits the exposure time in speckle interferometry.

Seeing monitors have also been developed for real time selection of the best images (RÖSCH [1958b, 1960]). As we have seen (§ 9) this is only worthwhile with telescopes of moderate size ($D/r_0 \approx 3$ to 5). Post-detection frame selection is now considered a much easier solution (MULLER [1973]). Calibration of atmospheric effects for a given observation remains a difficult problem. With high signal-to-noise ratios calibration is better made on the image itself, using some a priori knowledge of the object or using a self-consistent method, as reported by RICORT and AIME [1979]. For speckle work on faint objects, simultaneous offset measurements on a bright star could be envisaged.

§ 11. Conclusion

During the last decade, considerable advances have been achieved in high angular resolution optical imaging in astronomy, as attested by the I.A.U. Symposium no 50 held in August 1978 at the University of Maryland (DAVIS and TANGO [1979]). Diffraction limited resolution has been obtained with large telescopes up to magnitude 13 by means of speckle interferometry. A Michelson interferometer is already working in the visible on a 20 m baseline up to magnitude 4 and many projects are nearing completion. However, such technological progress will be fully useful only if accurate quantitative measurements prove to be feasible through atmospheric turbulence. As pointed out by Hanbury Brown (in DAVIS and TANGO [1979]), the accuracy needed on stellar diameters is of the order of 2%. Furthermore, most of the physical information is in the centre-to-limb brightness distribution as a function of wavelength. The considerable progress made recently in the understanding of atmospheric effects gives strong hopes that such a goal will be achieved in the near future. There will be strong competition between spatial and ground

based techniques. However, spatial techniques are extremely expensive and a telescope larger than 2.4 m is very unlikely to be launched before decades. The next step might be to launch a long baseline interferometer in space. Better support will be given to this project once ground based techniques are proven to be scientifically productive.

As pointed out in § 9, the quality of seeing is of fundamental importance for achieving high angular resolution from the ground. International efforts should be made to find the most appropriate site for such observations, and at existing sites, priority should be given to these observations whenever the seeing is exceptionally good. Considerable progress could also be made by the proper modification of domes and their environment, as carried out at the Pic du Midi observatory.

Much work remains to be done before achieving a full understanding of atmospheric effects. The relationship between isoplanicity or speckle boiling and the structure of the atmosphere is still not clear. The statistics of the fluctuations of seeing with time remain unknown. The effects of the finite outer scale of turbulence have never been experimentally investigated. The low frequency part of the spectrum of image motion is almost entirely unknown, although long term fluctuations are known to exist from astrometric measurements. Such a lack of knowledge has dramatic consequences in the selection of the astrometric satellite Hypparcos, since there still remains considerable controversy over the fundamental limitations imposed by the atmosphere on astrometric measurements. A whole area of investigation remains open and results are urgently needed. As a by-product, astronomical instruments may become useful for atmospheric remote sensing, as is now the case in studies of stellar scintillation.

References

- AIME, C., 1978, Opt. Commun. **26**, 139.
AIME, C., S. KADIRI, G. RICORT, C. RODDIER and J. VERNIN, 1979, Opt. Acta **26**, 575.
AIME, C., G. RICORT and G. GREC, 1975, Astron. Astrophys. **43**, 313.
AIME, C., G. RICORT and G. GREC, 1977, Astron. Astrophys. **54**, 505.
AIME, C. and F. RODDIER, 1976, Opt. Commun. **19**, 57.
AIME, C. and F. RODDIER, 1977, Opt. Commun. **21**, 435.
ANDERSON, J. A., 1920, Astrophys. J. **51**, 263.
ANTONIA, R. A., A. J. CHAMBERS and C. A. FRIEHE, 1978, Boundary Layer Meteor. **15**, 243.
ASSUS, P., H. CHOPLIN, J. P. CORTEGGIANI, E. CUOT, J. GAY, A. JOURNET, G. MERLIN and Y. RABBIA, 1979, J. Opt. **10**, 345.

- AUBRY, M., 1975, Les sondages acoustiques de l'atmosphère, Review paper presented at the U.R.S.I. 18th General Assembly (Lima), note technique C.R.P.E./7.
- AZOUIT, M., J. BORGNO and J. VERNIN, 1978, J. Opt. **9**, 291.
- AZOUIT, M. and J. VERNIN, 1980, J. Atmos. Sci. **37**, 1550.
- BABCOCK, H. W., 1953, Pub. Astr. Soc. Pac. **65**, 229.
- BABCOCK, H. W., 1958, J. Opt. Soc. Am. **48**, 500.
- BABCOCK, H. W., 1963, Pub. Astr. Soc. Pac. **75**, 1.
- BALEGA, Y. Y. and N. A. TIKHONOV, 1977, Sov. Astr. Letters **3**, 272.
- BARLETTI, R., G. CEPPATELLI, E. MORODER, L. PATERNO and A. RIGHINI, 1974, J. Geophys. Res. **79**, 4545.
- BARLETTI, R., G. CEPPATELLI, L. PATERNO, A. RIGHINI and N. SPERONI, 1976, J. Opt. Soc. Am. **66**, 1380.
- BARLETTI, R., G. CEPPATELLI, L. PATERNO, A. RIGHINI and N. SPERONI, 1977, Astron. Astrophys. **54**, 649.
- BARLETTI, R., P. LEMMETI and L. PATERNO, 1974, Rev. Sci. Instrum. **45**, 1563.
- BARNETT, M. E. and G. PARRY, 1977, Opt. Commun. **21**, 60.
- BARNHART, P. E., G. KELLER and W. E. MITCHELI, 1959, Air Force Cambridge Research Center, Final Tech. Report 59-291, Geophys. Research Directorate, Bedford, Mass. (U.S.A.).
- BATCHELOR, G. K., 1970, The Theory of Homogeneous Turbulence (Cambridge Univ. Press, Cambridge, G.B.).
- BATES, R. H. T., M. O. MILNER, G. I. LUND and A. D. SEAGAR, 1978, Opt. Commun. **26**, 22.
- BECKERS, J. M., 1966, Appl. Opt. **5**, 301.
- BEDDOES, D. R., J. C. DAINTY, B. L. MORGAN and R. J. SCADDAN, 1976, J. Opt. Soc. Am. **66**, 1247.
- BELVEDERE, G. and L. PATERNO, 1976, Astron. Astrophys. **51**, 199-207.
- BERTOLOTTI, M., L. MUZII, D. SETTE, 1970, J. Opt. Soc. Am. **60**, 1603.
- BIRAUD, Y. G., 1969, Astron. Astrophys. **1**, 124.
- BLAZIT, A., L. KOEHLIN and J. L. ONETO, 1975, On Line Digital Correlation of Photon Counting TV Images for Stellar Interferometry, in: Proc. Conf. on Image Processing Techniques in Astronomy, ed. C. de Jager (D. Reidel, Holland).
- BORGNO, J., G. CEPPATELLI, G. RICORT and A. RIGHINI, 1980, submitted to Astron. Astrophys.
- BORGNO, J. and F. MARTIN, 1977, J. Opt. Soc. Am. **67**, 1065.
- BORGNO, J. and J. VERNIN, 1978, J. Opt. Soc. Am. **68**, 1056.
- BORGNO, J., J. VERNIN, C. AIME and G. RICORT, 1979, Solar Phys. **64**, 403.
- BOURICIUS, G. M. B. and S. F. CLIFFORD, 1970, J. Opt. Soc. Am. **60**, 1484.
- BOYD, R. W., 1978, J. Opt. Soc. Am. **68**, 877.
- BOZEC, P., M. CAGNET and G. ROGER, 1971, Nouv. Rev. d'Opt. **2**, 197.
- BRANDT, P. N., 1969, Solar Phys. **7**, 187.
- BRANDT, P. N., 1970, Solar Phys. **13**, 243.
- BRECKINRIDGE, J. B., 1972, Appl. Opt. **11**, 2996.
- BRECKINRIDGE, J. B., 1974, Appl. Opt. **13**, 2760.
- BRECKINRIDGE, J. B., 1976, J. Opt. Soc. Am. **66**, 143.
- BRECKINRIDGE, J. B., H. A. McALISTER and W. G. ROBINSON, 1979, Appl. Opt. **18**, 1034.
- BROWN, D. S. and R. J. SCADDAN, 1979, Observatory **99**, 125.
- BROWNING, G. K. A., 1971, Quart. J. Meteor. Soc. **97**, 283.
- BRUCK, Y. M. and L. G. SODIN, 1979, Opt. Commun. **30**, 304.

- BRUCK, Y. M. and L. G. SODIN, 1980, *Astron. Astrophys.* **87**, 188.
- BUFFINGTON, A., F. S. CRAWFORD, R. A. MULLER and C. D. ORTH, 1977, *J. Opt. Soc. Am.* **67**, 304.
- BUFFINGTON, A., F. S. CRAWFORD, R. A. MULLER, A. J. SCHWEMIN and R. G. SMITS, 1977, *J. Opt. Soc. Am.* **67**, 298.
- BUFTON, J. L., 1973a, *J. Atmos. Sci.* **30**, 83.
- BUFTON, J. L., 1973b, *Appl. Opt.* **12**, 1785.
- BUFTON, J. L. and S. H. GENATT, 1971, *Astron. J.* **76**, 378.
- BUSER, R. G., 1971, *J. Opt. Soc. Am.* **61**, 488.
- BUTLER, H. E., 1952, *Proc. Roy. Irish Acad.* **A54**, 321.
- BUTLER, H. E., 1954, *Quart. J. R. Meteor. Soc.* **80**, 241.
- CHANDRASEKHAR, S., 1952, *Mon. Not. R. Astr. Soc.* **112**, 475.
- CHELLI, A., 1979, Thèse de 3e cycle, University of Paris 7 (France).
- CHELLI, A., P. LENA, C. RODDIER, F. RODDIER and F. SIBILLE, 1979, *Opt. Acta* **26**, 583.
- CHERNOV, L. A., 1955, *Akust. Zh.* **1**, 89.
- CHERNOV, L. A., 1960, *Wave Propagation in a Random Medium* (Dover, New York).
- CLIFFORD, S. F., 1978, *The Classical Theory of Wave Propagation in a Turbulent Medium*, in: *Laser Beam Propagation in the Atmosphere*, Topics in Applied Physics, vol. 25, ed. J. W. Strohbehn (Springer-Verlag, Berlin) pp. 9-43.
- CLIFFORD, S. F., G. M. B. BOURICIUS, G. R. OCHS and M. H. ACKLEY, 1971, *J. Opt. Soc. Am.* **61**, 1279.
- CLIFFORD, S. F., G. R. OCHS and R. S. LAWRENCE, 1974, *J. Opt. Soc. Am.* **64**, 148.
- CORRSIN, S., 1951, *J. Appl. Phys.* **22**, 469.
- COULMAN, C. E., 1973, *Boundary-Layer Meteor.* **4**, 196.
- COULMAN, C. E., 1974, *Solar Phys.* **34**, 491.
- COUPINOT, G., 1973, *Icarus* **19**, 212.
- COUPINOT, C. and J. HECQUET, 1979, *J. Opt.* **10**, 335.
- CURRIE, D. G., S. L. KNAPP and K. M. LIEWER, 1974, *Astrophys. J.* **187**, 131.
- DAINTY, J. C., 1974, *Mon. Not. R. Astr. Soc.* **169**, 631.
- DAINTY, J. C., 1975, *Stellar Speckle Interferometry*, in: *Laser Speckle and Related Phenomena*, Topics in Applied Physics, vol. 9, ed. J. C. Dainty (Springer-Verlag, Berlin) pp. 255-280.
- DAINTY, J. C., 1976, *The Statistics of Speckle Patterns*, in: *Progress in Optics*, vol. 14, ed. E. Wolf (North-Holland, Amsterdam) pp. 1-46.
- DAINTY, J. C. and A. H. GREENAWAY, 1978, *The Signal-to-Noise Ratio in Speckle Interferometry*, in: *Proc. I.A.U. Colloquium no 50*, Univ. of Maryland, eds. J. Davis and W. J. Tango (Chatterton Astr. Dept., Sydney) pp. 23/1-23/18.
- DAINTY, J. C. and A. H. GREENAWAY, 1979, *J. Opt. Soc. Am.* **69**, 786.
- DAINTY, J. C. and R. J. SCADDAN, 1974, *Mon. Not. R. Astr. Soc.* **167**, 69P.
- DAINTY, J. C. and R. J. SCADDAN, 1975, *Mon. Not. R. Astr. Soc.* **170**, 519.
- DANJON, A., 1955, *Vistas in Astronomy* **1**, 382.
- DAVIS, J. and W. J. TANGO, editors, 1979, *Proc. I.A.U. Colloquium no 50 on High Angular Resolution Stellar Interferometry*, Univ. of Maryland (Chatterton Astr. Dept., Sydney).
- ELLISON, M. A., 1954, *Quart. J. R. Meteor. Soc.* **80**, 246.
- ELLISON, M. A. and H. SEDDON, 1952, *Mon. Not. R. Astr. Soc.* **112**, 73.
- FANTE, R. L., 1979, *J. Opt. Soc. Am.* **69**, 1394.
- FIDDY, M. A. and A. H. GREENAWAY, 1978, *Nature* **276**, 421.
- FIENUP, J. R., 1978, *Opt. Letters* **3**, 27.
- FRIED, D. L., 1965, *J. Opt. Soc. Am.* **55**, 1427.
- FRIED, D. L., 1966, *J. Opt. Soc. Am.* **56**, 1372.

- FRIED, D. L., 1967, Proc. I.E.E.E. **55**, 57.
- FRIED, D. L., 1969, Proc. I.E.E.E. **57**, 415.
- FRIED, D. L., 1973, Theoretical Analysis of Aperture Averaging, Optical Sciences Consultants, Report DR-015.
- FRIED, D. L., 1974, R.A.D.C. Technical Reports TR-74-185 and TR-74-276.
- FRIED, D. L., 1975, Radio Sci. **10**, 71.
- FRIED, D. L., 1976, in: Proc. S.P.I.E. Seminar on Imaging through the Atmosphere **75**, 20.
- FRIED, D. L., 1978, J. Opt. Soc. Am. **68**, 1651.
- FRIED, D. L., 1979, Opt. Acta **26**, 597.
- FRIEHE, C. A. and J. C. LARUE, 1974, Dependence of Optical Refractive Index on Humidity and Temperature, in: Digest of Technical Papers, Topical Meeting on Optical Propagation through Turbulence, Boulder, pp. WB2/1-WB2/4.
- GAVIOLA, E., 1949, Astron. J. **54**, 155.
- GEZARI, D. Y., A. LABEYRIE and R. V. STACHNIK, 1972, Astrophys. J. Letters **173**, L 1.
- GOODMAN, J. W., 1968, Introduction to Fourier Optics (McGraw Hill, New York).
- GOODMAN, J. W., 1975, Statistical Properties of Laser Speckle Patterns, in: Laser Speckle and Related Phenomena, Topics in Applied Physics, vol. 9, ed. J. C. Dainty (Springer-Verlag, Berlin) pp. 9-75.
- GOODMAN, J. W. and J. F. BELSHER, 1976a, Technical Reports RADC-TR-76-50, RADC-TR-76-382 and RADC-TR-77-165. Rome Air Development Center.
- GOODMAN, J. W. and J. F. BELSHER, 1976b, in: Proc. S.P.I.E. Seminar on Imaging through the Atmosphere **75**, 141.
- GREENAWAY, A. H., 1977, Opt. Letters **1**, 10.
- GREENAWAY, A. H., 1979, Opt. Commun. **29**, 279.
- GREENAWAY, A. H. and J. C. DAINTY, 1978, Opt. Acta **25**, 181.
- GRIFFIN, R. F., 1973, Observatory **93**, 3.
- GUSH, H. P., 1979, J. Opt. Soc. Am. **69**, 187.
- HANBURY BROWN, R., 1977, Intensity Interferometry versus Michelson Interferometry, in: Proc. E.S.O. Conf. on Optical Telescopes of the Future, Geneva, eds. F. Pacini, W. Richter and R. N. Wilson (E.S.O. c/o C.E.R.N., Geneva 23) pp. 391-407.
- HANBURY BROWN, R., 1978, A Review of the Achievements and Potential of Intensity Interferometry, in: I.A.U. Colloquium no 50, Univ. of Maryland, eds. J. Davis and W. J. Tango (Chatterton Astr. Dept., Sydney) pp. 11/1-11/17.
- HARDY, J. W., 1978a, Proc. I.E.E.E. **66**, 651.
- HARDY, J. W., 1978b, The Role of Active Optics in Large Telescopes, in: E.S.O. Conf. on Optical Telescopes of the Future, Geneva, eds. F. Pacini, W. Richter and R. N. Wilson (E.S.O. c/o C.E.R.N., Geneva 23) pp. 455-467.
- HARLAN, E. A. and M. F. WALKER, 1965, Pub. Astr. Soc. Pac. **77**, 246.
- HARRIS, J. L., 1966, J. Opt. Soc. Am. **56**, 569.
- HARVEY, J. W., 1972, Nature Phys. Sci. **235**, 90.
- HARVEY, J. W., 1978, Adaptive Optics for Solar Observations?, in: Proc. J.O.S.O. Workshop on Future Solar Optical Observations, Needs and Constraints, Firenze, eds. G. Godoli, G. Noci and A. Righini (Baccini & Chiappi, Firenze) pp. 81-95.
- HAWKINS, M. R. S., 1979, Astron. Astrophys. **76**, 46.
- HESS, S. L., 1959, Introduction to Theoretical Meteorology (Holt, New York).
- HILL, R. J. and S. F. CLIFFORD, 1978, J. Opt. Soc. Am. **68**, 892.
- HINZE, J. O., 1959, Turbulence (McGraw-Hill, New York).
- HUFNAGEL, R. E., 1966, in: Restoration of Atmospherically Degraded Images, Woods Hole Summer Study, vol. 2 (Nat. Acad. of Sci., Washington D.C.) p. 14.
- HUFNAGEL, R. E., 1974, Variations of Atmospheric Turbulence, in: Digest of Technical

- Papers, Topical Meeting on Optical Propagation through Turbulence, Boulder, pp. WA1/1-WA1/4.
- HUFNAGEL, R. E. and N. R. STANLEY, 1964, J. Opt. Soc. Am. **54**, 52.
- IRWIN, J. W., 1966, Astron. J. **71**, 28.
- ISHIMARU, A., 1978, Wave Propagation and Scattering in Random Media, vol. 2 (Academic Press, New York).
- IYER, S. and J. L. BUFTON, 1977, Opt. Commun. **22**, 377.
- JAKEMAN, E., G. PARRY, E. R. PIKE and P. N. PUSEY, 1978, Contemp. Phys. **19**, 127.
- JAKEMAN, E., E. R. PIKE and P. N. PUSEY, 1976, Nature **263**, 215.
- JAKEMAN, A. and P. N. PUSEY, 1976, I.E.E.E. trans. AP **24**, 806.
- KADIRI, S., 1979, Thèse de 3e cycle, University of Nice (France).
- KALLISTRATOVA, M. A., 1966, Radiofizika **9**, 50.
- KALLISTRATOVA, M. A. and D. F. TIMANOVSKIY, 1971, Izv. Akad. Nauk. S.S.S.R., Atmos. Ocean. Phys. **7**, 46; Russ. **1**, 73.
- KARO, D. P. and A. M. SCHNEIDERMAN, 1967a, J. Opt. Soc. Am. **66**, 1065 A.
- KARO, D. P. and A. M. SCHNEIDERMAN, 1967b, J. Opt. Soc. Am. **66**, 1252.
- KARO, D. P. and A. M. SCHNEIDERMAN, 1977, J. Opt. Soc. Am. **67**, 1277.
- KARO, D. P. and A. M. SCHNEIDERMAN, 1978, J. Opt. Soc. Am. **68**, 480.
- KELLER, G., 1953, Astron. J. **58**, 113.
- KELLER, G., 1955, J. Opt. Soc. Am. **45**, 845.
- KELSALL, D., 1973, J. Opt. Soc. Am. **63**, 1472.
- KENKNIGHT, C. E., 1972, Astrophys. J. Letters **176**, L 43.
- KENKNIGHT, C. E., 1975, Imaging with the Small Angle Meter, in: Digest of Technical Papers, Meeting on Imaging in Astronomy, Cambridge Mass., pp. WB 12/1-WB 12/4.
- KIEPENHEUER, K. O., 1972, J.O.S.O. Annual Report, ed. C. de Jager, p. 11.
- KIEPENHEUER, K. O., 1973, J.O.S.O. Annual Report, ed. C. de Jager, p. 67.
- KINAHAN, B. F., 1976, Astrophys. J. **209**, 282.
- KING, J. R., 1971, Pub. Astr. Soc. Pac. **83**, 199.
- KNOX, K. T. and B. J. THOMPSON, 1974, Astrophys. J. Letters **193**, L 45.
- KOLCHINSKI, I. G., 1952, Astron. Zh. **29**, 350.
- KOLCHINSKI, I. G., 1957, Astron. Zh. **34**, 638.
- KOLMOGOROV, A. N., 1941, Dan. S.S.S.R. **30** (4), 229.
- KORFF, D., 1973, J. Opt. Soc. Am. **63**, 971.
- KORFF, D., G. DRYDEN and R. P. LEAVITT, 1975, J. Opt. Soc. Am. **65**, 1321.
- KORFF, D., G. DRYDEN and M. G. MILLER, 1972, Opt. Commun. **5**, 187.
- KOZHEVNIKOV, N. I., 1961, Solnechnye Dan. **8**, 75.
- KRASILNIKOV, V. A., 1949, Doklady Akad. Nauk. S.S.S.R. **65**, 291.
- KUCHEROV, N. I., editor, 1965, Optical Instability in the Earth's Atmosphere (I.P.S.T., Jerusalem).
- LABEYRIE, A., 1970, Astron. Astrophys. **6**, 85.
- LABEYRIE, A., 1974, Nouv. Rev. Opt. **5**, 141.
- LABEYRIE, A., 1975, Astrophys. J. Letters **196**, L 71.
- LABEYRIE, A., 1976, High Resolution Techniques in Optical Astronomy, in: Progress in Optics, Vol. 14, ed. E. Wolf (North-Holland, Amsterdam) pp. 49-87.
- LABEYRIE, A., 1977, Coherent Arrays, in: Proc. E.S.O. Conf. on Optical Telescopes of the Future, Geneva, eds. F. Pacini, W. Richter and R. N. Wilson (E.S.O. c/o C.E.R.N., Geneva 23) pp. 375-386.
- LABEYRIE, A., 1978, Stellar Interferometry Methods, in: Annual Review of Astronomy and Astrophysics, vol. 16, eds. G. Burbridge, D. Layzer and J. G. Phillips (Annual Rev. Inc., Palo Alto) pp. 77-102.

- LAWRENCE, R. S., G. R. OCHS and S. F. CLIFFORD, 1970, J. Opt. Soc. Am. **60**, 826.
- LEE, R. W. and J. C. HARP, 1969, Proc. I.E.E.E. **57**, 375.
- LINFOOT, E. H. and R. C. WITCOMB, 1972, Mon. Not. R. Astr. Soc. **158**, 199.
- LITTLE, C. G., 1951, Mon. Not. R. Astr. Soc. **111**, 289.
- LOOS, G. C. and C. B. HOGGE, 1979, Appl. Opt. **18**, 2654.
- LUMLEY, J. L. and PANOFSKY, H. A., 1964, *The Structure of Atmospheric Turbulence* (Interscience Pub., New York).
- LUTOMIRSKI, R. F. and H. T. YURA, 1971, J. Opt. Soc. Am. **61**, 482.
- LYNDS, C. R., S. P. WORDEN and J. W. HARVEY, 1976, Astrophys. J. **207**, 174.
- MCCARTHY, D. W. and F. J. LOW, 1975, Astrophys. J. Letters **202**, L 37.
- MCCARTHY, D. W., F. J. LOW and R. HOWELL, 1977, Astrophys. J. Letters **214**, L 85.
- MCGLAMERY, B. L., 1967, J. Opt. Soc. Am. **57**, 293.
- MEINEL, A. B., 1960, Astronomical Seeing and Observatory Site Selection, in: *Stars and Stellar Systems*, vol. 1, Telescopes, eds. G. P. Kuiper and B. M. Middlehurst (Chicago Univ. Press, Chicago) pp. 154-175.
- METCALF, J. I., 1975, J. Atmos. Sci. **32**, 362.
- MICHELSON, A. A., 1920, Astrophys. J. **51**, 257.
- MICHELSON, A. A. and F. G. PEASE, 1921, Astrophys. J. **53**, 249.
- MIKESELL, A. H., 1955, Pub. U.S. Naval Observ., 2nd series, vol. 17, part 4.
- MIKESELL, A. H., A. A. HOAG and J. S. HALL, 1951, J. Opt. Soc. Am. **41**, 689.
- MILLER, M. G., 1977, J. Opt. Soc. Am. **67**, 1176.
- MILLER, M. G. and P. F. KELLEN, 1975, Astronomical Differential Angle of Arrival Measurements, in: *Digest of Technical Papers, Meeting on Imaging in Astronomy*, Cambridge Mass., pp. WB3/1-WB3/4.
- MILLER, M. G. and P. L. ZIESKE, 1977, J. Opt. Soc. Am. **67**, 1680.
- MINOTT, P. O., 1972, J. Opt. Soc. Am. **62**, 885.
- MORODER, E. and A. RIGHINI, 1973, Astron. Astrophys. **23**, 307.
- MUELLER, P. F. and G. O. REYNOLDS, 1967, J. Opt. Soc. Am. **57**, 1338.
- MULLER, R., 1973, Solar Phys. **32**, 409.
- MULLER, R. A. and A. BUFFINGTON, 1974, J. Opt. Soc. Am. **64**, 1200.
- NEFF, W. D., 1975, N.O.A.A. Technical Report, E.R.L. 322, W.P.L. 38.
- NETTLEBALD, F., 1951, Observatory **71**, 111.
- NISENSON, P. and R. V. STACHNIK, 1978, J. Opt. Soc. Am. **68**, 169.
- NISENSON, P. and R. V. STACHNIK, 1978, Restoration of Turbulence Degraded Images - A Review, in: *Proc. I.A.U. Colloquium no 50*, Univ. of Maryland, eds, J. Davis and W. J. Tango (Chatterton Astr. Dept., Sydney) pp. 34 1-34/14.
- OBUKHOV, A. M., 1949, Izv. Akad. Nauk S.S.R., Ser Geograf. Geofiz. **13**, 58.
- OCHS, G. R. and R. S. LAWRENCE, 1972, N.O.A.A. Technical Report, E.R.L. 251, W.P.L. 22.
- OCHS, G. R., TING-I-WANG, R. S. LAWRENCE and S. F. CLIFFORD, 1976, Appl. Opt. **15**, 2504.
- O'NEILL, E. L., 1963, *Introduction to Statistical Optics* (Addison-Wesley).
- PACINI, F., W. RICHTER and R. N. WILSON, editors, 1978, *Proc. E.S.O. Conf. on Optical Telescopes of the Future*, Geneva (E.S.O. c/o C.E.R.N., Geneva 23).
- PARRY, G., J. G. WALKER and R. J. SCADDAN, 1979, Opt. Acta **26**, 563.
- PATERNO, L., 1976, Astron. Astrophys. **47**, 437.
- PESKOFF, A., 1968, J. Opt. Soc. Am. **58**, 1032.
- POLLAIN, S., A. BUFFINGTON and F. S. CRAWFORD, 1979, J. Opt. Soc. Am. **69**, 84.
- PROTHEROE, W. M., 1955a, Preliminary Report on Stellar Scintillation, Centr. Perkins Obs., Ohio Wesleyan Univ. and Ohio State Univ., Series II, no 4, 127.

- PROTHEROE, W. M., 1955b, J. Opt. Soc. Am. **45**, 851.
PROTHEROE, W. M., 1961a, Publ. Univ. of Pennsylvania (Flower and Cook Observatory) **90**, 27.
PROTHEROE, W. M., 1961b, Science **134**, 1593.
PROTHEROE, W. M., 1964, Quart. J. R. Meteor. Soc. **90**, 27.
PROTHEROE, W. M. and K. Y. CHEN, 1960, Air Force Cambridge Research Center, Technical Report AF19(604)-1570. Geophys. Research Directorate, Bedford, Mass. (U.S.A.).
RABBIA, Y., 1978. Thèse de 3e cycle, University of Nice (France).
REIGER, S. H., 1962, Atmospheric Turbulence and the Scintillation of Starlight, U.S. Air Force Project Rand, Report R-406-PR.
REIGER, S. H., 1963, Astron. J. **68**, 395.
RHODES, W. T. and J. W. GOODMAN, 1973, J. Opt. Soc. Am. **63**, 647.
RICORT, G. and C. AIME, 1979, Astron. Astrophys. **76**, 324.
RICORT, G., C. AIME, C. RODDIER and J. BORGNO, 1980, Solar Physics, in press.
ROCCA, A., F. RODDIER and J. VERNIN, 1974, J. Opt. Soc. Am. **64**, 1000.
RODDIER, C., 1976, J. Opt. Soc. Am. **66**, 478.
RODDIER, C. and F. RODDIER, 1973, J. Opt. Soc. Am. **63**, 661.
RODDIER, C. and F. RODDIER, 1975, J. Opt. Soc. Am. **65**, 664.
RODDIER, C. and F. RODDIER, 1976a, J. Opt. Soc. Am. **66**, 580.
RODDIER, C. and F. RODDIER, 1976b, J. Opt. Soc. Am. **66**, 1347.
RODDIER, F. 1974, Opt. Commun. **10**, 103.
RODDIER, F., 1975, Signal-to-Noise Ratio in Speckle Interferometry, in: Digest of Technical Papers, Meeting on Imaging in Astronomy, Cambridge Mass., pp. ThC 6/1-ThC 6/4.
RODDIER, F., 1978a, Observations of the Sun with Interferometry and Speckle Interferometry Techniques, in: Proc. J.O.S.O. Workshop on Future Solar Optical Observations, Needs and Constraints, eds. G. Godoli, G. Noci and A. Righini (Baccini & Chiappi, Firenze) pp. 96-109.
RODDIER, F., 1978b, Rotation-Shearing Interferometry, in: Proc. I.A.U. Colloquium no 50, Univ of Maryland, eds. J. Davis and W. J. Tango (Chatterton Astr. Dept., Sydney) pp. 32/1-32/15.
RODDIER, F., G. RICORT and C. RODDIER, 1978, Opt. Commun. **24**, 281.
RODDIER, F. and C. RODDIER, 1978, Imaging with a Multi-Mirror Telescope, in: Proc. E.S.O. Conf. on Optical Telescopes of the Future, Geneva, eds. F. Pacini, W. Richter and R. N. Wilson (E.S.O. c/o C.E.R.N., Geneva 23) pp. 359-370.
RÖSCH, J., 1954a, C. R. Acad. Sci. (Paris) **239**, 222.
RÖSCH, J., 1954b, J. Phys. Radium **15**, 39 S.
RÖSCH, J., 1957, C. R. Acad. Sci. (Paris) **244**, 3027.
RÖSCH, J., 1958a, C. R. Acad. Sci. (Paris) **246**, 559.
RÖSCH, J., 1958b, C. R. Acad. Sci. (Paris) **247**, 422.
RÖSCH, J., 1960, Astronomie **74**, 485.
RÖSCH, J., 1972, Space Res. **12**, 1633.
RÖSCH, J., G. COURTES and J. DOMMANGET, editors, 1963, Proc. I.A.U. Symp. no 19 on Site Testing. Bull. Astr. Obs. Paris, Vol. 24, no 2 and 3.
RUSSELL, F. D. and J. W. GOODMAN, 1971, J. Opt. Soc. Am. **61**, 182.
SAUNDERS, J. B., 1964, Astron. J. **69**, 449.
SAUNDERS, J. B., 1967, Precision Measurements, in: Advanced Optical Techniques, ed. A. C. S. Van Heel (North-Holland, Amsterdam) pp. 1-22.
SCADDAN, R. J. and J. G. WALKER, 1978, Appl. Opt. **17**, 3779.
SCHNEIDERMAN, A. M. and D. P. KARO, 1978a, J. Opt. Soc. Am. **68**, 338.
SCHNEIDERMAN, A. M. and D. P. KARO, 1978b, J. Opt. Soc. Am. **68**, 348.

- SEDMAK, G., 1973, *Astron. Astrophys.* **25**, 41.
SELBY, M. J., R. WADE and C. SANCHEZ MAGRO, 1979, *Mon. Not. R. Astr. Soc.* **187**, 553.
SHAPIRO, J. H., 1976, *J. Opt. Soc. Am.* **66**, 469.
SIBILLE, F., A. CHELLI and P. LENA, 1979, *Astron. Astrophys.* **79**, 315.
SINGAL, S. P., 1974, *J. Sci. Ind. Res.* **33**, 162.
STACHNIK, R. V., P. NISENSON, D. C. EHN, R. H. HUDGIN and V. E. SCHIRF, 1977, *Nature* **266**, 149.
STOCK, J. and G. KELLER, 1960, *Astronomical Seeing*, in: *Stars and Stellar Systems*, vol. 1, Telescopes, eds. G. P. Kuiper and B. M. Middlehurst (Chicago Univ. Press, Chicago) pp. 138-153.
STROHBEHN, J. W., 1968, *Proc. I.E.E.E.* **56**, 1301.
STROHBEHN, J. W., 1970a, *Proc. I.E.E.E.* **58**, 1523.
STROHBEHN, J. W., 1970b, *J. Geophys. Res.* **75**, 1067.
STROHBEHN, J. W., 1970c, *J. Opt. Soc. Am.* **60**, 948.
STROHBEHN, J. W., 1971, *Optical Propagation through the Turbulent Atmosphere*, in: *Progress in Optics*, vol. 9, ed. E. Wolf (North-Holland, Amsterdam) pp. 75-122.
STROHBEHN, J. W., 1973, *Boundary-Layer Meteor.* **4**, 397.
STROHBEHN, J. W., 1978, *Modern Theories in the Propagation of Optical Waves in a Turbulent Medium*, in: *Laser Beam Propagation in the Atmosphere*, Topics in Applied Physics, vol. 25, ed. J. W. Strohbehn (Springer-Verlag, Berlin) pp. 45-106.
STROHBEHN, J. W. and S. F. CLIFFORD, 1967, *I.E.E.E. Trans. AP-15*, 416.
SUTTON, E. C., 1978, *Results and Future Uses of Heterodyne Spatial Interferometry at 11 Microns*, in: *Proc. I.A.U. Colloquium no 50*, Univ. of Maryland, eds. J. Davis and W. J. Tango (Chatterton Astr. Dept., Sydney) pp. 16/1-16/14.
TATARSKI, V. I., 1956, *Doklady Akad. Nauk S.S.R.* **107**, 245.
TATARSKI, V. I., 1961, *Wave Propagation in a Turbulent Medium* (Dover, New York).
TATARSKI, V. I., 1971, *The Effects of the Turbulent Atmosphere on Wave Propagation* (I.P.S.T., Jerusalem).
TENNEKES, H. and J. L. LUMLEY, 1972, *A first Course in Turbulence* (M.I.T. Press, Cambridge, Mass.).
TEXEREAU, J., 1961, *La construction du télescope d'amateur* (Soc. Astr. de France, Paris).
TOWNSEND, A. A., 1965, *Quart. J. R. Meteorol. Soc.* **91**, 1.
TSVANG, L. R., 1969, *Radio Sci.* **4**, 1175.
USCINSKI, B. J., 1977, *The Elements of Wave Propagation in Random Media* (McGraw-Hill, New York).
VALLEY, G. C., 1979, *Appl. Opt.* **18**, 984.
VAN ISACKER, J., 1954, *Quart. J. R. Meteor. Soc.* **80**, 251.
VAN SCHOONEVELD, C., editor, 1979, *Proc. I.A.U. Colloquium no 49 on Image Formation from Coherence Functions in Astronomy*, Groningen, 1978 (Reidel, Dordrecht).
VANZANDT T. E., J. L. GREEN, K. S. GAGE and W. L. CLARK, 1977, *Reflectivity Studies with the Sunset VHF Pulsed Doppler Radar*, in: *Proc. of U.R.S.I. commission F open Symposium*, La Baule, 1977 (C.N.E.T., Paris) pp. 519-524.
VANZANDT, T. E., J. L. GREEN, K. S. GAGE and W. L. CLARK, 1978, *Radio Sci.* **13**, 819.
VERNIN, J., 1979, *Thèse d'Etat*, University of Nice, France.
VERNIN, J., R. BARLETTI, G. CEPPATELLI, L. PATERNO, A. RIGHINI and N. SPERONI, 1979, *Appl. Opt.* **18**, 243.
VERNIN, J. and F. RODDIER, 1973, *J. Opt. Soc. Am.* **63**, 270.
WADE, R. and M. J. SELBY, 1978, *Speckle Interferometry in the Near Infrared*, in: *Proc. I.A.U. Colloquium no 50*, Univ. of Maryland, eds. J. Davis and W. J. Tango (Chatterton Astr. Dept., Sydney) pp. 29/1-29/10.

- WALKER, J. G., 1978, Optimum Exposure Time and Filter Bandwidth in Speckle Interferometry, in: Proc. I.A.U. Colloquium no 50, Univ. of Maryland, eds. J. Davis and W. J. Tango (Chatterton Astr. Dept., Sydney) pp. 25/1-25/24.
- WALKER, J. G., 1979, Opt. Commun. **29**, 273.
- WALTERS, D. L., D. L. FAVIER and J. R. HINES, 1979, J. Opt. Soc. Am. **69**, 828.
- WANG, C. P., 1975, Opt. Commun. **14**, 200.
- WEIGELT, G. P., 1978a, Astron. Astrophys. **67**, L 11.
- WEIGELT, G. P., 1978b, Astron. Astrophys. **68**, L 5.
- WEIGELT, G. P., 1978c, Appl. Opt. **17**, 2660.
- WELTER, G. L. and S. P. WORDEN, 1978, J. Opt. Soc. Am. **68**, 1271.
- WESELY, M. L. and E. C. ALCARAZ, 1973, J. Geophys. Res. **78**, 6224.
- WESSELY, H. W. and J. O. BOLSTAD, 1970, J. Opt. Soc. Am. **60**, 678.
- WORDEN, S. P., 1977, Vistas in Astronomy **20**, 301.
- WYNGAARD, J. C., Y. IZUMI and S. A. COLLINS JR., 1971, J. Opt. Soc. Am. **61**, 1646.
- YAGLOM, A. M., 1949, Dan. S.S.S.R. **69** (6), 743.
- YOUNG, A. T., 1967, Astron. J. **72**, 747.
- YOUNG, A. T., 1969, Appl. Opt. **8**, 869.
- YOUNG, A. T., 1970, J. Opt. Soc. Am. **60**, 248.
- YOUNG, A. T., 1974, Astron. J. **189**, 587.
- ZHUKOVA, L. N., 1958, Izv. Glav. Astron. Observ., Akad. Nauk S.S.S.R. **21**, no 162.